# FABRICATION OF BIOACTIVE GLASS BASED ORALLY ADMINISTERED DRUG CARRIERS FOR BONE REGENERATION

**Thesis Submitted to**

DELHI TECHNOLOGICAL UNIVERSITY

**For the Award of the Degree of**

DOCTOR OF PHILOSOPHY

**Submitted By**

MANJOT KAUR

**2K18/PhD/AC/09**

*Under the Guidance of*

Dr. Deenan Santhiya



**Department of Applied Chemistry**

**Delhi Technological University**

**Shahbad Daulatpur, Main Bawana Road,**

**Delhi- 110042, INDIA**

**May 2024**

# DELHI TECHNOLOGICAL UNIVERSITY

**(Formerly Delhi College of Engineering)**

## Department of Applied Chemistry

**Shahbad Daulatpur, Bawana Road, Delhi- 110042, India**

---

**DELHI TECHNOLOGICAL UNIVERSITY**

(Formerly Delhi College of Engineering)

**Department of Applied Chemistry**

Shahbad Daulatpur, Bawana Road, Delhi- 110042, India

## DECLARATION

This is to declare that the research work embodied in this thesis entitled **"Fabrication of Bioactive Glass based orally administered drug carriers for bone regeneration"** submitted to the Delhi Technological University **is an original work and carried out by me for the degree of Doctor of Philosophy** under the supervision of **Dr. Deenan Santhiya, Assistant Professor**, Department of Applied Chemistry. This thesis is a contribution to my original research work. The extent of information derived from the existing literature has been indicated in the body of the thesis at appropriate places giving the source of information. Every effort has been made to make sure that the scientific contributions of others are appropriately cited. To the best of my knowledge, this research work has not been submitted in part or full for award of any degree or diploma in Delhi Technological University or in any other university/institution.

Date: 27.05.2024

**MANJOT KAUR**
Research Scholar
Reg. No. 2K18/PhD/AC/09
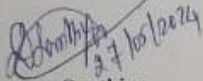
# DELHI TECHNOLOGICAL UNIVERSITY

## (Formerly Delhi College of Engineering)

## Shahbad Daulatpur, Bawana Road Delhi- 110042, India
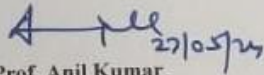
## CERTIFICATE

This is to certify that the thesis entitled **"Fabrication of Bioactive Glass based orally administered drug carriers for bone regeneration"** submitted to the Delhi Technological University, Delhi-110042, in fulfillment of the requirement for the award of the degree of **Doctor of Philosophy** has been carried out by the candidate, **Mrs. MANJOT KAUR**, (Reg. No. 2K18/PhD/AC/09) under the supervision of **Dr. Deenan Santhiya, Assistant Professor**, Department of Applied Chemistry. It is further certified that the work embodied in this thesis has neither partially nor fully been submitted to any other university or institution for the award of any degree or diploma.

27/05/2024

**Dr. Deenan Santhiya**
Supervisor
Department of Applied Chemistry
Delhi Technological University, Delhi

27/05/24

**Prof. Anil Kumar**
Head of the Department
Department of Applied Chemistry
Delhi Technological University, Delhi.

*Dedicated To*

*My Parents, My Husband &*
*Family…*

# Acknowledgment

The most important attribute of an individual is "an attitude of GRATITUDE". This brings to me the opportunity to thank every single individual who in one way or the other has helped me complete my PhD journey.

Nothing can be done without "HIS" grace. I think I have no words to thank GOD for helping me out and guiding me all through this phase. For making me keep going, giving me the enduring power to pursue the things, for all the strength that he has imparted and the blessings and mercy he has bestowed over me……." It's so true that there are no enough words to thank GOD because we are sustaining only because of him".

I would like to convey my thanks and regards to Prof. Jai Prakash Saini, Hon'ble Vice Chancellor, DTU, and Prof. Yogesh Singh (Former Vice Chancellor, DTU) to provide a platform and infrastructure for the research study.

The most important thing while pursuing Ph.D. is the freedom of thought and how your research ideas are perceived. In this regard, I am fortunate to have Dr. Deenan Santhiya as my mentor, my supervisor who has always guided me in the best possible direction. I thank her for showing tremendous faith and confidence in me and helping me grow in my research vision. Her encouragement has always helped to maintain my pace during this research journey. Her scientific and analytical approach to things helps me discover the uniqueness of simple things. I thank her and pay my gratitude to her for sharpening my research skills.

I would like to thank Prof. Anil Kumar, Head, Department of Applied Chemistry, Delhi Technological University, and Prof. S.G Warkar (Former Head of, the Department of Applied Chemistry, DTU) for providing a healthy and progressive environment to carry out research work. I would like to extend my thanks to both of them for their positive work culture and humility and guidance in all research work as well as Administrative work. I am grateful to all

You always need the driving force to keep going. And for me, it is my parents, my mother, and my father, I am living their dream. This Ph.D. is for them. No words can express this feeling. I will always be thankful to them for giving the best to their kids always. They have always encouraged me through thick and thin.

The person without whom I couldn't have dreamt of pursuing my Ph.D. after the five-year academic gap, MY HUSBAND. It is only due to him I was able to maintain the 3 Ps of my Ph.D. (Patience, Persistence, and Perseverance). Sometimes you remain short of words to express your feelings. I would like to conclude here, It's been always said: "Behind every successful man, there is a woman". I would like to add one more line, "behind every successful woman, there is a visionary father and a supporting husband"

I pay my regards to every single individual who has helped me in one way or the other during this journey.


Manjot Kaur

# Overview of thesis
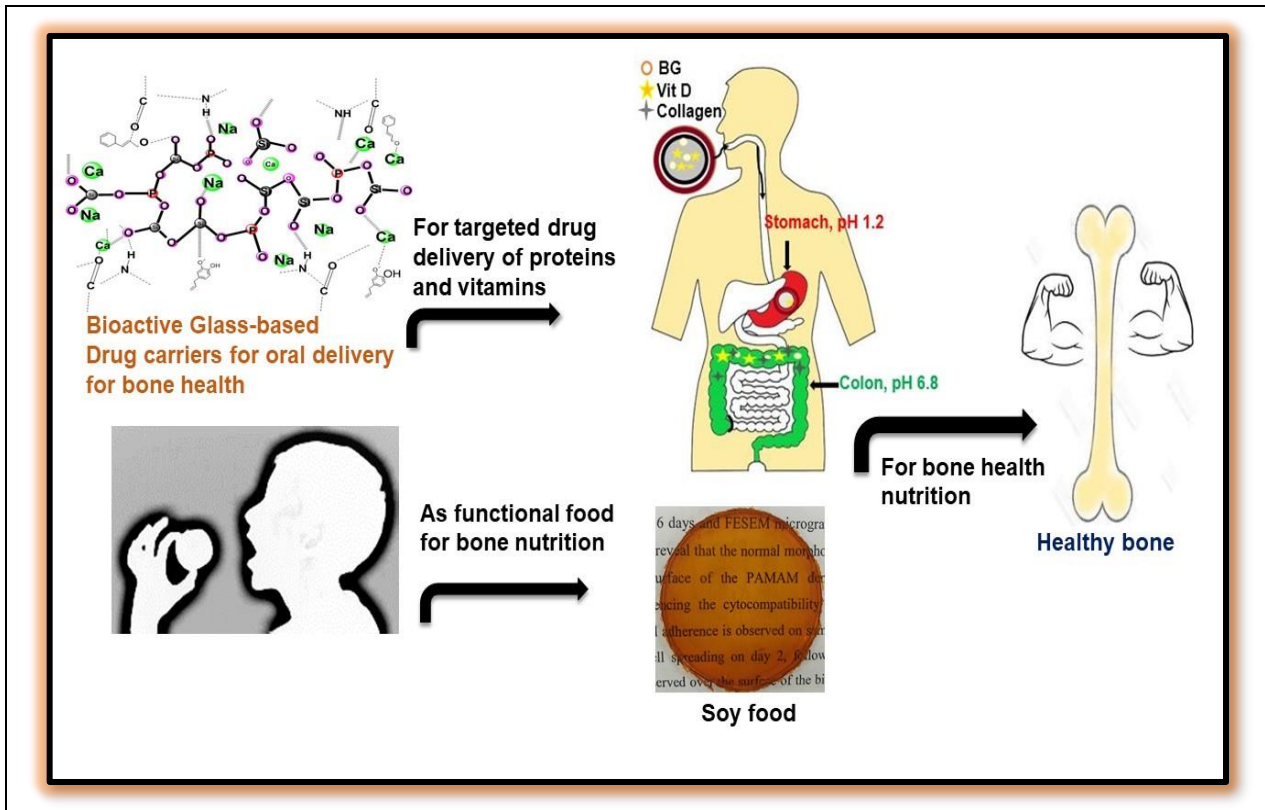
# Abstract

Bone disorders are one of the most prevalent diseases throughout the world, ranking Asia among the top list of people suffering from Osteoporosis (OP), especially women. There is an accelerated increase in OP during early postmenopausal years. Other prevalent bone disorders include osteomalacia, osteoarthritis, osteopenia, osteomyelitis, osteodystrophy, etc. The main cause for the prevalence of OP is the reduction of the organic matrix of bones i.e. protein leading to the fragility of bone and ultimately breaking of the bone. Treatment of bone disorders includes various techniques and measures like collagen fillers, collagen injections, tissue grafts (autograft, allograft), bone implants, tissue engineering, health supplements, etc. With the advent of third-generation biomaterial, bioactive glass (BG) has been widely used for bone regeneration as scaffolds and tissue engineering as it stimulates the natural bone to repair itself. In this view, emphasis is laid on the targeted oral delivery of protein and nutrients along with bioactive glass for bone regeneration using a polymeric matrix. To the best of our knowledge, it is the first time that oral delivery of bioactive glass is carried out for bone health applications due to its osteoinductive and osteoconductive properties. Also, BG is the reservoir of essential micronutrients that are essential for bone mineralization. For this, the synthesis of Nano-sized BG particles is carried out and it is radiolabelled with Technetium-99m (Tc-99m) and the labeling efficiency is calculated at different pH ranges. BG formed is found to be bioactive and biocompatible and is easily taken up by the intestinal cell lines (Caco-2). These studies made these nanoparticles a suitable candidate for oral drug delivery application. To provide complete nutrition for overall bone health various edible protein films have been fabricated fortified with BG network and essential vitamins like vitamin D and vitamin K. We have explored the application of BG in drug delivery and as functional food by carrying out *in-situ* mineralization of bioactive glass in food-grade polymer for targeted protein delivery and fabrication of bioactive glass fortified functional food for bone health respectively. The materials thus formed

are tested for cytocompatibility and found to be biocompatible. Finally, to protect against micro-organisms and pathogens and to prevent photo-oxidation, the active packaging material is fabricated that can be used for the packaging of the drug and food. Further, the radiolabeling of BG and its binding stability in different gastrointestinal pH conducted in the present study can be explored in the future in an animal model where the whole ADME process (Absorption, Distribution, Metabolism, and Excretion) can be studied when these particles are ingested orally. The pharmacokinetics and pharmacodynamic studies will help in deducing the efficacy of bioactive glass through the oral route in bone regeneration.

This thesis is summarized in five chapters.

**Chapter 1** Discusses a brief introduction to bone disorders and their prevalent treatments. It also talks about the application of biomaterials and the advantages of bioactive glass for bone regeneration applications.

**Chapter 2** This chapter describes the synthesis, characterization, and functionalization of bioactive glass nanoparticles through an *in-situ* mineralization process. Physico-chemical characterization is carried out to investigate the morphology, crystallinity, and functionality of the nanoparticles. An *in-vitro* cell proliferation assay is conducted to check the cytocompatibility against caco-2 and U2OS cell lines. The cellular uptake studies of the said nanoparticles for caco-2 cell lines are studied to prove it to be an efficient oral delivery nanocarrier. The radiolabeling efficiency of $^{99m}$Tc with formed nanoparticles is monitored at different pH levels at various time intervals. Thus, this work demonstrated the fabrication of biomaterial that can be employed as a potent radiopharmaceutical for long-term follow-up studies and in-vivo imaging.

**Chapter 3** The present chapter focuses on fabricating sandwiched film as a controlled drug delivery system using dextran for the delivery of collagen and vitamin D along with bioactive

glass to the colon site. To provide both organic and inorganic nutrients to the bone framework, *in-situ* mineralization of the bioactive glass network is carried out in a collagen matrix and is cast into a film. This film is sandwiched between the dextran film as the latter is considered to be important in colon-specific delivery. CD spectra depict the conformational changes in the secondary structure of collagen due to the inter- and intramolecular interactions of the BG network with the collagen fibrils. The rheological study is done to depict the visco-elastic nature of the sandwiched film in different GI tract pH. UV-Visible spectroscopy reveals the release of vitamin D and collagen at pH 6.8. The SDS-PAGE profile helps deduce the targeted delivery of collagen at the colon site having pH 6.8. Cellular cytotoxic studies are employed to deduce the biocompatible nature of the film.

**Chapter 4** The chapter focuses on the fabrication of soy films as a functional food for bone nutrition. The film formed is fortified with an *in-situ* mineralized bioactive glass (BG) network containing essential minerals required for good bone health. Also, vitamin K1 is supplemented into the films. Nutritional analysis is carried out to show that the films are a rich source of protein containing about 67% of protein per 100 g having energy calories of 330 Kcal/100 g and essential micronutrients required for bones. The rheological studies are conducted for the functional soy-based film. The mechanical analysis of the formed film is done along with its antimicrobial assay.

**Chapter 5** A comprehensive study on Zein film blended with glycerol and essential oils (EOs) is presented in this work. In particular, UV shielding properties and antimicrobial efficacy of developed active zein films are tested. Antibacterial assays are conducted to prove that the films are effective against spoilage microorganisms. Thermal and mechanical characterization of the film is carried out. To deduce its efficacy as packaging/coating material, water vapor permeability testing, and oxygen transmission rate are also investigated.

# Contents

# List of Figures

# List of Tables

# List of Abbreviations and Symbols

| | |
|---|---|
| **AOAC** | Association of official analytical chemists |
| **AR** | Analytical reagent |
| **ASTM** | American society for testing and materials |
| **ATCC** | American type cell culture |
| **BET** | Brunauer–Emmett–Teller |
| **BG** | Bioactive glass |
| **BGC** | Vitamin C templated bioactive glass |
| **BJH** | Barrett–Joyner–Halenda |
| **Ca** | Calcium |
| **Ca2+** | Calcium ion |
| **CaAc** | Calcium acetate |
| **Caco-2** | Human colorectal adenocarcinoma cell lines |
| **CBG** | Collgen with bioactive glass |
| **Cu** | Copper |
| **DCD** | Sandwich film contain dextran-collagen+bioactive glass-dextran |
| **DMA** | Dynamic mechanical analyzer |
| **DMEM** | Dulbecco's Modified Eagle's Medium |
| **DSC** | Differential scanning caloriemeter |
| **E. coli** | Escherichia coli |
| **ECM** | Extracellular matrix |

| | |
|---|---|
| **EDAX** | Energy dispersive X-ray analysis |
| **EO** | Essential oil |
| **FITC** | Fluorescein isothiocyanate |
| **FTIR** | Fourier transform infrared spectroscopy |
| **HA** | Hydroxyapatite |
| **HCA** | Hydroxycarbonate apatite |
| **HCl** | Hydrochloric acid |
| **HDPE** | High density polyethylene |
| **ICP-MS** | Inductively coupled plasma mass spectrometry |
| **ITLC** | Instant thin layer chromatography |
| **IS** | Indian standards |
| **IUPAC** | International union of pure and applied chemistry |
| **JCPDS** | Joint committee on powder diffraction standard |
| **K** | Potassium |
| **LC-MS** | Liquid chromatography mass spectroscopy |
| $^{99}$**Mo** | Molybdenum-99 (radioisotope) |
| **MTT** | 3-(4,5-Dimethylthiazol-2-yl)-2,5-diphenyltetrazolium bromide |
| **Na** | Sodium |
| **NaAc** | Sodium acetate |
| **NaOH** | Sodium hydroxide |
| **NH2** | Amine group |
| **NH3+** | Ammonium ion |
| **OP** | Osteoporosis |
| **OP** | Oxygen permeability |

| | |
|---|---|
| **OTR** | Oxygen transmission rate |
| **PBS** | Phosphate buffer saline |
| **pI** | Isoelectric point |
| **PI** | Propidium iodide |
| **PP** | Polypropylene |
| **PS** | Polystyrene |
| **PVC** | Polyvinyl chloride |
| **S. aureus** | *Staphylococcus aureus* |
| **SBF** | Simulated body fluid |
| **SBGK** | Soy protein film with glycerol, bioactive glass and vitamin K |
| **SDS-PAGE** | Sodium dodecyl sulphate-polyacrylamide gel electrophoresis |
| **SGF** | Simulated gastric fluid |
| **SIF** | Simulated intestinal fluid |
| **SEM** | Scanning electron microscopy |
| **SF** | Soy protein film with glyderol |
| **SP** | Soy Protein |
| **SPI** | Soy protein isolate |
| **SEO** | Soy protein film with glycerol and essential oil |
| **SEOBGK** | Soy protein film with glycerol, essential oil, Bioctive glass and vitamin K |
| **tan δ** | Loss tangent |
| **TEM** | Transmission electron microscope |
| **$^{99m}$Tc** | Technetium-99m (radioisotope) |
| **TEOS** | Tetraethyl orthosilicate |

| | |
|---|---|
| **TEP** | Triethyl phosphate |
| **TGA** | Thermogravimetric analysis |
| **U2OS** | human osteoblast-like osteosarcoma cell line |
| **WVP** | Water vapor permeability |
| **WVTR** | Water vapor transmission rate |
| **XRD** | X-Ray Diffraction |
| **ZEO** | Zein film with glycerol and essential oil |
| **ZF** | Zein film with glycerol |
| **ZP** | Zein protein |
| **%** | Percentage |
| **Å** | Angstrom |
| **cc** | Cubic centimeter |
| **cm** | Centimetre |
| **d** | Inter-planar spacing |
| **eV** | Electron-volt |
| **G'** | Storage modulus |
| **G"** | Loss modulus |
| **gm** | Gram |
| **h** | Hour |
| **Hz** | Hertz |
| **K** | Kelvin |
| **kD** | Kilo Dalton |
| **KJ** | Kilojoule |
| **kV** | Kilo Volts |

| | |
|---|---|
| **M** | Molar |
| **mA** | Milliampere |
| **mg** | Milligram |
| **Mg** | Magnesium |
| **MHz** | Megahertz |
| **min** | Minutes |
| **mL** | Milliliter |
| **mM** | Millimolar |
| **mm** | Millimetre |
| **MPa** | Mega pascal |
| **MW** | Molecular weight |
| **nm** | Nanometer |
| **°C** | Degree Celsius |
| **Pa** | Pascal |
| **v/v** | Volume per volume |
| **w/v** | Weight per volume |
| **wt.** | Weight |
| **λ** | X - ray wavelength |
| **λmax** | Wavelength |
| **μg** | Microgram |
| **μm** | Micrometer |
| **ω** | angular frequency |
| **θ** | Diffraction angle |

# Chapter 1
# Introduction

# Chapter 1

# Introduction

## 1.1 Overview

Bone health plays an important role in jovial sustainable life. It helps in movement and locomotion alongside protects our internal organs. For a jovial and healthful lifestyle, bones need to be strong, flexible, and healthy. Bones play a crucial role in a human body structure. Besides serving as storage for minerals and helping regulating blood sugar levels, bones also act as a shield for softer organs like ribs in the chest for the heart and lungs, and the skull protecting the brain. With the advent of bone health issues including lowbone mass density, Osteoporosis (OP), and Osteomalacia, it is been estimated that by 2030, the number of individuals affected by OP and low bone density will increase to 71.2 million (a 29 % increase from 2010) [1].
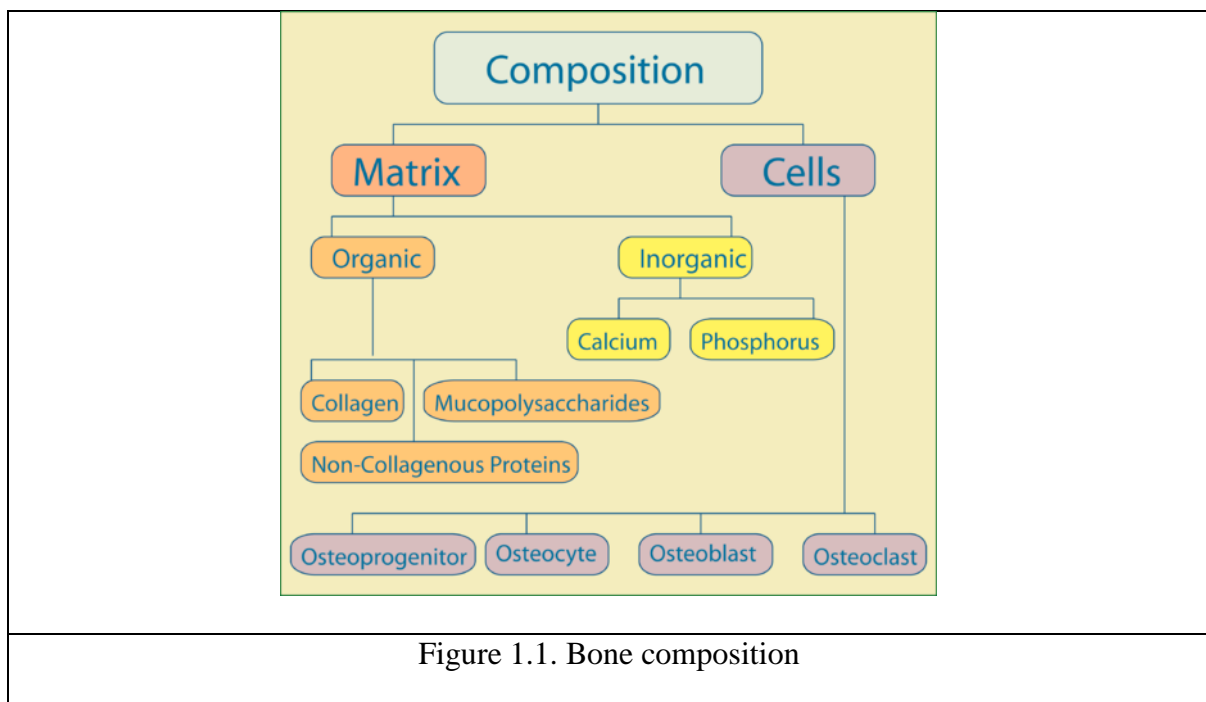


Figure 1.1. Bone composition

The bone framework consists of an organic matrix nd inorganic salts. The organic matrix contains 90 % of collagen protein [2] . Consitituting the major portion of the extracellular matrix,it plays a crucialrole in the structure and functioning of bone tissues [3]. It is  structural protein that forms white fibres of the skin, cartilage, bones, tendon, and all other connective tissues [4,5]. The inorganic portion primarily consists of phosphate and calcium ions. The nucleation of calcium and phosphate ions forms a hydroxyapatite layer and its association with collagen is responsible for the typical stiffness and strength of bone tissue. Other factors accountable fpr maintaining bones include parathyroid hormone (PTH), estrogens, and Vitamin D [3]. Vitamin D3 (cholecalciferol) and vitamin D2 (ergocalciferol) are the two main physiological forms of vitamin D. Physical activity also appears to be crucial for bone mass. A healthy nutitional diet combined with exercise is always advisable to maintain overall bone health [6].

**Table 1.1 List of essential nutrients for good bone health**

| Essential nutrients for bone health | Biological response (in-vivo & in-vitro) | Reference |
|---|---|---|
| **Collagen** | Stimulate osteoinduction | Hum, J. and Boccaccini, A.R., 2018. Collagen as coating material for 45S5 bioactive glass-based scaffolds for bone tissue engineering. International journal of molecular sciences, 19(6), p.1807. |

| Soy Protein | Protect against bone loss and beneficial against osteoporosis | Bawa, S.E., 2010. The significance of soy protein and soy bioactive compounds in the prophylaxis and treatment of osteoporosis. Journal of osteoporosis, 2010. |
|---|---|---|
| **Vitamin D** | Essential for calcium absorption and bone mineralization | Amrein, Karin, et al. "Vitamin D deficiency 2.0: an update on the current status worldwide." European journal of clinical nutrition 74.11 (2020): 1498-1513. |
| **Vitamin K** | Prevent vascular calcification and promote bone metabolism | Wasilewski, Grzegorz B., Marc G. Vervloet, and Leon J. Schurgers. "The bone—vasculature axis: calcium supplementation and the role of vitamin K." Frontiers in cardiovascular medicine (2019): 6. |
| **Vitamin C** | Collagen synthesis | DePhillipo, Nicholas N., et al. "Efficacy of vitamin C supplementation on collagen synthesis and oxidative stress after musculoskeletal injuries: a systematic review." Orthopaedic journal of sports medicine 6.10 (2018): 2325967118804544. |

| | | |
|---|---|---|
| **Silicon (Si)** | Essential for metabolic processes, formation and calcification of bone tissue, Dietary intake of Si increases bone mineral density. | Costa-Rodrigues, J., S. Reis, A. Castro, and M. H. Fernandes. "Bone anabolic effects of soluble Si: in vitro studies with human mesenchymal stem cells and CD14+ osteoclast precursors." Stem cells international 2016 (2016). Jugdaohsingh, Ravin, Katherine L. Tucker, Ning Qiao, L. Adrienne Cupples, Douglas P. Kiel, and Jonathan J. Powell. "Dietary silicon intake is positively associated with bone mineral density in men and premenopausal women of the Framingham Offspring cohort." Journal of Bone and Mineral Research 19, no. 2 (2004): 297-307. |
| **Calcium (Ca)** | Favors osteoblast proliferation, Extracellular matrix mineralization (ECM) | Rizzoli, René, Emmanuel Biver, and Tara C. Brennan-Speranza. "Nutritional intake and bone health." The lancet Diabetes & endocrinology 9, no. 9 (2021): 606-621. Maeno, Shinichi, Yasuo Niki, Hideo Matsumoto, Hideo Morioka, Taku Yatabe, Atsushi Funayama, Yoshiaki Toyama, Tetsushi Taguchi, and Junzo Tanaka. "The effect of calcium ion concentration on osteoblast viability, proliferation and |

| | | differentiation in monolayer and 3D culture." Biomaterials 26, no. 23 (2005): 4847-4855. |
|---|---|---|
| **Phosphorous (P)** | Stimulates expression of MGP (matrix gla protein) a key regulator in bone formation | Peacock, Munro. "Phosphate metabolism in health and disease." Calcified tissue international 108 (2021): 3-15. |

With the escalation of technology-related mental work, there is poor participation in physical activity leading to a sedentary lifestyle [7]. Physical inactivity reduces bone mineral density [8]. There is an increasing identification that inadequate exercise, poor vitain D, and low calcium intake are common in current society [9]. The consequence is that urban youngersters are getting affected by bone-related health issues including weakening of bones, bone fragility, etc. Nearly 70 % of children in the USA are deficient in vitamin D and calcium [10]. There is an increasing number of young adults complaining about osteoarthritis (OA) problems [11]. OA is the most common form of arthritis among people [12]. An unbalanced diet and wearing of cartilage surrounding the bone leads to OA. It can happen in any joint but the majority occur in the hip, spine, hand, and knee joints [13]. Apart from this, OP is another common problem that is more prevalent in females over the age of 50 due to postmenopausal changes in the body [14]. The main cause for OP is a decrease in estrogen levels during menopause which causes bone mass reduction and collagen protein depletion in the body with aging [15]. This eventually grounds the fragility of bones and ultimately the breaking of bones [16,17].

The aforementioned bone disorders are listed below along with the present treatments [15-17]:

1.  Osteoporosis (OP)

It is a bone disorder that results in a decrease in bone mass & mineral density. Overall bone structure and quality is also impacted. Osteoporosis can decrease bone strength and increase the risk of bone fracturing. The most commonly affected bones are the ribs, hips, and the bones of wrist and spine. The prevalence of Osteoporosis increases with age (especially after the age of 65 years) and hormonal changes in women during menopause. A study states that in Germany, the 12-month prevalence of Osteoporosis in adults aged 65 years and older is 24.0% in women and 5.6% in men. As the population ages due to demographic change, the prevention of osteoporosis and osteoporosis fractures is becoming more and more relevant.

Treatment involved:

*   <u>Bisphosphonates</u>

For both men and women at increased risk of broken bones, the most widely prescribed osteoporosis medications are bisphosphonates such as Alendronate (Binosto, Fosamax), Risedronate (Actonel, Atelvia), Ibandronate, Zoledronic acid (Reclast, Zometa).

The side effects of Bisphosphonates include nausea, abdominal pain and heartburn-like symptoms. Although these are less likely to occur if the medicine is taken properly.

*   <u>Denosumab</u>

Compared with bisphosphonates, denosumab (Prolia, Xgeva) produces similar or better bone density results and reduces the chance of all types of breaks. It is delivered via a shot under the skin every six months. Recent research indicates there could be a high risk of spinal column fractures after stopping the drug, therefore you might need to continue to take it indefinitely.

- <u>Hormone-related therapy</u>

Estrogen, especially when started soon after menopause, can help in maintaining bone density. However, estrogen therapy can increase the risk of breast cancer and blood clots, which can cause strokes. Therefore, estrogen is typically used for bone health in younger women or in women whose menopausal symptoms also require treatment. Osteoporosis medications have been better studied in men to treat it and thus are recommended alone or in addition to testosterone replacement therapy.

- <u>Bone-building medicines</u>

Teriparatide (Bonsity, Forteo), Abaloparatide (Tymlos), Romosozumab (Evenity). After stopping to take of these, you will need to take another osteoporosis drug to maintain the new bone growth.

2. Osteopenia

Osteopenia is a clinical term used to describe a decrease in Bone Mineral Density (BMD) below a normal level, though not to an extent to be referred as osteoporosis. Although it is similar to osteoporosis, the key difference is that osteopenia has NO symptoms. Some people can experience bone pain or weakness in rare cases.

The natural bone loss that occurs gradually during adulthood is considered to be the cause of primary forms of osteopenia and osteoporosis. Lifestyle factors such as alcohol use disorder, smoking, sedentary lifestyle, thin body habitus (BMI under 18.5 kg/m2) serves to accelerate the process in the form of secondary causes along with certain medications and disease states.

A study reflects that currently, 34 million Americans are afflicted with osteopenia. Overall, females have a four-fold higher overall prevalence of osteopenia as compared to males. In the United States, 54% of postmenopausal women are osteopenic, and an additional 30% are

already considered osteoporotic. By age 80, this relative trend predictably shifts in favour of osteoporosis as 27% of women are osteopenic, and 70% are osteoporotic. According to a survey, Asia has reported the lowest average t-scores by region worldwide.

Treatment involved:

- <u>Physical activity and exercise</u>

 Physical activities that make body work against gravity like walking, yoga, Pilates and tai chi can improve strength and balance without putting too much stress on your bones.

- <u>Vitamin and mineral supplements</u>
- <u>Following an eating plan that's healthy</u>

Eating enough and getting the right kinds of vitamins and minerals can strengthen the bones and improve the overall health.

3. Osteoarthritis

Osteoarthritis is the most common type of arthritis. It is a degenerative joint disease, in which the tissues in the joint break down over time. Most common in older people, osteoarthritis affects each person differently. For some, it is relatively mild and does not hamper day-to-day activities while for others, it can cause significant pain and disability.

Women are more prone to having osteoarthritis than men, especially after age of 50 years. For many women, it develops after menopause. Usually, joint injuries, abnormal joint structure and genetic defect in joint cartilage can result in developing osteoarthritis in younger people. Osteoarthritis happens when the cartilage and other tissues within the joint break down or have a change in their structure.

Treatment involved:

- <u>Medications</u>

Acetaminophen, Nonsteroidal anti-inflammatory drugs (NSAIDs), Duloxetine (Cymbalta)

- <u>Therapy</u>

Physical & Occupational Therapy, Transcutaneous electrical nerve stimulation (TENS)

- <u>Surgical and other procedure</u>

Cortisone injections, Lubrication injections, Realigning bones, Joint replacement, Knee osteotomy, Artificial hip.

4. Osteogenesis Imperfecta

Osteogenesis Imperfecta (OI) is a disorder in which the bones fracture (break) easily. Also referred as brittle bone disease OI results from a change or mutation in the genes that carry information for making a protein known as type I collagen. This protein is necessary for making the bones stronger. Since, Type I collagen is also in other connective tissues like tendon, ligament, lung, and skin, these tissues can also be affected sometimes. The symptoms can range from mild with only a few fractures to severe with many medical complications.

Treatment involved:

OI treatments are designed to prevent or control symptoms and vary from person to person.

- <u>Fracture care</u>
- <u>Physical therapy</u>

Preferably, combination of muscle strengthening with aerobic conditioning exercises/work out

- <u>Bracing</u>

Braces can allow people to get around and function more easily.

- <u>Surgical procedures</u>

- <u>Medication</u>

Bisphosphonates are drugs used to treat osteoporosis. These drugs do not build new bone, but they slow the loss of existing bone. They have been shown to reduce vertebral compressions and some long bone fractures.

5. Osteomalacia

Osteomalacia, often referred to as "soft bone disease" is a metabolic bone disorder specified by the inadequate mineralization of bone tissue. Mineralization refers to the process where minerals coat the inner layer of the bone, forming a hard outer shell. The incomplete formation of this shell leaves the collagen soft and vulnerable.

The main reason behind this condition is deficiency in Vitamin D, calcium or phosphate, weakening and softening bones. While osteoporosis is a more widely recognized bone disorder, osteomalacia represents a distinct but equally significant concern within the realm of bone health. Osteomalacia can cause a range of exhausting symptoms and complications, including bone pain, muscle weakness, and an increased risk of fractures.

Vitamin D deficiency is the most common nutritional deficiency among children and adults. The present lifestyle of the people also contributes for the same. In children, inadequate concentrations of vitamin D may even cause rickets. Osteomalacia describes a disorder of "bone softening" in adults, a condition where the bone does not harden the way it should after forming, is usually due to prolonged deficiency of vitamin D. Result of this deficiency is abnormal osteoid mineralization. Contrarily, rickets results from deficient mineralization at the cartilage of growth plates in children.

Common symptoms of Osteomalacia include pain in the bones and hips, bone fractures, and muscle weakness along with difficulty in walking for the patients.

Treatment involved:

Depending on the individual case, patients who have osteomalacia can take vitamin D, calcium or phosphate supplements.

With the increase in the number of bone health issues among individuals, various health treatments have evolved in recent times. As mentioned earlier, these treatments include surgery (bone grafts, knee transplant) [18], bisphosphonate injections, collagen fillers [19], and numerous oral bone health supplements. Modern bone grafts, bone substitutes attempt to facilitate and enhance healing process. Various bone grafts have been employed such as autologous bone grafts where the osseous matter is harvested from one anatomic site and transplanted to another site in the same patient. This type of bone grafting confers MHC (Major histocompatibility Complex) compatibility while processing healing. The limitations lie in the harvesting process of autografts such as increased blood loss, increased operative time, etc. Allopathic bone grafts are the other version of bone grafts that is harvested from the human cadavers and transplanted to the recipient. It has high success rate with less surgical time. But high cost and susceptible to viral infections are among its drawbacks. Another treatment that has been widely used for bone disorders include bisphosphonate. They help in inhibiting bone resorption and prevent bone fractures. But studies have shown that oral bisphosphonates have been associated with several gastrointestinal side effects such as oesophageal ulcers, upper gastrointestinal hemorrhage [20]. Collagen supplements and collagen fillers are generally used in dermal applications but pose some side effects like hypersensitive reactions type IV in human body. [21] Figure 1.2 below depicts the possible treatments for bone diseases and the side effects of health supplements.
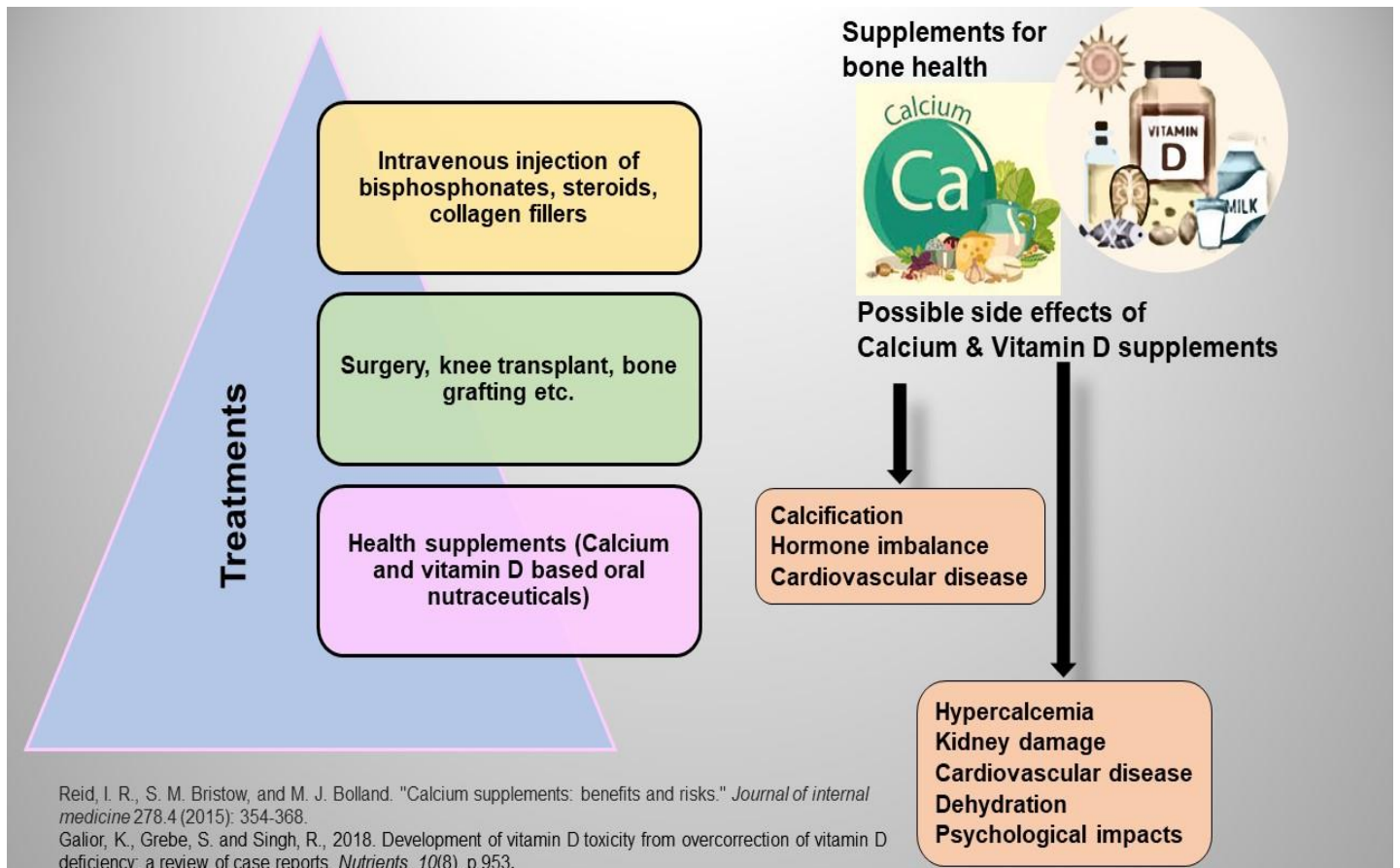
Figure 1.2 Treatments for bone diseases and the side effects of health supplements.

Among all these regimens, oral health supplements for bone are preferred as oral delivery is the most amicable route for patients. Oral delivery is considered to be the most widely used, cost-effective, non-invasive, and placable strategy for patients to treat any disease. The compliance of patients towards is generally higher that other routes such as intravenous, subcutaneous, and intramuscular injections which can be painful to the patients. Also, these injections may cause infections if not handled with care. But, the major concern that remains with the oral administration of drugs is their bioavailability. The drug following the oral route may show poor absorption due to insufficient stability in a harsh gastric environment and also due to poor solubility [22]. Thus, new pharmaceutical approaches such as multifunctional sustainable nanoparticle (NP) formulations can be adopted to make the drug available after oral

administration. In this respect, there has been growing interest in multifunctional NPs that can be explored as drug carriers enclosing active pharmaceutical ingredients (API) for biomedical and diagnostic applications. Notable, mesoporous NPs (pore size 2 to 50 nm) with tailorable properties have been of great interest to be used as lucrative biomaterials for targeted drug delivery applications [23]. Variations of such nanomaterials such as silicas, metal, metal oxides, bioactive glass (BG), polymers, lipids, etc. have been explored for biomedical and drug delivery applications.

Through the onset of biomaterials, the biomedical sector has been revolutionized. These materials can be engineered to support, augment, replace, or restore damaged tissues or a biological function. Metals, ceramics, pol ceramics, polymers, and glass can be used in creating biomaterial. Biomaterials are used for a wide range of applications in treating bone ailments like medical implants, as scaffolds for hard and soft tissue engineering. An ideal biomaterial should be non-toxic, biocompatible, biodegradable, and bioactive. With the advent of third-generation biomaterials, bioactive glass (BG) has substantial properties, making it a central choice for use in bone tissue engineering applications. BG being osteoconductive, osteoinductive, and osteostimulative [24], has received great attention for treating bone defects. Studies have shown that dissolution of BG enhances osteoblast activity and bone mineralization [25]. First introduced in 1969, this FDA (Food and Drug Administration) approved [26,27] has been commercially used in different healthcare sectors like orthopedics and dental with a trading name of Perioglas, Novabone, Novamin, etc.[28]. It has been used in soft tissue engineering as saffolds, bone grafts, and coating over metallic implants [29,30]. It has the potential to anchorage new bone tissue growth and bone mineralization by forming hydroxyapatite (HA) like material in in-vitro and in-vivo conditions showing promising bioactivity [31,32]. BG has been used as scaffolds for tissue engineering [30], has been

employed as dental implants, and as a particulate substitute in toothpaste for hypersensitivity [24,33]. Figure 1.3. below depicts the biomedical applications of BG.
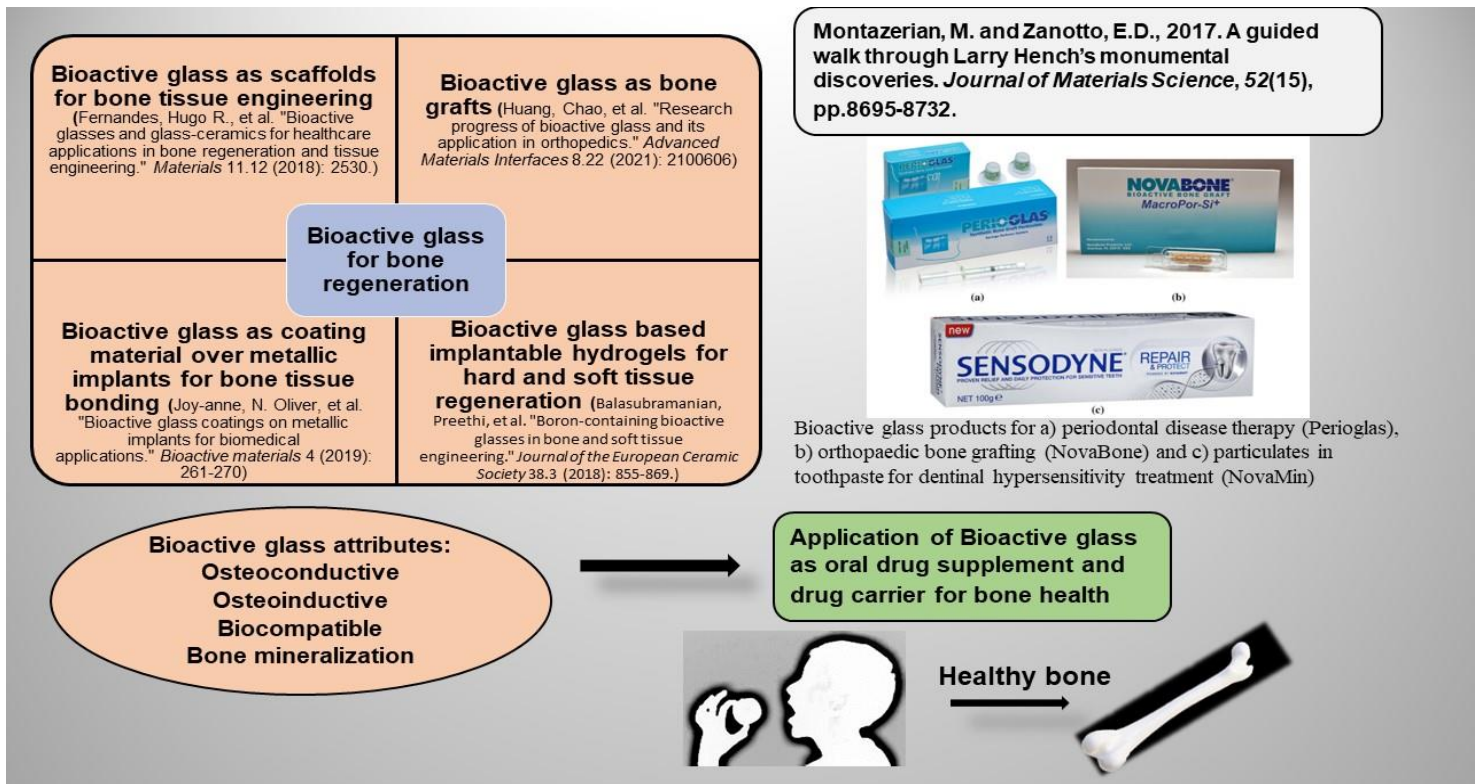


Figure 1.3  Biomedical applications of BG

Importance of oral medicine and its implications:

Oral delivery of drugs and health supplements plays a pivotal role in treating health ailments. It is considered to be the most amicable and placable way to treat patients. Oral drug delivery is the most convenient, high patient compliance, cost effective, and safe route of administration to treat various diseases. But oral availability becomes a concern. Though oral delivery is considered to be the most amicable way to consume drugs and other health supplements, due to the harsh GI tract environment, there is much loss of drug in the upper GI tract before systemic absorption causing the bioavailability of drugs often questionable through oral route. This leads to a larger amount of drug dosage formulations that may impose side effects like

calcification due to Ca deposition , nausea & polyuria due to higher dosages of Vit D [34,35]. Therefore, to ensure adequate bioavailability and optimum dosage of essential nutrients and vitamins, these need to be protected in the digestive tract. For this purpose, there comes the role of biopolymers in drug delivery system for the efficient delivery of drugs to the targeted site.

Biopolymers in oral delivery: Biopolymers have revolutionized medical and pharmaceutical field. They are considered to be the important class of materials due to their specific characteristics such as biodegradability, biocompatibility, non-toxicity, non-immunogenicity and extensive blood circulation time. They also pose an advantage of high drug loading ration for both macro and micro- sized drug molecules. Biopolymers successfully act as efficient drug delivery system by ensuring the availability of drug to the specific site. Various polysaachrides and protein have been explored as biopolymers and are FDA approved. Chitosan, dextran, alginate, collagen, silk fibroin, etc. are few examples. Figure 1.4 depicts the types of biopolymers used in oral drug delivery system.
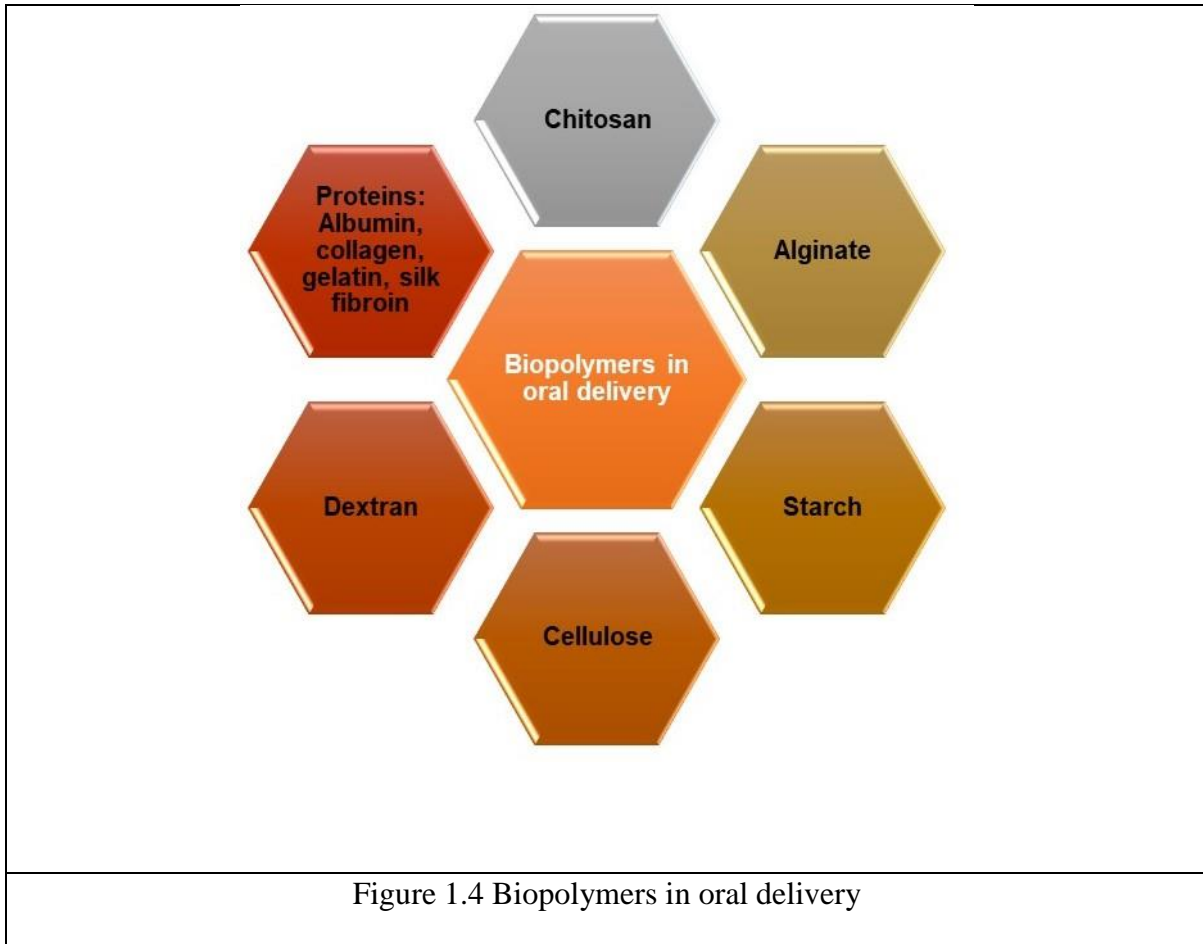
Figure 1.4 Biopolymers in oral delivery

Reviewing all its applications in bone regeneration, the present thesis work focuses on the oral delivery of BG for bone health applications. The basic composition of 45S5 BG includes 45 wt % $SiO_2$, 24.5 wt % $CaO$, 24.5 wt % $Na_2O$ and 6 wt % $P_2O_5$ [28]. Micronutrients like Si, Ca, and P play a pivotal role in bone mineral density.Various researchers have shown the potential application of $SiO_2$ nanoparticles in oral delivery of macromolecules[36]. BG has also been explored as an oral delivery vehicle for gastrointestinal regeneration [37]. All these findings have led us to explore the application of oral delivery of BG as a bone health supplement.

For this purpose, several formulations of BG were prepared in combination with collagen, soy protein, and fortification of essential vitamins for bone health. Soy foods contain varying levels of various types of isoflavones known to be osteogenic compounds that help prevent bone loss especially in postmenopausal condition. Soy protein has been reported to have positive effect

both on bone metabolism and cardiovascular health [38]. Soy consumption hs also shown improvement in the bone markers that stimulates the osteoblast activity and shows a positive impact on bone mineral density and bone microstructure [39]. These studies led to the usage of soy protein as base food material mineralized with BG and vitamin K for bone health applications. Vitamin K mediates the carboxylation of glutamyl residues on bone protein i.e. osteocalcin and maintain bone health. It has been studied that low serum concentration of vit K is associated with low bone mineral density and increased of fracture thus depicting vit K as an essense for good bone health. Collagen has also been explored in the present study to fabricate oral edible film fortified with BG. Collagen is the most abundant fibre like protein on our body [2]. It the main constituent of bone mass and is found throughout the body [3]. Collagen peptides significantly inreases the organic substance of the bone. Collagen may help people with osteoporosis. Various studies have demonstrated that collagen peptides increase bone mineral density and enhance bone markers thus indicating a reduction in bone loss and elevation in bone formation [40]. Collagen peptides have also shown positive effect on cartilage, tendons due to the production of elastin [41]. Herein, we have explored the application of BG in drug delivery and as functional food by carrying out *in-situ* mineralization of bioactive glass in food-grade polymer for targeted protein delivery and fabrication of bioactive glass-fortified functional food for bone health respectively. The materials thus formed are tested for cytocompatibility and found to be biocompatible. Finally, to protect against micro-organisms and pathogens and to prevent photo-oxidation, the active packaging material is fabricated that can be used for the packaging of the drug and food. It is for the first time BG has been introduced as a radiopharmaceutical by radiolabelling it with $^{99m}$Tc (Technetium-99m). $^{99m}$Tc is widely used radiopharmaceutial in medical sector for dynamic imaging and diagnostic purposes of organs and tissues. Its applications are oriented to study renal, hepatic, helatobiliary, bone, cardiac, and oncological diseases. Once entered into the human body, $^{99m}$Tc

concentrates in the thyroid gland and the gastrointestinal tract and its excretion is rapid mostly in the urine and in the form of feces. The short six hour half-life and its rapid elimination from the body limit its toxic effects and make it a valuable agent in imaging and diagnosics, all while curbing the radiation exposure to the patient [42,43]  Subsequently, the radiolabeling of BG and its binding stability in different gastrointestinal pH conducted in the present study. This can further be explored in future in an animal model where the whole ADME process (Absorption, Distribution, Metabolism, and Excretion) can be studied when these particles are ingested orally.

**1.2 Major Objectives of the Thesis:**

- ✓ To synthesize radiolabelled Nano-sized bioactive glass particles for bone regeneration.

- ✓ Application of bioactive glass in drug delivery and as a functional food.

- ➤ In-situ mineralization of bioactive glass in food-grade polymer for targeted protein delivery.

- ➤ Fabrication of bioactive glass-fortified functional food for bone health.

- ✓ To evaluate cytocompatibility and cellular uptake of bioactive glass for intestinal and bone cells.

- ✓ To fabricate active polymeric film for drug/ food packaging applications

**1.3 Outline of the thesis:**

The chapters included in the thesis are as follows:

**Chapter II** discusses the synthesis of BG nanoparticles using vitamin C as a template followed by its radiolabelling with $^{99m}$Tc and explored BG as a potent radiopharmaceutical.

**Chapter III** involves the fabrication of dextran sandwiched film for the targeted delivery of collagen-BG complex along with vitamin D at the targeted site. Structural and functional characterization was carried out for the formed film.

**Chapter IV** discusses the formulation of BG in functional food applications. Soy-based functional food was fabricated and fortified with BG network and vitamin K for bone health applications. A detailed structural analysis of the edible film was carried out. The nutritional analysis was also conducted to showcase its potential as food for bone health.

**Chapter V** elaborates on the fabrication of the UV shielding antimicrobial edible active packaging material to be used for drug and food packaging materials.

**References:**

[1]     N. Wright, A. Looker, K. Saag, J. Curtis, E. Delzel, S. Randall, M. Dawson-Hughes, The recent prevalence of osteoporosis and low bone mass in the United States, J. Bone Miner. Res. 29 (2014) 2520–2526. https://doi.org/10.1002/jbmr.2269.The.

[2]     X. Feng, Chemical and Biochemical Basis of Cell-Bone Matrix Interaction in Health and Disease, Curr. Chem. Biol. 3 (2012) 189–196. https://doi.org/10.2174/2212796810903020189.

[3]     R. Florencio-Silva, G.R.D.S. Sasso, E. Sasso-Cerri, M.J. Simões, P.S. Cerri, Biology of Bone Tissue: Structure, Function, and Factors That Influence Bone Cells, Biomed Res. Int. 2015 (2015). https://doi.org/10.1155/2015/421746.

[4]     S.N. Deshmukh, A.M. Dive, R. Moharil, P. Munde, Enigmatic insight into collagen, J. Oral Maxillofac. Pathol. 20 (2016) 276–283. https://doi.org/10.4103/0973-029X.185932.

[5]     M. Yazaki, Y. Ito, M. Yamada, S. Goulas, S. Teramoto, M. aki Nakaya, S. Ohno, K. Yamaguchi, Oral Ingestion of Collagen Hydrolysate Leads to the Transportation of Highly Concentrated Gly-Pro-Hyp and Its Hydrolyzed Form of Pro-Hyp into the Bloodstream and Skin, J. Agric. Food Chem. 65 (2017) 2315–2322. https://doi.org/10.1021/acs.jafc.6b05679.

[6]     R.M. Bielemann, J. Martinez-Mesa, D.P. Gigante, Physical activity during life course and bone mass: A systematic review of methods and findings from cohort studies with young adults, BMC Musculoskelet. Disord. 14 (2013). https://doi.org/10.1186/1471-2474-14-77.

[7]     S.F. Chastin, O. Mandrichenko, D.A. Skelton, The frequency of osteogenic activities and the pattern of intermittence between periods of physical activity and sedentary

behaviour affects bone mineral content: The cross-sectional NHANES study, BMC Public Health. 14 (2014). https://doi.org/10.1186/1471-2458-14-4.

[8]     J.H. Park, J.H. Moon, H.J. Kim, M.H. Kong, Y.H. Oh, Sedentary Lifestyle: Overview of Updated Evidence of Potential Health Risks, Korean J. Fam. Med. 41 (2020) 365–373. https://doi.org/10.4082/KJFM.20.0165.

[9]     A.G.A.G. M, The effect of exercise and nutrition on the mechanostat, J. Musculoskelet. Neuronal Interact. 5 (2005) 239–254. https://doi.org/10.4103/jmsr.jmsr.

[10]    C.T. Price, J.R. Langford, F.A. Liporace, Essential Nutrients for Bone Health and a Review of their Availability in the Average North American Diet, Open Orthop. J. 6 (2012) 143–149. https://doi.org/10.2174/1874325001206010143.

[11]    J.B. Driban, M.S. Harkey, S.-H. Liu, M. Salzler, T.E. McAlindon, Osteoarthritis and Aging: Young Adults with Osteoarthritis, Curr. Epidemiol. Reports. 7 (2020) 9–15. https://doi.org/10.1007/s40471-020-00224-7.

[12]    A. Mobasheri, A. Mahmoudian, U. Kalvaityte, I. Uzieliene, C.E. Larder, M.M. Iskandar, S. Kubow, P.C. Hamdan, C.S. de Almeida, L.J. Favazzo, L.J.C. van Loon, P.J. Emans, P.G. Plapler, M.J. Zuscik, A White Paper on Collagen Hydrolyzates and Ultrahydrolyzates: Potential Supplements to Support Joint Health in Osteoarthritis?, Curr. Rheumatol. Rep. 23 (2021). https://doi.org/10.1007/s11926-021-01042-6.

[13]    D.R. Coates, J.M. Chin, S.T.L. Chung, 基因的改变NIH Public Access, Bone. 23 (2011) 1–7. https://doi.org/10.1002/art.34453.Osteoarthritis.

[14]    T. Sozen, L. Ozisik, N. Calik Basaran, An overview and management of osteoporosis, Eur. J. Rheumatol. 4 (2017) 46–56. https://doi.org/10.5152/eurjrheum.2016.048.

[15]  D.M. Reilly, J. Lozano, Skin collagen through the lifestages: importance for skin health and beauty, Plast. Aesthetic Res. 2021 (2021). https://doi.org/10.20517/2347-9264.2020.153.

[16]  F. Pouresmaeili, B. Kamalidehghan, M. Kamarehei, Y.M. Goh, A comprehensive overview on osteoporosis and its risk factors, Ther. Clin. Risk Manag. 14 (2018) 2029–2049. https://doi.org/10.2147/TCRM.S138000.

[17]  S. Stevenson, J. Thornton, Effect of estrogens on skin aging and the potential role of SERMs., Clin. Interv. Aging. 2 (2007) 283–297. https://doi.org/10.2147/cia.s798.

[18]  T.T. Roberts, A.J. Rosenbaum, Bone grafts, bone substitutes and orthobiologics the bridge between basic science and clinical advancements in fracture healing, Organogenesis. 8 (2012) 114–124. https://doi.org/10.4161/org.23306.

[19]  J.A. Sunyecz, Zoledronic acid infusion for prevention and treatment of osteoporosis, Int. J. Womens. Health. 2 (2010) 353–360. https://doi.org/10.2147/IJWH.S7322.

[20]  C. Reyes, M. Hitz, D. Prieto-Alhambra, B. Abrahamsen, Risks and Benefits of Bisphosphonate Therapies, J. Cell. Biochem. 117 (2016) 20–28. https://doi.org/10.1002/jcb.25266.

[21]  P. Lucey, D.J. Goldberg, Complications of collagen fillers, Facial Plast. Surg. 30 (2014) 615–622. https://doi.org/10.1055/s-0034-1396904.

[22]  J. Lou, H. Duan, Q. Qin, Z. Teng, F. Gan, X. Zhou, X. Zhou, Advances in Oral Drug Delivery Systems: Challenges and Opportunities, Pharmaceutics. 15 (2023). https://doi.org/10.3390/pharmaceutics15020484.

[23]  N. Sreeharsha, M. Philip, S.S. Krishna, V. Viswanad, R.K. Sahu, P.N. Shiroorkar, A.H. Aasif, S. Fattepur, S.M.B. Asdaq, A.B. Nair, M. Attimarad, K.N. Venugopala,

Multifunctional Mesoporous Silica Nanoparticles for Oral Drug Delivery, Coatings. 12 (2022). https://doi.org/10.3390/coatings12030358.

[24]    M. Montazerian, E.D. Zanotto, A guided walk through Larry Hench's monumental discoveries, J. Mater. Sci. 52 (2017) 8695–8732. https://doi.org/10.1007/s10853-017-0804-4.

[25]    S. Kargozar, F. Baino, S. Hamzehlou, R.G. Hill, M. Mozafari, Bioactive Glasses: Sprouting Angiogenesis in Tissue Engineering, Trends Biotechnol. 36 (2018) 430–444. https://doi.org/10.1016/j.tibtech.2017.12.003.

[26]    S. Kargozar, F. Kermani, S.M. Beidokhti, S. Hamzehlou, E. Verné, S. Ferraris, F. Baino, Functionalization and surface modifications of bioactive glasses (BGs): Tailoring of the biological response working on the outermost surface layer, Materials (Basel). 12 (2019). https://doi.org/10.3390/ma12223696.

[27]    F. Baino, S. Hamzehlou, S. Kargozar, Bioactive glasses: Where are we and where are we going?, J. Funct. Biomater. 9 (2018). https://doi.org/10.3390/jfb9010025.

[28]    L.L. Hench, J.R. Jones, Bioactive glasses: Frontiers and Challenges, Front. Bioeng. Biotechnol. 3 (2015) 1–12. https://doi.org/10.3389/fbioe.2015.00194.

[29]    G.M. Calori, E. Mazza, M. Colombo, C. Ripamonti, The use of bone-graft substitutes in large bone defects: Any specific needs?, Injury. 42 (2011) S56–S63. https://doi.org/10.1016/j.injury.2011.06.011.

[30]    H.R. Fernandes, A. Gaddam, A. Rebelo, D. Brazete, G.E. Stan, J.M.F. Ferreira, Bioactive glasses and glass-ceramics for healthcare applications in bone regeneration and tissue engineering, Materials (Basel). 11 (2018) 1–54. https://doi.org/10.3390/ma11122530.

[31]   T. Kokubo, H. Takadama, How useful is SBF in predicting in vivo bone bioactivity?, Biomaterials. 27 (2006) 2907–2915.

https://doi.org/10.1016/j.biomaterials.2006.01.017.

[32]   A.L.B. Maçon, T.B. Kim, E.M. Valliant, K. Goetschius, R.K. Brow, D.E. Day, A. Hoppe, A.R. Boccaccini, I.Y. Kim, C. Ohtsuki, T. Kokubo, A. Osaka, M. Vallet-Regí, D. Arcos, L. Fraile, A.J. Salinas, A. V. Teixeira, Y. Vueva, R.M. Almeida, M. Miola, C. Vitale-Brovarone, E. Verné, W. Höland, J.R. Jones, A unified in vitro evaluation for apatite-forming ability of bioactive glasses and their variants, J. Mater. Sci. Mater. Med. 26 (2015) 1–10. https://doi.org/10.1007/s10856-015-5403-9.

[33]   N. Esfahanizadeh, M. Montazeri, M. Nourani, M. Harandi, Use of bioactive glass doped with magnesium or strontium for bone regeneration: A rabbit critical-size calvarial defects study, Dent. Res. J. (Isfahan). 19 (2022) 18.

https://doi.org/10.4103/1735-3327.338781.

[34]   G.B. Wasilewski, M.G. Vervloet, L.J. Schurgers, The Bone—Vasculature Axis: Calcium Supplementation and the Role of Vitamin K, Front. Cardiovasc. Med. 6 (2019) 1–16. https://doi.org/10.3389/fcvm.2019.00006.

[35]   K. Galior, S. Grebe, R. Singh, Development of vitamin d toxicity from overcorrection of vitamin D deficiency: A review of case reports, Nutrients. 10 (2018).

https://doi.org/10.3390/nu10080953.

[36]   M.M. Abeer, P. Rewatkar, Z. Qu, M. Talekar, F. Kleitz, R. Schmid, M. Lindén, T. Kumeria, A. Popat, Silica nanoparticles: A promising platform for enhanced oral delivery of macromolecules, J. Control. Release. 326 (2020) 544–555.

https://doi.org/10.1016/j.jconrel.2020.07.021.

[37]   V. Miguez-Pacheco, L.L. Hench, A.R. Boccaccini, Bioactive glasses beyond bone and

teeth: Emerging applications in contact with soft tissues, Acta Biomater. 13 (2015) 1–15. https://doi.org/10.1016/j.actbio.2014.11.004.

[38]   K.S. George, J. Muñoz, N.S. Akhavan, E.M. Foley, S.C. Siebert, G. Tenenbaum, D.A. Khalil, S.C. Chai, B.H. Arjmandi, Is soy protein effective in reducing cholesterol and improving bone health?, Food Funct. 11 (2020) 544–551. https://doi.org/10.1039/c9fo01081e.

[39]   A.J. Lanou, Soy foods: Are they useful for optimal bone health?, Ther. Adv. Musculoskelet. Dis. 3 (2011) 293–300. https://doi.org/10.1177/1759720X11417749.

[40]   H. Song, S. Zhang, L. Zhang, B. Li, Effect of orally administered collagen peptides from bovine bone on skin aging in chronologically aged mice, Nutrients. 9 (2017). https://doi.org/10.3390/nu9111209.

[41]   H. Wang, A review of the effects of collagen treatment in clinical studies, Polymers (Basel). 13 (2021). https://doi.org/10.3390/polym13223868.

[42]   T. Banerjee, A.K. Singh, R.K. Sharma, A.N. Maitra, Labeling efficiency and biodistribution of Technetium-99m labeled nanoparticles: Interference by colloidal tin oxide particles, Int. J. Pharm. 289 (2005) 189–195. https://doi.org/10.1016/j.ijpharm.2004.09.022.

[43]   B. Lasa-Saracíbar, S.H. El Moukhtari, T. Tsotakos, S. Xanthopoulos, G. Loudos, P. Bouziotis, M.J. Blanco-Prieto, In vivo biodistribution of edelfosine-loaded lipid nanoparticles radiolabeled with Technetium-99 m: Comparison of administration routes in mice, Eur. J. Pharm. Biopharm. 175 (2022) 1–6. https://doi.org/10.1016/j.ejpb.2022.04.007.

# Chapter 2

# Synthesis and functionalization of bioactive glass as a potent radiopharmaceutical for bone regeneration



| pH | Labelling efficiency |
|-----|---------------------|
| 1.2 | 95.01 % |
| 6.8 | 95.74 % |
| 7.0 | 94.44 % |
| 7.4 | 91.50 % |
| 8.5 | 96.26 % |
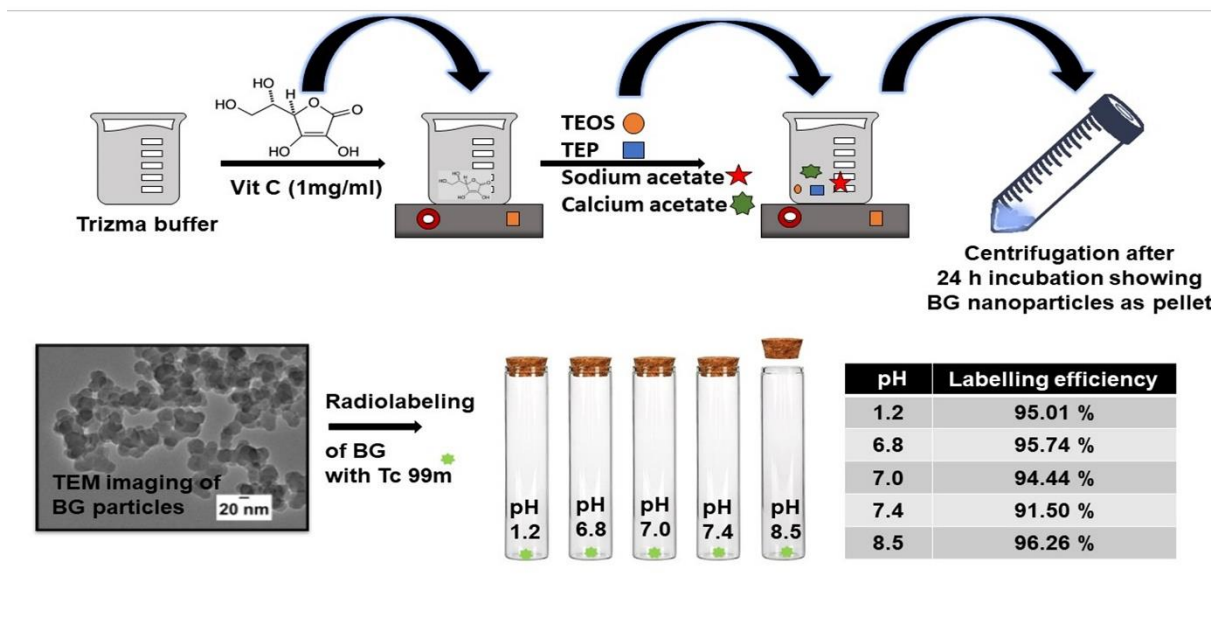
# Chapter 2

# Synthesis and functionalization of bioactive glass as a potent radiopharmaceutical for bone regeneration

## 2.1 Introduction:

Osteoporosis (OP), osteomalacia (often called soft bones), and osteopenia are some of the common bone disorders related to the decrease in the level of bone mineral density and often leading to fracture of bone and dependable lifestyle [1]. Bone fractures have become a global public health issue. The prevalent disorders related to bones are majorly due to the decreased mineralization of bones i.e. reduction in the inorganic matrix of bones [2]. Various organic and inorganic nutrients are required to keep the overall well-being of bones. For instance, collagen protein is the major protein in the extracellular matrix (ECM) and supports osteoconduction [3]. Similarly, various studies have shown a positive impact of soy protein against OP and prevent bone loss [4,5]. Micronutrients like vitamin C, vitamin D, and vitamin K play an essential part in nurturing bones. Vitamin C plays a vital role in collagen synthesis that helps maintains the organic matrix of the bone framework [6]. Likewise, vitamin K prevents vascular calcification and promotes bone metabolism [7]. For efficient calcium (Ca) absorption in our body, vitamin D plays a crucial role [8]. Along with organic nutrients, different inorganic constituents make a bone framework like Ca that favors osteoblast proliferation and ECM mineralization [9]. Phosphorous (P) stimulates the expression of MGP (matrix gla protein) [10], a key regulator in bone formation, and silicon (Si) is required for the formation and calcification of bone tissues [11]. For overall bone health, all these aforementioned nutrients perform an indispensable role. The deficiency of any of these nutrients may harm bone health. There are various treatments available to nurse bone disorders such as knee transplants, bone grafts [12], intravenous injections of bisphosphonates, steroids, collagen fillers, etc. [13], Ca and vitamin

D-based supplements in combination with collagen [14]. Among all these possible treatments, oral delivery of nutraceuticals is widely accepted as it is most placable for patients.

With the advent of third-generation biomaterials, bioactive glass (BG) has widely been used and explored for bone regeneration applications. BG has been used as scaffolds for bone tissue engineering [15] and has also been proposed as a potential biomaterial for bone grafts [16] BG has also been explored as coating material over metallic implants [17] as they are osteoconductive and osteoinductive [18]. Commercially, various BG products like Perioglass for periodontal disease therapy, Novabone for orthopedic bone grafting, and Novamin as particulates of BG in toothpaste for dentinal hypersensitivity treatment are available [19]. These attributes of BG make it a potent biomaterial for bone mineralization applications. To serve the purpose of bone health issues, the present investigation proposes the oral delivery of BG nanoparticles for bone regeneration and a healthy skeletal system. Oral delivery of BG has been studied for gastrointestinal regeneration [20–22]. It is the first time that oral delivery of bioactive glass is proposed to be explored as a bone health supplement for bone regeneration. The basic composition of 45S5 BG is 45 wt % (weight) $SiO_2$, 24.5 wt % CaO, 24.5 wt % $Na_2O$, and 6 wt % $P_2O_5$ and is found to form a bond with a bone showing bioactivity [20,23]. This composition of BG showcases it as a reservoir of micronutrients for bones. Also, the phenomenon of bioactivity plays an essential role in bone mineralization by forming a hydroxyapatite (HA) i.e. calcium phosphate layer. Herein, a well-established method of *in-situ* mineralization of bioactive glass is carried out [24,25] using vitamin C as a template. The choice of vitamin C as a reacting surface for precursors of BG is done as the former plays an important role in the synthesis of collagen. The synthesized nanoparticles are thoroughly characterized for their functional and structural properties including XRD, FTIR, and TEM. The mineralization of BG nanoparticles is confirmed by SEM/EDAX. The nanoparticles are subjected to *in-vitro* biocompatibility studies against Caco-2 (human colorectal

adenocarcinoma cells) and U2OS (human osteosarcoma cells) cell lines. The cellular uptake studies are also conducted against Caco-2 cell lines since the proposed delivery method of nanoparticles is through an oral route. To the best of our knowledge, this is the first time that BG nanoparticles have been radiolabeled with technetium- 99m ($^{99m}$Tc) and is subjected to oral delivery, unlike the conventional method of $^{99m}$Tc incorporation via injection. The labeling efficiency is checked using ITLC (instant thin layer chromatography) at different pH variants of GI tract and physiological pH. This attempt may help in knowing the biodistribution of BG through *in-vivo* imaging.

## 2.2 Experimental section

### 2.2.1 Materials

Precursors for the *in-situ* mineralization of bioactive glass (BG) nanoparticles namely tetraethyl orthosilicate (TEOS), triethyl phosphate (TEP), sodium acetate, and calcium acetate monohydrate along with vitamin C were obtained from Sigma-Aldrich, USA. Hanks's Balanced Salt Solution, HBSS (also known as simulated body fluid, SBF) was also procured from Sigma-Aldrich, USA for the *in-vitro* bioactivity analysis. Cell studies were carried out for Caco-2 cell lines (human colorectal adenocarcinoma) and U2OS cell lines (human osteoblast-like osteosarcoma) obtained from National Centre for Cell Science (NCCS), Pune, India. $^{99m}$Tc-pertechnetate freshly eluted from $^{99}$Mo (Molybdenum-99) by solvent extraction method was acquired from the Regional Centre, Board of Radiation and Isotope Technology (BRIT), Department of Atomic Energy, India. For all experiments, Milli-Q water was used. All the reagents used in the experiments were of analytical reagent (AR) grade of high purity. All the procedures were performed at room temperature of 25 °C unless otherwise stated.

### 2.2.2 Methods

#### 2.2.2.1 Synthesis of vitamin C templated bioactive glass nanoparticles (BGCNPs)

For the *in-situ* mineralization of vitamin C templated BG nanoparticles, vitamin C (1mg/ml) was dissolved in 10mM TRIZMA buffer at pH 8 under constant stirring at 25 °C. After complete dissolution, precursors namely TEOS, TEP, sodium acetate, and calcium acetate monohydrate were gradually added successively as reported by our previous lab work [26] and the particles thus formed were named BGC.

*2.2.3 Characterization techniques*

*2.2.3.1 FTIR*

FTIR spectra were recorded by grounding the sample with potassium bromide (KBr) in the ratio of 1:100 and pelleted. The spectra were recorded by NICOLET 380 FTIR spectrometer in an operating range of 4000 – 400 cm$^{-1}$ with a resolution of 4 cm$^{-1}$.

*2.2.3.2 XRD*

To deduce the amorphous and crystalline nature of the nanoparticles, XRD was performed on Rikagu Miniflex-II. The operating specifications were 20 kV and a current of 10 mA using Cu – Kα radiations with a scanning range 2θ of 10 ° to 70 ° at a scanning rate of 0.2 °/min.

*2.2.3.3 Particle size and distribution*

The particle size and size of distribution were investigated using Transmission Electron Microscopy (TEM), JEOL 100 TEM, operating at 100 kV. Before imaging, BGC nanoparticles were sonicated for 30 min using ethanol as dispersing medium. Consequently, 5 µl of that solution was pipetted over 200 mesh C-coated Cu grid.

*2.2.3.4 Nitrogen sorption analysis*

The porosity of BGC was determined by nitrogen adsorption-desorption analysis at -196 °C using Microtrac BEL (Model BELSORP-max), Japan, and with nitrogen as adsorptive gas (N$_2$, cross-sectional area 0.162 nm$^2$). As per the procedure, BGC nanoparticles were vacuum heated

at 300 °C for 3 h. The surface area was determined using Brunauer-Emmett-Teller (BET) equation. The pore size distribution was determined by the Barrett-Joyner-Halenda (BJH) method applied to the desorption branch of isotherm.

*2.2.3.5 Morphological and elemental evaluation*

The surface morphology of BGC was observed using Scanning Electron Microscopy (SEM, ZEISS EVO MA15). The samples were gold coated and then observed at an accelerating voltage of 5.0 kV at 500 X magnification. The elemental evaluation was done using EDAX (Energy Dispersive X-Ray Analysis) at a running voltage of 20 kV using ZEISS EVO MA15 to investigate the presence of Si, P, Na, and Ca ions in a sample.

*2.2.3.6 In-vitro formation of hydroxyapatite- Bioactivity test*

The bioactive nature of BGC was studied concerning hydroxyapatite forming ability when immersed in simulated body fluid (SBF) as described by Kokubo et. al [27]. The samples were prepared with a BGC/SBF ratio of 3:1 and were placed in an incubator shaker at 37 °C under constant shaking at 120 rpm. The SBF solution was replaced every 3 days and the study was conducted for 30 days. At required time intervals, the solution was centrifuged and particles were rinsed with absolute ethanol, dried, and stored for further analysis using XRD, FTIR, SEM, and ICP-MS (Inductively coupled plasma mass spectrometry).

*2.2.3.7 ICP-MS*

After in-vitro bioactivity assay, the leftover SBF after recovery of BGC via centrifugation, was analyzed by ICP-MS. This helps in highlighting the ionic exchange that took place between the BGC surface and SBF during the bioactivity process. Concentrations of Si, P, and Ca in the remaining SBF were measured for all periods. This estimation was done using Agilent 7900, ICP-MS, USA. As per the standard procedure, BGC nanoparticles were heated at 900 °C for

24 h. The resulting ash was dissolute in aqua-regia followed by dilution using Milli Q. The solution was then filtered and administered into the ICP plasma chamber, followed by desolvation and ionization. The ionized plasma was analyzed using a mass spectrometer.

*2.2.3.8 Biocompatibility and cell viability*

The cytotoxicity of BGC was examined by MTT assay. Since the oral delivery of BGC is proposed in the present investigation, therefore, cellular toxicity against intestinal cell lines (Caco-2 cell line) becomes indispensable. Also, bioactive glass is considered to be osteogenic [28], thus cytocompatibility is monitored against human osteosarcoma cell lines (U2OS cell lines). The study was conducted for 24 h and 48 h for both cell lines. The basic principle behind the MTT assay is that only metabolically functioning cells can transform MTT (3-[4,5-dimethylthiazol-2-yl]-2,5 diphenyl tetrazolium bromide) to purple formazan. The extent of formazan generated can be quantified using TECAN multimode microplate reader at a wavelength of 570 nm and is directly proportional to the number of living cells. The standardized protocol was followed as reported by other researchers to carry out this assay [29,30]. The cell viability was calculated as described elsewhere [30].

*2.2.3.9 Cellular uptake*

The uptake of extracellular material across the plasma membrane of eukaryotic cells is characterized by different routes i.e. from passive to active transport as discussed [31]. Internalization of particles > 1 μm can occur through micropinocytosis and nanoparticles are transported mainly via Caveolae and Clathrin-mediated and independent endocytosis [32]. The cellular uptake efficiency of BGC nanoparticles was evaluated using a flow cytometer (Becton Dickinson LSR II, San Jose, SA, USA) equipped with cell quest software. Initially, BGC nanoparticles were made fluorescent by tagging them with FITC (Fluorescein isothiocyanate) to be estimated via flow cytometry. The uptake efficacy was examined for Caco-2 cell line.

Caco-2 cells were seeded in a 6-well plate at a density of $2.0 \times 10^5$ cells per well (counted by hemocytometer). The cells were allowed to adhere overnight. As the cell confluency reached 70 %, the culture medium was removed and cells were rinsed with 1 ml PBS (phosphate buffer saline). Subsequently, cells were incubated with FITC-BGC at a concentration of 25, 50, and 100 µg/ml for 24 h. After incubation, the cells were washed three times with ice cold PBS, trypsinized and centrifuged at 4000 rpm at 4 °C for 5 min. The pelleted cells thus obtained were resuspended in 500 µl of PBS and were acquired on flow cytometer. A total of 10,000 events per sample were obtained at the excitation wavelength of 375 nm and emission wavelength of 510 nm. The fluorescence signal from the cells were recorded and the cells without any treatment were used as a control for autofluorescence. Each analysis was done in triplicate.

*2.2.3.10 Radiolabeling of BGC nanoparticles with Technetium-99m ($^{99m}$Tc)*

Radiolabeling of BGC with $^{99m}$Tc is concluded to fabricate BGC as a radiopharmaceutical that can further be employed for biodistribution profile studies. In the present study, the stability/labeling efficiency of BGC-$^{99m}$Tc is studied at pH variants of the GI tract (pH 1.2 & 6.8), neutral pH (7), physiological pH (7.4), and alkaline pH (8.5). These ranges of pH were chosen as radiolabeled BGC has to travel through the GI tract following oral delivery and after cellular uptake may enter the systemic circulation. Five different vials were taken having designated pH values containing 1 mg/ml of BGC and 100 µl of SnCl$_2$ (Stannous Chloride) followed by the addition of $^{99m}$Tc (4.0 mCi). The labeling efficiency was assessed by ascending instant thin-layer chromatography (ITLC). The radiochemical purity of free and labeled BGC was checked by using a 31ET Whatman strip having acetone as the mobile phase. The labeling efficiency was calculated using the following equation [33]:

Labeling efficiency % = (total counts – counts of free pertechnetate/total counts) × 100

*Statistical analysis*

Data are expressed as mean ± SD. Statistical analysis was carried out through Origin Pro 8.6 32-bit software using two-way ANOVA, (least significant difference) at the significance level of p-value <0.05. The results are reported as the mean ± standard deviations of at least three replicates.

## 2.3 Results and Discussions

### 2.3.1 FTIR

When IR radiation passes through a sample, some of the radiation is absorbed, and the rest passing through the sample is recorded. Fig.1 (b) shows the FTIR spectra of BG, BGC, and Vit C. BG (without template) and BGC are depicted separately just to indicate the presence of vitamin C in the formed nanoparticles thus showing the presence of template with BG nanoparticles. The peak at 1103 $cm^{-1}$ and 473 $cm^{-1}$ corresponds to Si-O-Si stretching. A small peak at 959 $cm^{-1}$ is assigned to the non-bridging oxygen with the surface of active silanol (Si-OH) [25,34,35]. The peak at 674 $cm^{-1}$ indicates the P-O bending vibration. The peak at 1649 $cm^{-1}$ of Vit C refers to the C=O vibration present in the lactone ring [36]. The -OH stretching and vibration can be seen around peaks 1412 $cm^{-1}$ and 1565 $cm^{-1}$ that also be visualized in BGC with a slight deviation of 1412 $cm^{-1}$ to 1446 $cm^{-1}$ addressing the ionic interaction among Vit C and BG precursors. The bands between 1400 – 1100 $cm^{-1}$ of Vit C are ascribed to C-OH vibrations. The peak at 3374 $cm^{-1}$ in Vit C depicts O-H stretching and can also be seen in BGC at 3436 $cm^{-1}$ confirming the in-situ mineralization of BG nanoparticles using Vit C as a template and signifies ionic interactions among different moieties [25,36].
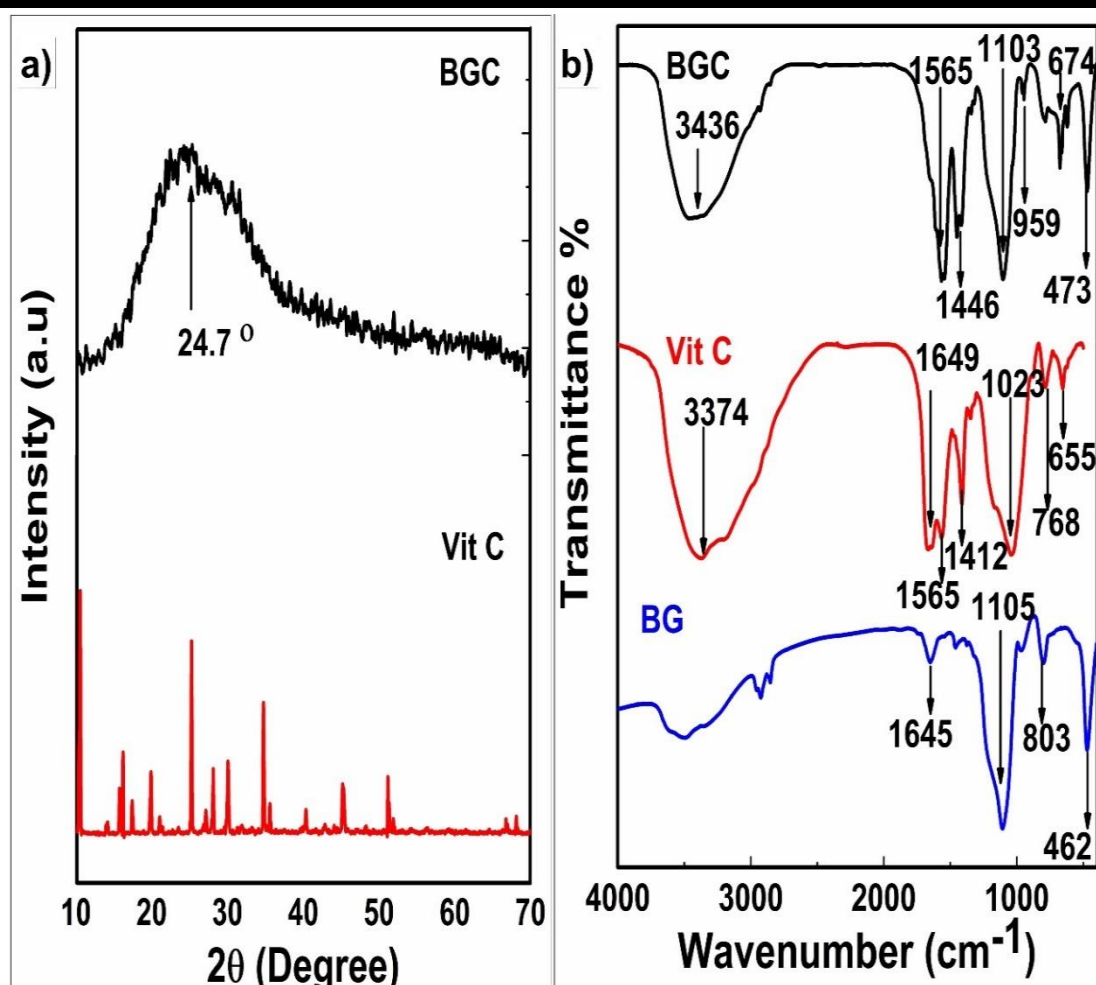
Fig.2.1 a) XRD pattern b) FTIR spectra

*2.3.2 XRD*

As crystalline size approaches the nanoscale, the XRD peak broadens [37]. Broadening of the diffraction peak escalates as the crystalline size drops from 50 nm to 25 nm [38]. Fig.1 (a) depicts the possibility of the synthesized BGC to be nanosized as there can be seen a broad diffraction domain at 2θ value range from 15 ° to 30 °. It can also be inferred from the diffraction pattern that the formed BGC is highly amorphous as depicted by various researchers [39,40]. Vit C, on the other hand, is highly crystalline in its pure form. During ionic/physical interaction of Vit C as a template with BG precursors during in-situ mineralization of BG, there

occurs alteration in its structural integrity of Vit C according to reaction sites of the same. Alike observations can also correspond to FTIR spectra (fig.1 (b))

*2.3.3 TEM*

TEM micrographs confirmed the size of the BGC in the Nano range (Fig.2 (a & b). Using Image J-analysis, particle size distribution was evaluated and the mean diameter of BGC came out to be $25.36 \pm 1.2$ nm as depicted in Fig 2 (d). The nanoparticles formed are spherical. Further, the amorphous nature of the prepared BGC has also been reflected by the selected area electron diffraction (SAED) pattern (Fig. 2 (c)) that is consistent with the XRD (Fig.1(a)) The EDAX spectra confirm the *in-situ* mineralization of BG nanoparticles employing Vit C as a template. (Fig.2 (e)). The elemental analysis of the formed nanoparticles using EDAX is shown in Table 1.

**Table 2.1: Elemental analysis of BGC using EDAX spectra. ($p < 0.05$)**

| Element | Atomic % EDAX analysis | |
|---|---|---|
| | Observed | Calculated |
| **P** | 6.75 | 7.22 |
| **Ca** | 3.11 | 1.72 |
| **Si** | 42.89 | 37.74 |
| **Na** | 35.55 | 29.23 |
| **C** | 11.70 | 24.05 |
| **Total** | 100 | 99.96 |
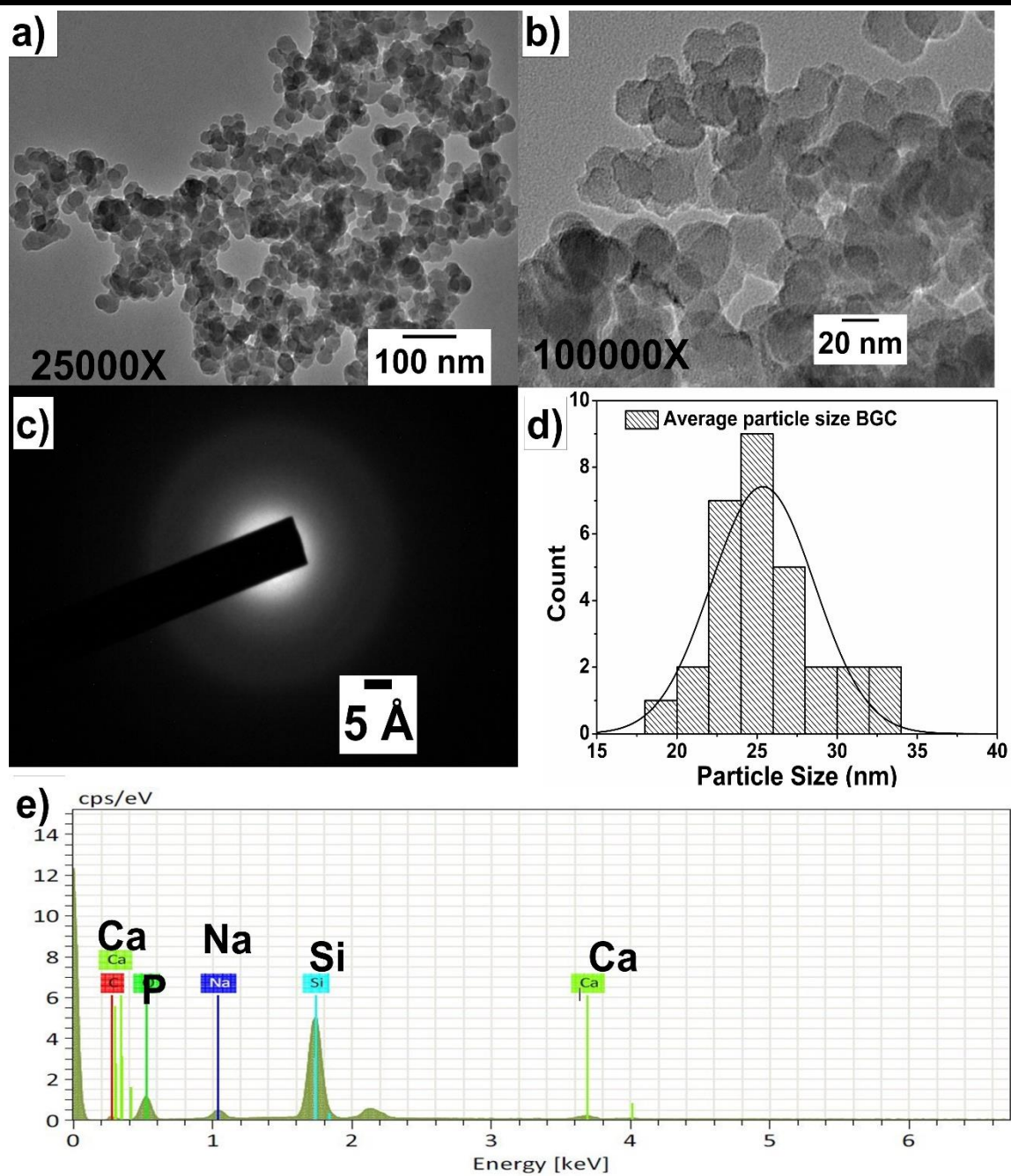
Fig. 2.2  a) & b) TEM images of BGC c) SAED pattern of BGC nanoparticles d) Particle size distribution based on TEM images using image J bundled with 64-bit Java-1.8.0_172 analysis software e) EDAX spectra of BGC nanoparticles

*2.3.4 Nitrogen sorption analysis*

To confirm the mesopores distribution of synthesized BGC, BET analysis was extended for the t-method and the result is displayed in Fig.3. The analysis depicted the mesoporous nature of the nanoparticles with a mean pore diameter of 8.18 nm as depicted in the inset image. Pore size was not homogenous and can be attributed to the ionic interaction between ionic moieties of BG and vitamin C. The investigation represents type IV isotherm with hysteresis loop H4 [41,42]. The surface area was calculated using the BJH method and was found to be 75.912 $m^2$/g.



| Pore Characterization: | |
|---|---|
| BJH surface area ($m^2$/g) | 75.912 |
| Average pore radius (A°) | 7.480 |
| BJH cumulative desorption pore volume (cc/g) (at P/Po=0.997 | 0.971 |
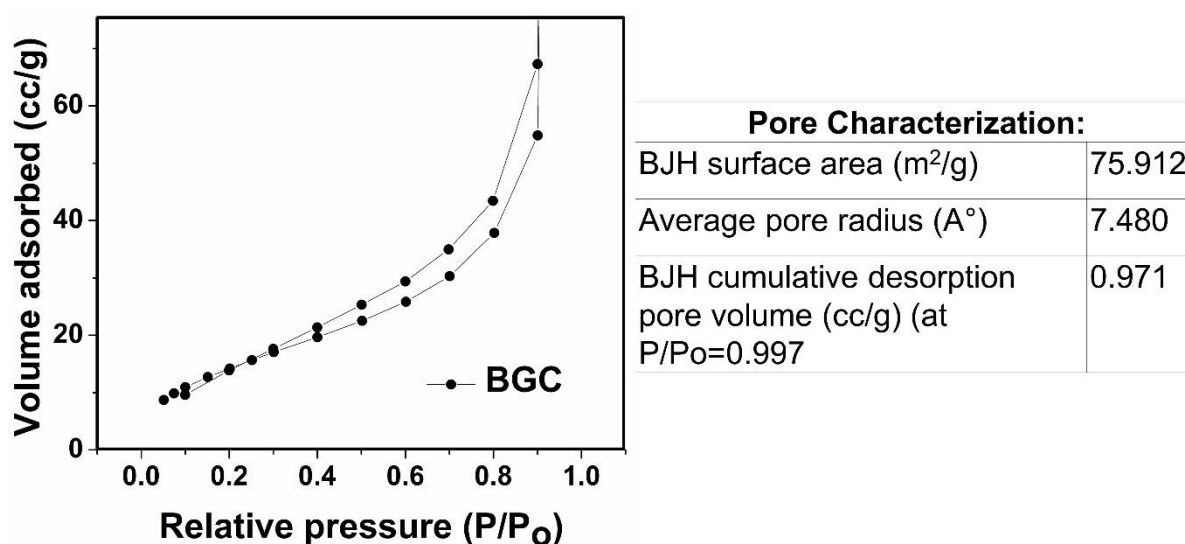
Fig. 2.3 Nitrogen adsorption-desorption isotherm and pore size characterization of BGC nanoparticles

*2.3.5 Bioactivity test*

Bioactivity can be defined as the potential of the material to interact with the living tissue by forming body-like constituents [27]. In terms of bones, bioactivity is a property of a material to bond with the bone tissues by forming a hydroxyapatite (HA) like layer which constitutes

the major portion of the inorganic matrix of the bones [43]. The *in-vitro* bioactivity of BGC was evaluated by soaking it in simulated body fluid (SBF). The particles were examined for up to 1 month and thorough structural, functional, and morphological characterization were studied. Also, changes in the chemical composition of the counterpart of BGC i.e. the ion concentration of the SBF solution after immersion of the sample as a function of time were examined by ICP-MS. Fig.4(a) illustrates the XRD pattern obtained after the interaction of BGC with SBF at different time intervals. When compared with BGC before immersion in SBF as shown in Fig.1 (a), there is an occurrence of small peak at about $2\theta \approx 32°$[39,40]. The intensity of this aforementioned peak keeps on increasing with direct proportionality with time, thus showing increased crystallization. This crystallization is an outcome of the development of an HA-like layer (Calcium phosphate silicate, JCPDS-00-049-1674) on the surface of BGCNPs. Further, the formation of HA is also confirmed by FTIR spectroscopy (Fig 4(b)). The peak at 1642 $cm^{-1}$ corresponds to the -OH group after the interaction of BGC with SBF. Apart from this, the peak at 803 $cm^{-1}$ is attributed to the carbonate group [34,40,42]. The absorption band for phosphate can be visualized at 1108 and 953 $cm^{-1}$. The peak at 471 $cm^{-1}$ is attributed to the bending vibration of the phosphate group [24]. The presence of all these peaks confirms the formation of HA over the BGC surface. It is critical to note that the intensity of the prior mentioned peaks has significantly increased as the interactivity time for BGC and SBF is augmented to 30 days.
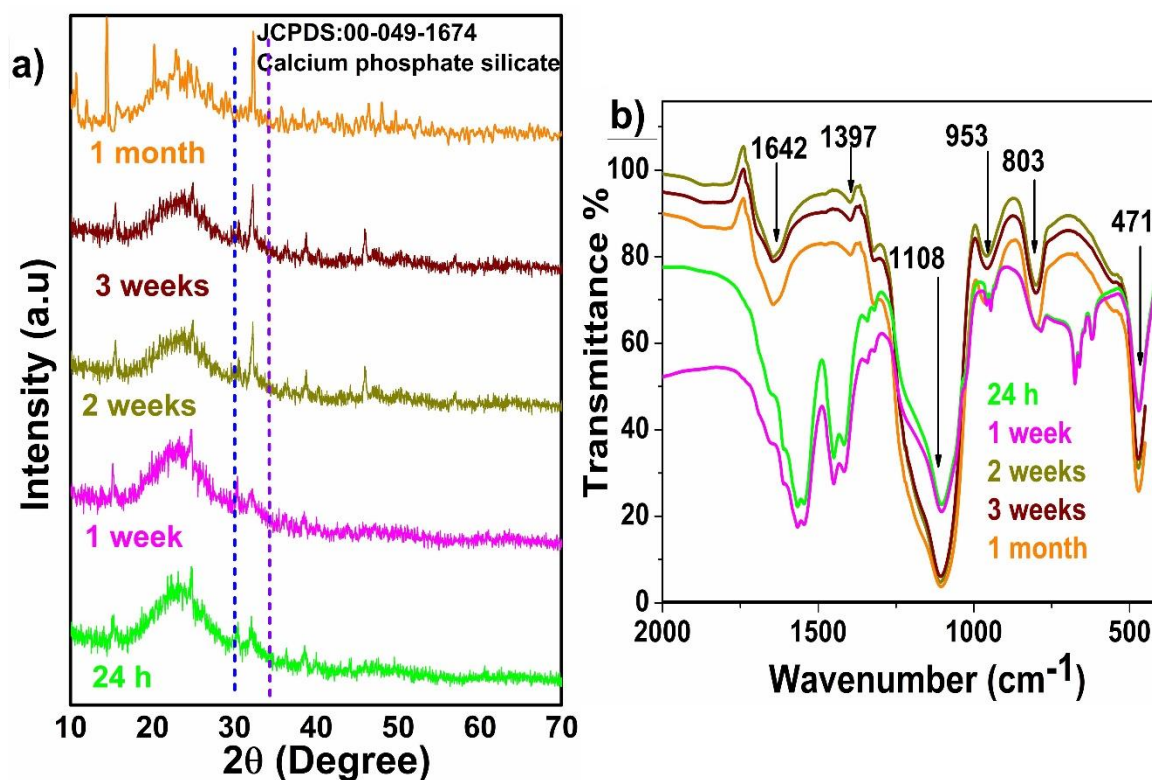
Fig.2. 4 Bioactivity analysis of BGC nanoparticles by its immersion in SBF a) XRD b) FTIR

To further validate the bioactivity mechanism of nanoparticles in SBF, ICP-MS plays a vital role. It allows the determination of ionic exchanges established between the glass surface and SBF. Measurements have been carried out on the remaining SBF. The results obtained show variations in the concentration of calcium (Ca), phosphorous (P), and silicon (Si) with respect to time. The presence of Si in SBF is an indication of the dissolution of silica from BGC to form silanol. This eventually leads to the formation of silica gel over the surface of said nanoparticles further forming the HA layer [44]. As depicted in Fig.6 (b), the concentration of Ca and P decreases with an increase in time. In contrast, the concentration of Si increases over time confirming the dissolution of the glass surface during the bioactivity process. These aforenamed results stand in accordance with various researchers [24,27,44]. After immersion of BGC in SBF, the samples were retrieved from SBF after a stipulated time interval, and the surface topography of the same was monitored using SEM. As depicted in Fig. 5, HA growth

over BGC in patches can be seen after 24 h. With the escalation in the time period, it is evident from the images that HA starts aggregating and spreads throughout the surface of the particles. EDAX spectra (Fig.5) depicting Ca, P, and O confirms the formation of calcium phosphate (HA) and stand as per FTIR (Fig.4(b)). Enhanced HA showing an increased percentage of Ca and P at day 30 when compared with day 1 from EDAX as shown in Fig.6 (a) (as a bar graph) validates the bioactivity phenomenon.
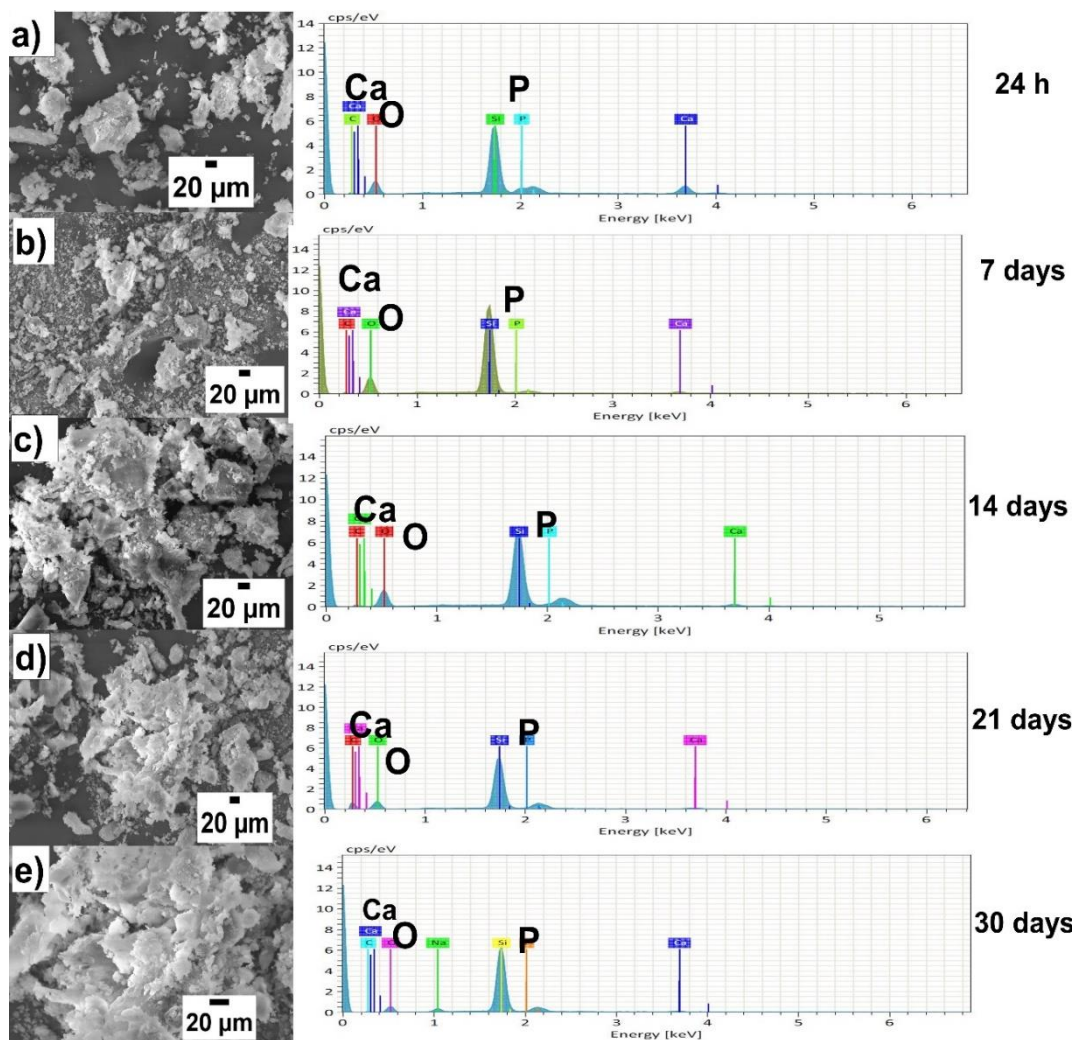


Fig. 2.5 Bioactivity analysis by SEM micrographs (500 X magnification) along with EDAX spectra
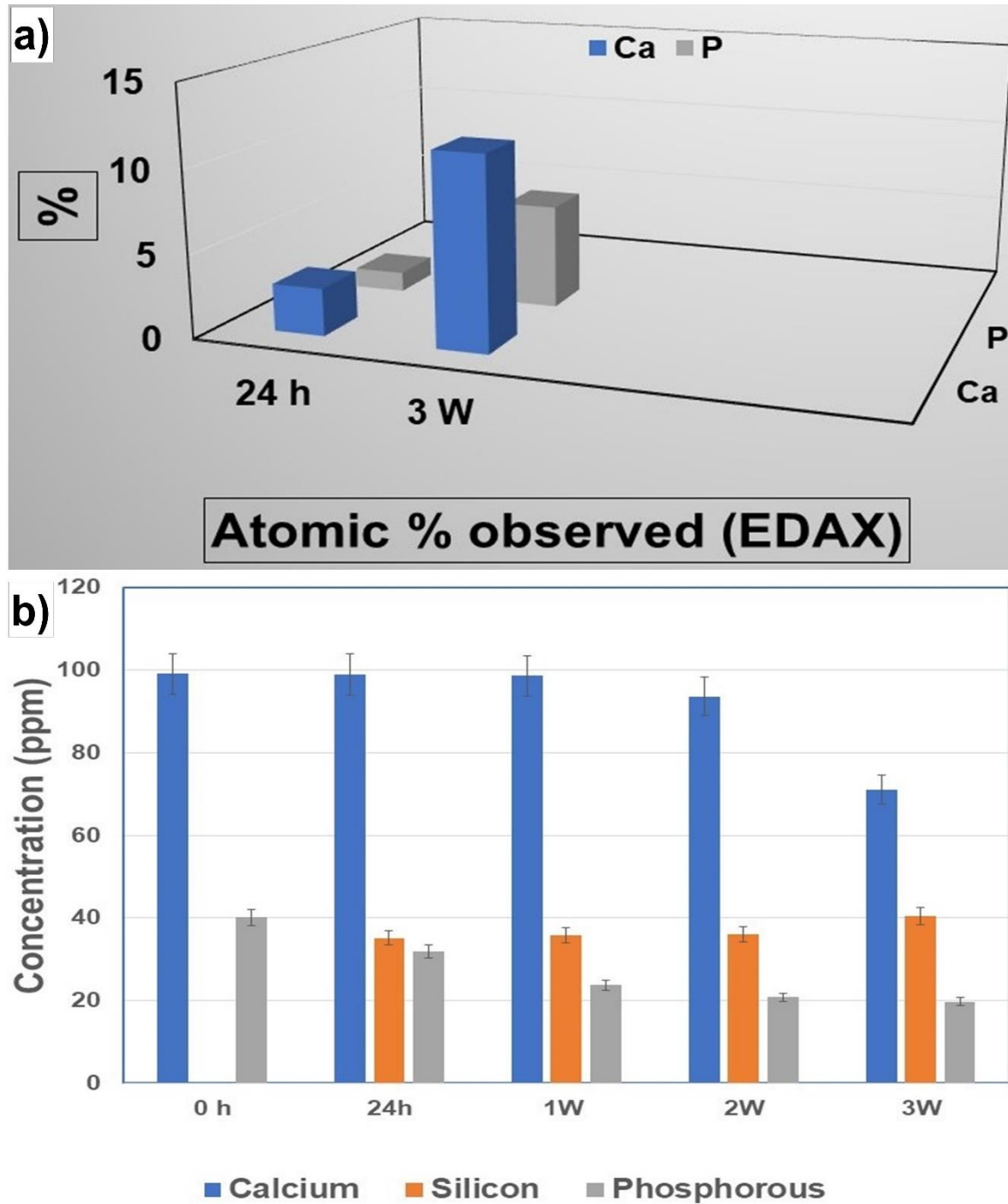
Fig. 2.6 a) Bioactivity analysis by atomic percentage calculation of Ca & P observed at 24 h and 3 weeks by EDAX. b) ICP-MS for leftover SBF fluid after bioactivity test (dissolution of Ca, P, and Si in SBF after immersion of BGC nanoparticles)

*2.3.6 Biocompatibility test*

With the advent of the application of nanoparticles in drug delivery systems (DDS), cellular viability is a crucial aspect to be studied. The cellular toxicity of BGC was evaluated at varying concentrations from 0.5 µg/ml to 100 µg/ml. The assay was carried out for the incubation period of 24 h and 48 h against Caco-2 cell lines and U2OS cell lines. It is evident from Fig.7 (a & b) that the viability of cells remains 80 % and above over the entire concentration range for both cell lines. This showcases the promising nature of BGC to be biocompatible and a potent oral delivery system. These results stand analogous to various researchers [45,46].

*2.3.7 Cellular uptake*

The cellular internalization of nanoparticles is highly influenced by the physiochemical properties of nanoparticles. Since the oral delivery of BGC has to follow the GI tract, therefore, the cellular uptake of FITC-tagged BGC at varying concentrations (25 µg/ml to 100 µg/ml) against Caco-2 cell line was evaluated using a flow cytometer. The fluorescence intensity produced is directly proportional to the amount of material internalized. From Fig. 7 (c), it can be inferred that as the concentration of BGC increases, there is a six-time increase in fold change when compared with blank cells. Due to its nanosized range, BGC is easily internalized via endocytosis through the intestinal cell line [31,46]. This study shows that BGC is a suitable candidate for oral delivery applications.
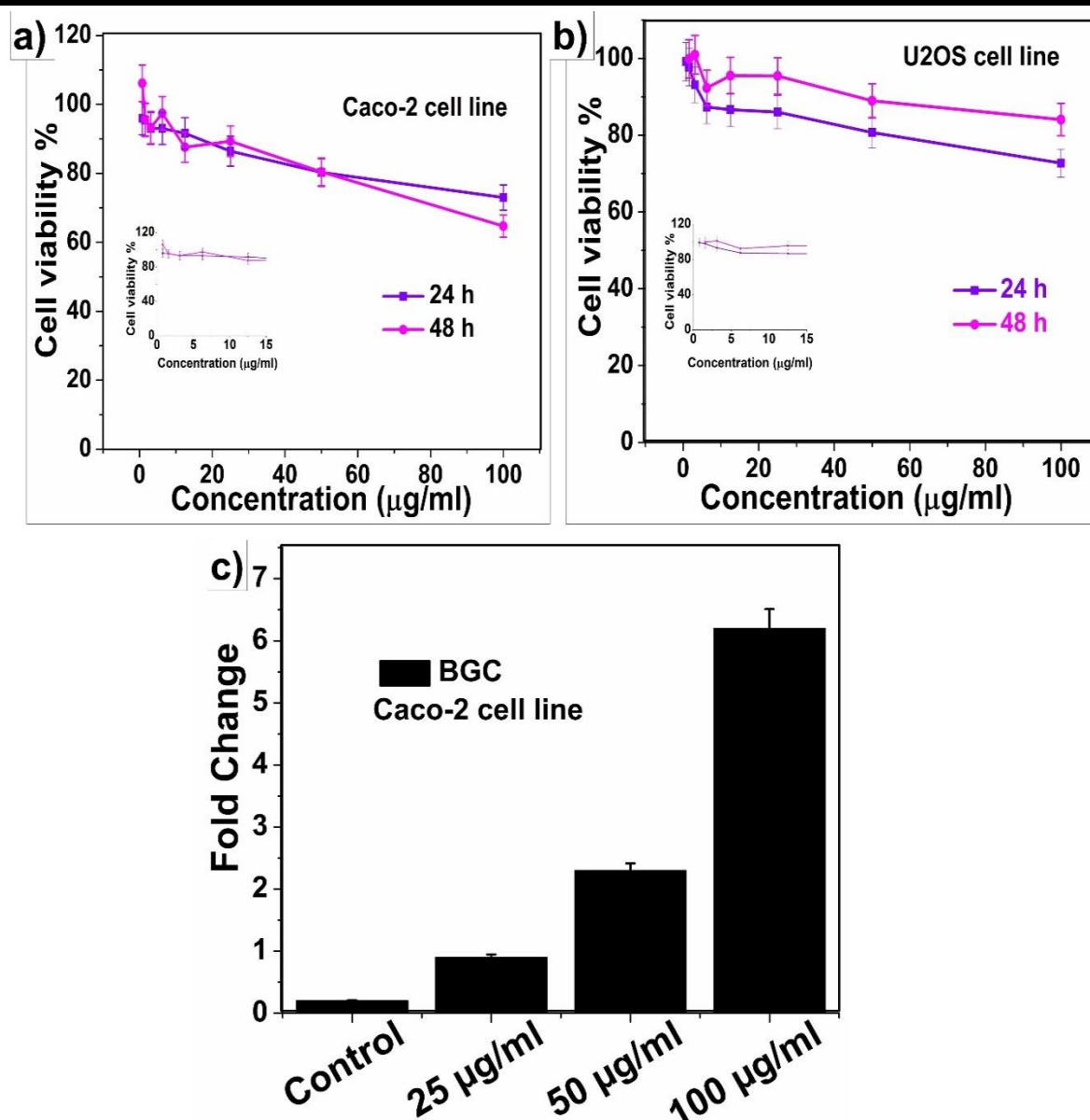
Fig. 2.7  Biocompatibility assay of BGC nanoparticles against a) Caco-2 cell lines b) U2OS cell lines c) Cellular uptake of BGC nanoparticles over Caco-2 cell lines.

*2.3.8 Radiolabeling efficiency*

One of the important requisites of radiopharmaceuticals is its stability in systemic body fluid. Numerous biomolecules in human body fluid tend to bind with Tc-99m. Therefore, the labeling efficiency of Tc-99m with BGC is checked using radio TLC. Also, the ingestion of nanoparticles is proposed to follow the oral route, which resonates that it has to encounter the

different pH conditions of the GI tract, consequently labeling efficiency is monitored at different pH ranges (acidic-neutral-basic). The residence time of any ingested material in the stomach is nearly about 2 h, therefore at pH 1.2 (stomach pH), labeling efficacy is checked up to 2 h. Subsequently, food descends to an intestinal region where residence time varies from 6 to 10 h, and eventually, it enters into the systemic circulation after being absorbed via intestines, for that reason at pH 6.8 & pH 7 (intestinal pH) and physiological pH (pH 7.4), the labeling effectiveness is checked up to 24 h. From Fig. 8, it can be comprehended that the labeling efficiency of BGC-Tc 99m is approximately more than 91 % after 6 h and is maintained at around 88 % even after 24 h. The TLC chromatographs depicted in Fig. 8 (b to e) reveal the major portion of labeled $^{99m}$Tc-BGC and a very less proportion of free $TcO_4^-$ (pertechnetate). The above data discern the application of Tc-99m labeled BGC as an effective radiopharmaceutical for oral delivery applications.
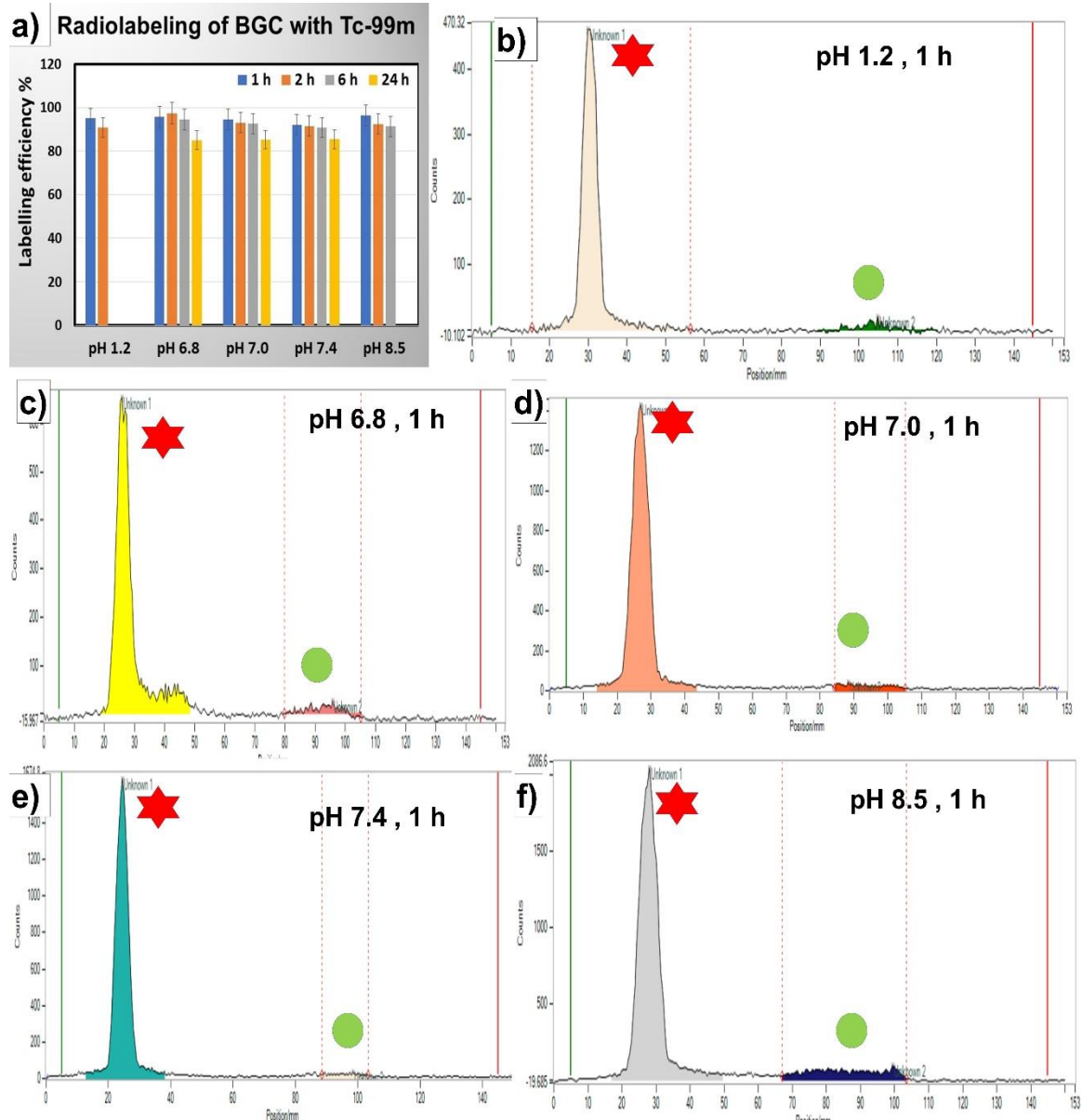
Fig.2.8 a) Radiolabeling efficiency of BGC with $^{99m}$Tc at different pH and at different time intervals. b) to e) Radio-TLC of $^{99m}$Tc (Tc-BGC) developed on ITLC with acetone as mobile phase ($^{99m}$Tc-BGC ⭐), (Free TcO$_4^-$ 🟢)

## 2.4 Conclusion

The present investigation describes the successful synthesis and characterization of BGC. It also demonstrates its productive interaction with SBF showing bioactivity thereby resulting in biomineralization. The *in-vitro* studies also show the biocompatible nature of the formed

particles for both intestinal and bone cells (caco-2 and U2OS cell lines respectively). The cellular uptake studies depict the potential of these particles for oral delivery application. The stable radiolabeling of BGC with $^{99m}$Tc at different pHs indicates its usage as a radiopharmaceutical, which in the future may be explored for *in-vivo* imaging for diagnosis and targeted delivery applications.

## References

[1]     N. Salari, H. Ghasemi, L. Mohammadi, M. hasan Behzadi, E. Rabieenia, S. Shohaimi, M. Mohammadi, The global prevalence of osteoporosis in the world: a comprehensive systematic review and meta-analysis, J. Orthop. Surg. Res. 16 (2021). https://doi.org/10.1186/s13018-021-02772-0.

[2]     M. Murshed, Mechanism of bone mineralization, Cold Spring Harb. Perspect. Med. 8 (2018) 1–11. https://doi.org/10.1101/CSHPERSPECT.A031229.

[3]     J. Hum, A.R. Boccaccini, Collagen as coating material for 45S5 bioactive glass-based scaffolds for bone tissue engineering, Int. J. Mol. Sci. 19 (2018). https://doi.org/10.3390/ijms19061807.

[4]     S. Bawa, The Significance of Soy Protein and Soy Bioactive Compounds in the Prophylaxis and Treatment of Osteoporosis, J. Osteoporos. 2010 (2010) 1–8. https://doi.org/10.4061/2010/891058.

[5]     K.S. George, J. Muñoz, N.S. Akhavan, E.M. Foley, S.C. Siebert, G. Tenenbaum, D.A. Khalil, S.C. Chai, B.H. Arjmandi, Is soy protein effective in reducing cholesterol and improving bone health?, Food Funct. 11 (2020) 544–551. https://doi.org/10.1039/c9fo01081e.

[6]     N.N. DePhillipo, Z.S. Aman, M.I. Kennedy, J.P. Begley, G. Moatshe, R.F. LaPrade, Efficacy of Vitamin C Supplementation on Collagen Synthesis and Oxidative Stress After Musculoskeletal Injuries: A Systematic Review, Orthop. J. Sport. Med. 6 (2018) 1–9. https://doi.org/10.1177/2325967118804544.

[7]     G.B. Wasilewski, M.G. Vervloet, L.J. Schurgers, The Bone—Vasculature Axis:

Calcium Supplementation and the Role of Vitamin K, Front. Cardiovasc. Med. 6 (2019) 1–16. https://doi.org/10.3389/fcvm.2019.00006.

[8]  K. Amrein, M. Scherkl, M. Hoffmann, S. Neuwersch-Sommeregger, M. Köstenberger, A. Tmava Berisha, G. Martucci, S. Pilz, O. Malle, Vitamin D deficiency 2.0: an update on the current status worldwide, Eur. J. Clin. Nutr. 74 (2020) 1498–1513. https://doi.org/10.1038/s41430-020-0558-y.

[9]  I.R. Reid, S.M. Bristow, M.J. Bolland, Calcium supplements: Benefits and risks, J. Intern. Med. 278 (2015) 354–368. https://doi.org/10.1111/joim.12394.

[10]  M. Peacock, Phosphate Metabolism in Health and Disease, Calcif. Tissue Int. 108 (2021) 3–15. https://doi.org/10.1007/s00223-020-00686-3.

[11]  J. Costa-Rodrigues, S. Reis, A. Castro, M.H. Fernandes, Bone anabolic effects of soluble si: In vitro studies with human mesenchymal stem cells and cd14+ osteoclast precursors, Stem Cells Int. 2016 (2016). https://doi.org/10.1155/2016/5653275.

[12]  T.T. Roberts, A.J. Rosenbaum, Bone grafts, bone substitutes and orthobiologics the bridge between basic science and clinical advancements in fracture healing, Organogenesis. 8 (2012) 114–124. https://doi.org/10.4161/org.23306.

[13]  J.A. Sunyecz, Zoledronic acid infusion for prevention and treatment of osteoporosis, Int. J. Womens. Health. 2 (2010) 353–360. https://doi.org/10.2147/IJWH.S7322.

[14]  K. Lampropoulou-Adamidou, E. Karlafti, C. Argyrou, K. Makris, G. Trovas, I.A. Dontas, S. Tournis, I.K. Triantafyllopoulos, Effect of Calcium and Vitamin D Supplementation With and Without Collagen Peptides on Volumetric and Areal Bone Mineral Density, Bone Geometry and Bone Turnover in Postmenopausal Women With Osteopenia, J. Clin. Densitom. 25 (2022) 357–372.

https://doi.org/10.1016/j.jocd.2021.11.011.

[15]  H.R. Fernandes, A. Gaddam, A. Rebelo, D. Brazete, G.E. Stan, J.M.F. Ferreira, Bioactive glasses and glass-ceramics for healthcare applications in bone regeneration and tissue engineering, Materials (Basel). 11 (2018) 1–54. https://doi.org/10.3390/ma11122530.

[16]  G.M. Calori, E. Mazza, M. Colombo, C. Ripamonti, The use of bone-graft substitutes in large bone defects: Any specific needs?, Injury. 42 (2011) S56–S63. https://doi.org/10.1016/j.injury.2011.06.011.

[17]  J. anne N. Oliver, Y. Su, X. Lu, P.H. Kuo, J. Du, D. Zhu, Bioactive glass coatings on metallic implants for biomedical applications, Bioact. Mater. 4 (2019) 261–270. https://doi.org/10.1016/j.bioactmat.2019.09.002.

[18]  M.N. Rahaman, X. Liu, B.S. Bal, D.E. Day, L. Bi, L.F. Bonewald, Bioactive glass in bone tissue engineering, Ceram. Trans. 237 (2012) 73–82. https://doi.org/10.1002/9781118511466.ch8.

[19]  M. Montazerian, E.D. Zanotto, A guided walk through Larry Hench's monumental discoveries, J. Mater. Sci. 52 (2017) 8695–8732. https://doi.org/10.1007/s10853-017-0804-4.

[20]  V. Miguez-Pacheco, L.L. Hench, A.R. Boccaccini, Bioactive glasses beyond bone and teeth: Emerging applications in contact with soft tissues, Acta Biomater. 13 (2015) 1–15. https://doi.org/10.1016/j.actbio.2014.11.004.

[21]  F. Baino, S. Hamzehlou, S. Kargozar, Bioactive glasses: Where are we and where are we going?, J. Funct. Biomater. 9 (2018). https://doi.org/10.3390/jfb9010025.

[22]  S. Kargozar, S. Hamzehlou, F. Baino, Can bioactive glasses be useful to accelerate the

healing of epithelial tissues?, Mater. Sci. Eng. C. 97 (2019) 1009–1020.

https://doi.org/10.1016/j.msec.2019.01.028.

[23]   L.L. Hench, J.R. Jones, Bioactive glasses: Frontiers and Challenges, Front. Bioeng.

Biotechnol. 3 (2015) 1–12. https://doi.org/10.3389/fbioe.2015.00194.

[24]   H. Goel, N. Gupta, D. Santhiya, N. Dey, H.B. Bohidar, A. Bhattacharya, Bioactivity

reinforced surface patch bound collagen-pectin hydrogel, Int. J. Biol. Macromol. 174

(2021) 240–253. https://doi.org/10.1016/j.ijbiomac.2021.01.166.

[25]   N. Gupta, D. Santhiya, In situ mineralization of bioactive glass in gelatin matrix,

Mater. Lett. 188 (2017) 127–129. https://doi.org/10.1016/j.matlet.2016.11.045.

[26]   N. Gupta, D. Santhiya, A. Aditya, K. Badra, Dendrimer templated bioactive glass-

ceramic nanovehicle for gene delivery applications, RSC Adv. 5 (2015) 56794–56807.

https://doi.org/10.1039/c5ra04441c.

[27]   T. Kokubo, H. Takadama, How useful is SBF in predicting in vivo bone bioactivity?,

Biomaterials. 27 (2006) 2907–2915.

https://doi.org/10.1016/j.biomaterials.2006.01.017.

[28]   L.B. Alves, S.L.S. De Souza, M.T. Jr, A.B. Novaes, P.T. De Oliveira, D.B. Palioto, B i

o a c t i v e G l a s s Pa r t i c l e s i n Two-Dimensional and Three- Dimensional

Osteogenic Cell Cultures, 28 (2017) 307–316.

[29]   M. Gautam, D. Santhiya, N. Dey, Zein coated calcium carbonate nanoparticles for the

targeted controlled release of model antibiotic and nutrient across the intestine, Mater.

Today Commun. 25 (2020) 101394. https://doi.org/10.1016/j.mtcomm.2020.101394.

[30]   S. Kamiloglu, G. Sari, T. Ozdal, E. Capanoglu, Guidelines for cell viability assays,

Food Front. 1 (2020) 332–349. https://doi.org/10.1002/fft2.44.

[31]  J.J. Rennick, A.P.R. Johnston, R.G. Parton, Key principles and methods for studying the endocytosis of biological and nanoparticle therapeutics, Nat. Nanotechnol. 16 (2021) 266–276. https://doi.org/10.1038/s41565-021-00858-8.

[32]  S. Mazumdar, D. Chitkara, A. Mittal, Exploration and insights into the cellular internalization and intracellular fate of amphiphilic polymeric nanocarriers, Acta Pharm. Sin. B. 11 (2021) 903–924. https://doi.org/10.1016/j.apsb.2021.02.019.

[33]  T. Banerjee, A.K. Singh, R.K. Sharma, A.N. Maitra, Labeling efficiency and biodistribution of Technetium-99m labeled nanoparticles: Interference by colloidal tin oxide particles, Int. J. Pharm. 289 (2005) 189–195. https://doi.org/10.1016/j.ijpharm.2004.09.022.

[34]  N. Gupta, D. Santhiya, A. Aditya, K. Badra, Dendrimer templated bioactive glass-ceramic nanovehicle for gene delivery applications, RSC Adv. 5 (2015) 56794–56807. https://doi.org/10.1039/c5ra04441c.

[35]  Z. Tabia, K. El Mabrouk, M. Bricha, K. Nouneh, Mesoporous bioactive glass nanoparticles doped with magnesium: Drug delivery and acellular: In vitro bioactivity, RSC Adv. 9 (2019) 12232–12246. https://doi.org/10.1039/c9ra01133a.

[36]  H. Yang, J. Irudayaraj, Rapid determination of vitamin C by NIR, MIR and FT-Raman techniques, J. Pharm. Pharmacol. 54 (2010) 1247–1255. https://doi.org/10.1211/002235702320402099.

[37]  C.F. Holder, R.E. Schaak, Tutorial on Powder X-ray Diffraction for Characterizing Nanoscale Materials, ACS Nano. 13 (2019) 7359–7365. https://doi.org/10.1021/acsnano.9b05157.

[38]  J. Madhavi, Comparison of average crystallite size by X-ray peak broadening and

Williamson–Hall and size–strain plots for VO2+ doped ZnS/CdS composite nanopowder, SN Appl. Sci. 1 (2019) 1–12. https://doi.org/10.1007/s42452-019-1291-9.

[39]    J. Chen, L. Zeng, X. Chen, T. Liao, J. Zheng, Preparation and characterization of bioactive glass tablets and evaluation of bioactivity and cytotoxicity in vitro, Bioact. Mater. 3 (2018) 315–321. https://doi.org/10.1016/j.bioactmat.2017.11.004.

[40]    N. Gupta, D. Santhiya, A. Aditya, Tailored smart bioactive glass nanoassembly for dual antibiotic: In vitro sustained release against osteomyelitis, J. Mater. Chem. B. 4 (2016) 7605–7619. https://doi.org/10.1039/c6tb01528j.

[41]    M. Thommes, K. Kaneko, A. V. Neimark, J.P. Olivier, F. Rodriguez-Reinoso, J. Rouquerol, K.S.W. Sing, Physisorption of gases, with special reference to the evaluation of surface area and pore size distribution (IUPAC Technical Report), Pure Appl. Chem. 87 (2015) 1051–1069. https://doi.org/10.1515/pac-2014-1117.

[42]    F. Kurtuldu, N. Mutlu, M. Michálek, K. Zheng, M. Masar, L. Liverani, S. Chen, D. Galusek, A.R. Boccaccini, Cerium and gallium containing mesoporous bioactive glass nanoparticles for bone regeneration: Bioactivity, biocompatibility and antibacterial activity, Mater. Sci. Eng. C. 124 (2021). https://doi.org/10.1016/j.msec.2021.112050.

[43]    X. Feng, Chemical and Biochemical Basis of Cell-Bone Matrix Interaction in Health and Disease, Curr. Chem. Biol. 3 (2012) 189–196. https://doi.org/10.2174/2212796810903020189.

[44]    N. Rocton, H. Oudadesse, B. Lefeuvre, H. Peisker, K. Rbii, Fine analysis of interaction mechanism of bioactive glass surface after soaking in SBF solution: AFM and ICP-OES investigations, Appl. Surf. Sci. 505 (2020) 144076. https://doi.org/10.1016/j.apsusc.2019.144076.

[45]   N. Dey, D. Santhiya, A. Das, Bio-Inspired Synthesis of Hollow Mesoporous Bioactive Glass Nanoparticles Using Calcium Carbonate as Solid Template, ChemistrySelect. 7 (2022). https://doi.org/10.1002/slct.202200392.

[46]   S. Labbaf, O. Tsigkou, K.H. Müller, M.M. Stevens, A.E. Porter, J.R. Jones, Spherical bioactive glass particles and their interaction with human mesenchymal stem cells in vitro, Biomaterials. 32 (2011) 1010–1018. https://doi.org/10.1016/j.biomaterials.2010.08.082.

# Chapter 3

# Characterizing Dextran-Sandwiched Collagen Bioactive Glass Film for Enhanced Oral Targeted Delivery: A Physicochemical and Structural Investigation

<div align="center">
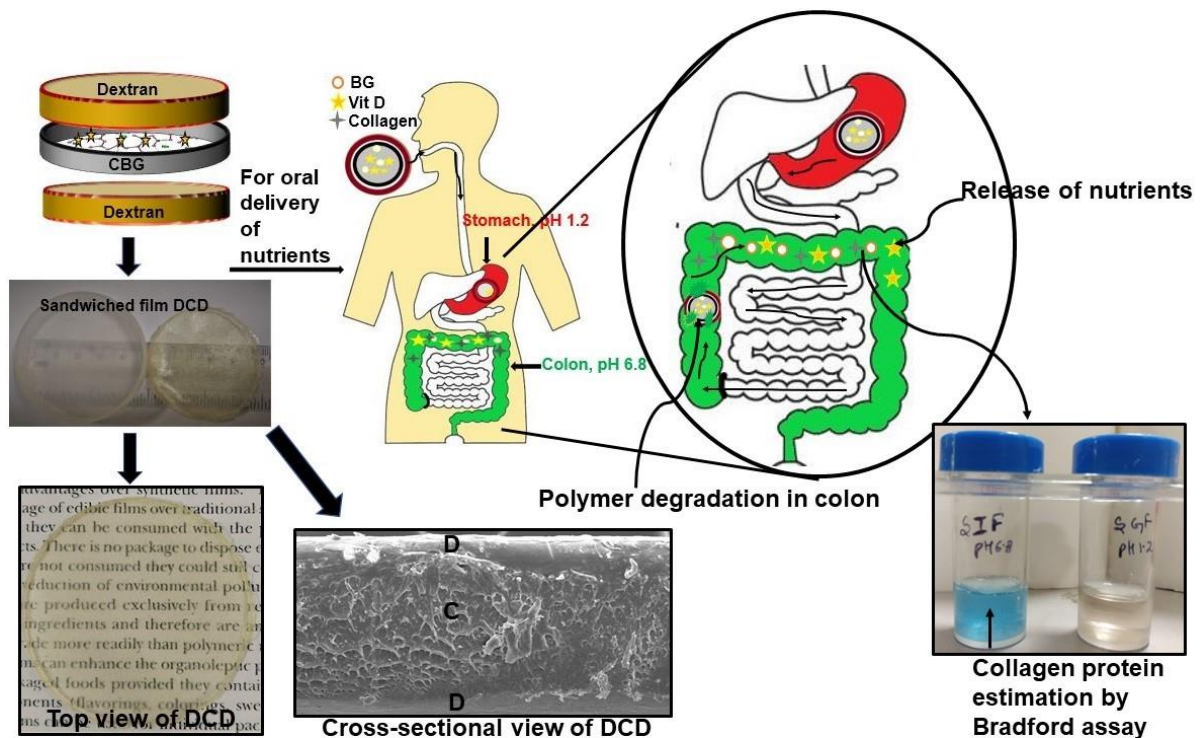
**Chapter 3**

**Characterizing Dextran-Sandwiched Collagen Bioactive Glass Film for Enhanced Oral Targeted Delivery: A Physicochemical and Structural Investigation**

</div>

### 3.1 Introduction:

The bone framework consists of an organic matrix and inorganic salts. The organic matrix contains 90 % of collagen protein [1]. Constituting the major portion of the extracellular matrix, it plays a crucial role in the structure and functioning of bone tissues [2]. It is a structural protein that forms white fibers of the skin, cartilage, bones, tendon, and all other connective tissues [3,4]. The inorganic portion primarily consists of phosphate and calcium ions. The nucleation of calcium and phosphate ions forms a hydroxyapatite layer and its association with collagen is responsible for the typical stiffness and strength of bone tissue. Other factors accountable for maintaining bones include parathyroid hormone (PTH), estrogens, and Vitamin D [2]. Physical activity also appears to be crucial for bone mass. A healthy nutritional diet combined with exercise is always advisable to maintain overall bone health [5]. With the escalation of technology-related mental work, there is poor participation in physical activity leading to a sedentary lifestyle [6]. Physical inactivity reduces bone mineral density [7]. There is an increasing identification that inadequate exercise, poor vitamin D, and low calcium intake are common in current society [8]. The consequence is that urban youngsters are getting affected by bone-related health issues including weakening of bones, bone fragility, etc. Nearly 70 % of children in the USA are deficient in vitamin D and calcium. [9]. There is an increasing number of young adults complaining about osteoarthritis (OA) problems [10], OA is the most common form of arthritis among people [11]. An unbalanced diet and wearing of cartilage surrounding the bone leads to OA. It can happen in any joint but the majority occur in the hip,

spine, hand, and knee joints [12]. Apart from this, Osteoporosis (OP) is another common problem that is more prevalent in females over the age of 50 due to postmenopausal changes in the body [13]. The main cause for OP is a decrease in estrogen levels during menopause which causes bone mass reduction and collagen protein depletion in the body with aging [14]. This eventually grounds the fragility of bone and ultimately the breaking of the bone [15,16]. Vitamin D3 (cholecalciferol) and vitamin D2 (ergocalciferol) are the two main physiological forms of vitamin D. Vitamin D3 is naturally produced by the skin when exposed to sunlight. It has been shown to have a more pronounced effect in elevating the concentration of 25(OH) D in serum [17]. With the exponential increase in skeletal ailments, a combination of Vit D and Ca appears to be substantial for bone health as Vit D is needed for Ca absorption in the body [18].

With the advent of third-generation biomaterial, bioactive glass (BG) has been widely used for bone regeneration as scaffolds and tissue engineering as it stimulates the natural bone to repair itself [19]. Mesoporous BG has a high drug-carrying capacity because of its structure and it is not only osteoconductive and osteoproductive but also osteoinductive, therefore it is considered an ideal component for bone repair mechanism [20]. Some examples of their applications are in orthodontics, maxillofacial, and orthopaedics [21]. In this study, 45S5 BG nanoparticles containing 45% $SiO_2$ are first time used for oral route. Apart from silica, it a rich repository of Calcium (Ca), phosphrous (P), and sodium (Na) [22]. It is to bring attention that biodegradable and biocompatible silica nanoparticles has been recently emerged with enormous potential as a oral delivery vehicle for various therapeutics including macromolecules [23]. Silica is considered "Generally regarded as safe" (GRAS) by US FDA and are employed in many nutraceuticals and cosmetics [24,25] This lead to the exploration of BG as oral drug delivery component. BG is well known for the mineralization of bone by forming a hydroxyapatite (HA) layer as it manifests bioactivity when contacted with simulated body fluid [26,27]. HA is

known to be very essential for bone regeneration *in-vivo* [28]. Thus, BG stands to be a fundamental oral bone health supplement since it is enriched with Ca, Si, andP which are very much required for bone mineralization.

Various health supplements containing Calcium (Ca), Vitamin D, and collagen derivatives are available in the market to support the skeletal system of the human body. Oral delivery of collagen hydrolysates has been used in practice and has exemplified their efficacy in alleviating discomfort caused due to bone-related problems. It has also proved to have beneficial effects on skin aging, OA, OP, rheumatoid arthritis, etc. [4]. But oral availability becomes a concern. Though oral delivery is considered to be the most amicable way to consume drugs and other health supplements, due to the harsh GI tract environment, there is much loss of drug in the upper GI tract before systemic absorption causing the bioavailability of drugs often questionable through oral route. Also,the burst release of drugs causes poor absorption in body due to erractic drug release. This leads to a larger amount of drug dosage formulations that may impose side effects like higher doses of Ca supplemnts causes calcification due to Ca deposition [29], nausea & polyuria are symptoms against higher dosages of Vit D [30]. Therefore, to ensure adequate bioavailability and optimum dosage of essential nutrients and vitamins, these need to be protected in the digestive tract. Studies have shown that sustained release of drugs are found to be more effective in treating ailments promising high bioavalability and fewer systemic side effects [31].

Taking into account all these aspects, this study aims at bringing the novel formulation of essential nutrients $Ca^{2+}$, vitamin D and collagen and their controlled delivery at colon to support bone framework.Colon is onsidered to be an ideal site for delivery of proteins and vitamins as it lacks proteases that degrade the protein in upper GI tract [32]. The combination of Ca with vitamin D and collagen shows a synergistic effect in bone metabolism as evident by various researchers [33]The formulation is not just pH sensitive but also enzyme specific to ensure the

targeted delivery of the desired nutrients to support bone framework. Herein, *in situ* mineralization of BG particles[19] is carried out in the collagen protein matrix followed by the addition of Vitamin D to form collagen BG (CBG) film. To assure the bioavailability of said nutrients at the targeted site i.e. delivery of collagen-bioactive glass assembly to the colon, it is necessary to protect the collagen protein from degradation in the upper GI tract. For this purpose, CBG is sandwiched between dextran film to promote colon-targeted delivery by forming a layered film Dextran-CBG-Dextran named DCD. Dextran is a neutral polysaccharide obtained from *Leuconostoc mesenteroides* with a backbone of α-(1,6)- glycosyl residues. It has a random coiled structure and has been approved to be used in the food industry. Also, its main applications are in pharmaceutics, medicine, coatings, etc. [34]. The degradation of dextran takes place in the presence of the dextranase enzyme found in colonic microflora [35]. Also, proteins that enter large intestine are digested by bacterial enzymes. Colon cells have the capacity to absorb peptides and amino acids due to the presence of amino acid transpoters. [36]   All these attributes of dextran make it a perfect choice for colonic delivery. Colon-specific protein delivery poses benefits as compared to the upper GI tract as it contains lesser protein degrading enzymes than the latter. Also, the residence time for food is longer and the colon has high responsiveness to agents that enhance the absorption of drugs [37,38]. Due to the targeted delivery, protein drug concentration can also be reduced simultaneously thus enhancing the bioavailability of the protein [39]. Being natural and FDA-approved [40], chosen biopolymers i.e. collagen and dextran are generally characterized by low toxicity which makes them advantageous for oral delivery applications. In-situ mineralized BG can prove to be the answers for the the above mentioned enigma of various health supplements since the BG network formed in collagen promises a sustained release of Ca and other ions accounts [19]. It also accounts for various application in bone regeneration [41].

Since the fabricated edible film in this study is composed of collagen protein, Vit D and BG that eventually form HA, therefore, it can serve as a health supplement to support complete bone health. The structural, morphological, and thermal analysis of the fabricated film is done by Fourier Transform Infrared Spectroscopy (FTIR), X-Ray Diffraction (XRD), Scanning Electron Microscopy (SEM), and Thermogravimetric Analysis (TGA). The conformational studies are conducted through Circular Dichroism Spectroscopy (CDS). The mineralization of the BG network in collagen protein is confirmed by SEM/EDAX. The release studies of nutrients from the film are carried out using UV-Visible spectroscopy followed by Sodium Dodecyl Sulphate Polyacrylamide Gel Electrophoresis (SDS-PAGE). The mechanical integrity of the fabricated film at different pHs of the GI tract is studied using a rheometer. Further *in-vitro* disintegration studies are performed at colonic pH followed by the biocompatibility testing of the fabricated film over Caco-2 cell lines.

## 3.2 Experimental Section

### 3.2.1 Materials

For the preparation of the film, dextran (70 M.W. 60,000-80,000 Da, pure, product code: D/0124/48) was purchased from Thermo Fischer Scientific, UK. Collagen and vitamin D (calciferol) were procured from Sisco Research Laboratories Pvt. Ltd., Mumbai, India. Glycerol, dextranase from Penicillium sp. (D8144-500 UN), precursors for in-situ mineralization of BG particles namely triethyl orthosilicate (TEOS), triethyl phosphate (TEP), sodium acetate, and calcium acetate monohydrate were acquired from Sigma Aldrich, USA. Cell studies were carried out using Caco-2 cell lines (human colorectal adenocarcinoma cells) that were obtained from National Centre for Cell Science (NCCS), Pune, India. Simulated gastric fluid (SGF) and simulated intestinal fluid (SIF) solutions were prepared as per the

protocol described earlier [42]. For SGF preparation, 2 g NaCl and 3.2 g pepsin were dissolved in 500 ml distilled water. Subsequently, 3 ml concentrated HCl was added to it and the final volume was made up to 1 L. The solution was adjusted to pH 1.2. The pH of intestinal region (small & large) of human digestive system ranges from 6 to 7.4 [43]. Therefore, for in-vitro experiments, working pH chosen for intestinal fluid is kept 6.8 . Thus, for SIF preparation, 6.8 g monobasic potassium phosphate ($KH_2PO_4$) was dissolved in 650 ml of water followed by the addition of 1 g pancreatin mixture and 0.1 % (w/v) of dextranase. The pH of the solution was adjusted to pH 6.8 by adding 0.2 N NaOH and the solution was made to 1 L. For all experimental procedures, Milli Q water was used and all other reagents used in this study were of analytical reagent (AR) grade of high purity. All experiments were carried out at room temperature i.e., 25 °C unless otherwise stated.

### *3.2.2 Film fabrication*

For the fabrication of sandwiched film DCD, primarily dextran film was obtained by dissolving 2 % dextran (w/v) in milli Q water for 30 min followed by the dropwise addition of glycerol (dextran/glycerol ratio 5:1) to the solution with constant stirring for further 30 min till the homogenous mixture is obtained. The solution was then cast onto a polypropylene (PP) petri-plate with a 5 cm diameter and was left undisturbed till it was partially dried. This film having dextran and glycerol was simply named dextran. Simultaneously, in another beaker, 10 % collagen (w/v) was dissolved in TRIZMA buffer at pH-8 and was stirred constantly for 45 min at room temperature (25 °C). *In-situ* mineralization of BG is carried out as it creates the homogenous system of BG network into collagen fibril network. BG precursors namely TEOS, TEP, sodium acetate, and calcium acetate monohydrate were sequentially added dropwise with an interval of 30 min with constant stirring, and the solution was kept in a silicon oil bath for 24 h at 37 °C to synthesize bioglass as reported earlier [19,44].During this mineralization process, the rate of hydrolysis of TEOS to silica gel takes place [45]. After 24 h, the solution

was again stirred while adding 20 µl of Vit D (1 mg/ml) and poured over the dextran that was cast previously and was left for drying at room temperature. This film was named CBG. Subsequently, another dextran layer was discharged over CBG to form sandwiched film DCD. To elucidate the interlinkage of various components of the fabricated film, all film variants i.e. dextran (having dextran and glycerol), collagen (pure collagen film), CBG, and DCD were prepared. The thickness of the dextran as measured by precision micrometer was $0.11 \pm 0.02$ mm and for collagen, it was $0.21 \pm 0.01$ mm. For CBG, the thickness came out to be $0.25 \pm 0.01$ mm irrespective of maintaining the same weight percentage of collagen in both collagen-based films. This might be due to the in-situ mineralization of the BG network in the collagen matrix while forming CBG. The thickness of DCD was observed to be $0.46 \pm 0.09$ mm.

### 3.2.3   Characterization of the films

#### 3.2.3.1 X-ray Diffraction (XRD)

XRD was performed on film variants. Measurements were carried out with Rikagu MIniflex-II operating at 20 kV and a current of 10 mA using Cu-Kα radiations with a scanning range of 2θ of 5° to 70° at 0.2 °/min.

#### 3.2.3.2 Fourier Transform Infrared Spectroscopy (FTIR)

Dried film samples were powdered and mixed thoroughly with potassium bromide at the ratio of 1:100 and pelleted. The IR spectra of pellets were then recorded using the NICOLET 380 FTIR operating in the range of $4000 - 400$ cm$^{-1}$ with a resolution of 4 cm$^{-1}$.

#### 3.2.3.3 Morphological characterization by Scanning Electron Microscopy (SEM)

The surface topography of film samples was studied with SEM (ZESIS EVO MA15). The samples were coated with gold and then observed at an accelerating voltage of 5.0 kV at 500 X magnifications.

### 3.2.3.4 Thermogravimetric analysis (TGA)

TGA serves in understanding the thermal events associated with polymeric substances and nanomaterials when subjected to heating under predetermined heating rate and temperature conditions. Thermal analysis of the films was measured over time with respect to temperature using TGA (TGA 4000, Perkin Elmer, USA). The samples were weighed approximately 5 mg and heated from 0 °C to 800 °C at a heating rate of 10 °C/min in an $N_2$ gas flow of 50 ml/min.

### 3.2.3.5 Circular Dichroism Spectroscopy (CDS)

The study of conformational stability and secondary structure of pure collagen and CBG was confirmed by CDS. CD spectra of the protein samples were recorded using a Jasco Spectropolarimeter (model J-815) equipped with a Peltier thermostat-controlled cell holder at 25 °C and a cuvette with a path length of 1 cm.

### 3.2.3.6 Rheological studies

The comprehensive rheological analysis of DCD in SGF and SIF was carried out with an MCR 702, advanced rheometer, Anton Paar, Austria, loaded with Rheoplus Software using parallel plate (PP-40) geometry at a measuring distance of 1 mm at 37 °C. Amplitude sweep studies were performed from 0.01 to 100 strain % at 10 rad/s to define rheological stability. The mechanical deformation and flow behavior were measured by frequency sweep experiments which exhibit storage modulus (G ') and loss modulus (G ") as a function of angular frequency (ω) in the range of 0.1 – 100 rad/s at 0.1 % strain. Loss factor versus strain % was depicted to demonstrate the stability of DCD in the GI tract environment.

### 3.2.3.7 Swelling and drug release studies

The swelling studies on various films i.e. dextran, collagen, and DCD were carried out by immersing aforementioned film variants (square shaped 5 cm × 5 cm) into SGF, pH 1.2 for 3

h. After 3 h, samples were rinsed and transferred to SIF, pH 6.8, and the swelling experiment was pursued in the same way for the next 6 h. The swelling ratio from the conducted experiment was calculated gravimetrically as reported earlier [46]. To explore the release study of collagen and Vit D from DCD, the supernatant of the film samples was quantified using a UV- VIS spectrophotometer. The release profile in the case of vit D was studied for 9 h at wavelength 281 nm in SGF and SIF as per the protocol described [47,48]. Similarly, collagen release was estimated in different GI tract buffers using Bradford assay by UV- Visible spectroscopy at wavelength 595 nm as per the procedure described  [49].

### *3.2.3.8 MTT assay*

The cytotoxicity of DCD was examined by MTT assay [50]. Caco-2 cell lines were maintained in Minimum Essential Medium (MEM) with 2 mM L-glutamine and Earle's BSS adjusted to contain 1.5 g/l sodium bicarbonate, 0.1 mM non-essential AA, 10 mM sodium pyruvate, 20 % FBS and 0.1 % penicillin/ streptomycin at 37 °C with 5 % $CO_2$. The cells were seeded onto 96 well plates at $10^4$ cells/ well and were incubated under standard culturing conditions. Once 70 % confluency was achieved, the film suspension was added at a varying concentration ranging from 0.5 µg/ml to 100 µg/ml followed by the incubation of cells for 24 h. The principle behind the MTT assay is that only metabolically active viable cells can convert MTT (3-[4,5-dimethylthiazol-2-yl]-2,5-diphenyl tetrazolium bromide) to purple formazan which has a maximum absorbance at 570 nm. The amount of formazan generated can be quantified and is directly proportional to the number of viable cells. To carry out the assay, initially, 10 % MTT reagent was added along with Opti MEM and incubated for 2 h at 37 °C under ambient cell-culture conditions. After 2 h, the plate was taken out followed by the addition of 10 µl DMSO (Dimethyl sulfoxide) in each well to dissolve formazan crystals.  After incubation, absorbance was measured at 570 nm using TECAN multimode plate reader. The cell viability was calculated as described elsewhere [51].

### 3.2.3.9 SDS-PAGE analysis

To investigate the protein release at different pH from DCD, SDS-PAGE was employed. The amount of collagen released from DCD was analyzed as explained in swelling and drug release studies. Herein, 200 µl were drawn from the release medium, and the concentration of collagen was determined using Bradford reagent and was adjusted to 10 µg/ml. Reducing SDS-PAGE was performed on discontinuous buffered using 5 % stacking gel and 7.5 % resolving gel (Mini Protean Tetra Cell: Bio-Rad Laboratories, Germany) as reported [46,52]. Before running the gel electrophoresis, the film suspension was dialyzed (using dialysis tubing cellulose membrane D9277, Sigma Aldrich) in dialysis buffer for 24 h at 4 °C.

### 3.2.3.10 Disintegration studies

*In-vitro* disintegration studies of DCD were examined in SIF, pH 6.8 at 37 °C. Herein, the film strip was sliced under sterile conditions into a square shape (5 cm × 5 cm), weighed precisely, and placed in 10 ml of SIF, pH 6.8. The sample was taken out at the required time interval (every 1 h to 9 h), washed with water, dried, and weighed. The media (SIF) was refreshed every 2 h. The percentage disintegration was calculated from dry weight before and after the immersion [53]. Also, to examine the changes in the molecular interaction and functional groups in DCD after dissolution, the said samples were analyzed by FTIR, and the alterations in surface morphology were studied by SEM/ EDAX. The dissolution of BG network was also studied in SIF after disintegration using ICP-MS (Inductively coupled plasma mass spectroscopy)

### Statistical analysis

Data are expressed as mean ± SD. Statistical analysis was carried out through Origin Pro 8.6 32-bit software using two-way ANOVA, (least significant difference) at the significance level

of p-value <0.05. The results are reported as the mean ± standard deviations of at least three replicates.

## 3.3 Results and discussion

### 3.3.1 XRD

XRD patterns were employed to examine the physical and crystallographic properties of the fabricated films. In Fig.1, the diffraction domain at $2\theta \approx 10.1$ ° and 22.4 ° of collagen represents the intermolecular lateral distance between triple helical collagen chains and diffuse scattering respectively. The diffraction peak at 30.4 ° resonates with a typical triple helical structure of collagen [54]. Broad diffraction at 22.4 ° is a result of unordered collagen depicting its amorphous nature. The determined d-spacing values d = 0.88 nm and d = 0.44 nm for the peak at 10.1° and 22.4 ° respectively provide the interlayer distance (lamellar layers) in collagen fibril. *In-situ* mineralization of BG in collagen matrix leads to a slight change in the diffractogram of CBG causing a decrease in d-spacing ≈ 0.83 nm at a peak of 10.1 °. This is due to the stacking of the BG network in the collagen matrix and suppression in peak 2 at 22.4 ° with the shift at 19.2 ° [50]. The mineralization of the BG network resulted in the crosslinking of its ionic moieties with collagen fibril that proceeds the orientation among collagen interlayers. Both CBG and DCD have lower intensity as compared to collagen portraying the changes in the triple helical structure of collagen protein. The broad peak of DCD at 19.1 ° and small bump at 10.6 ° shows the amorphous nature of the sandwiched film
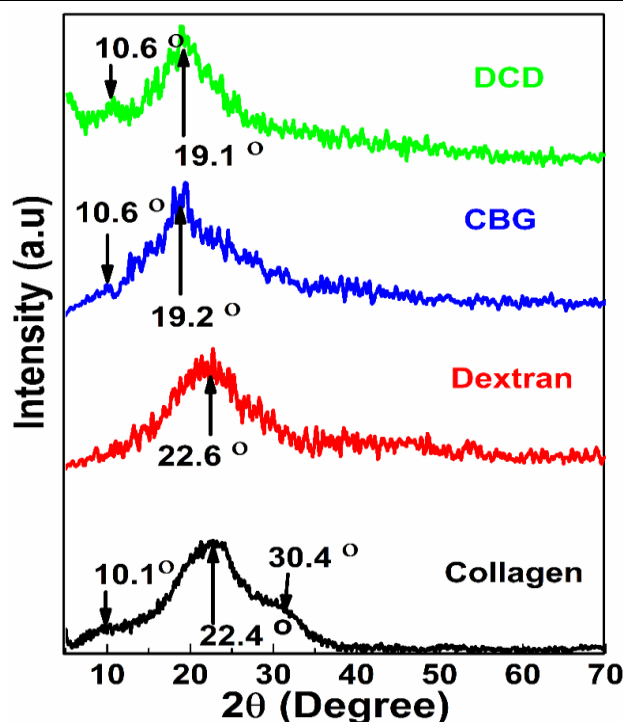
Fig. 3.1 XRD patterns of various films- collagen, dextran, CBG, and DCD

### 3.3.2 FTIR

To elucidate the physical and chemical interaction of biomacromolecules (collagen protein and dextran) with BG precursors and Vit D, functional groups in the films were examined by FTIR spectra (fig.2) The wide peak observed at 3414 cm$^{-1}$ (fig.2a) in collagen is related to N-H stretching of amide A. Spectral region observed at 1656 cm$^{-1}$ corresponds to the protein secondary structural components of amide I which is due to the C=O stretching vibrations of peptide linkages. The peak observed at 1531 cm$^{-1}$ is representative of amide II showing N-H deformation and C-N vibrations. O-H stretching located at 1401 cm$^{-1}$ represents the triple helical structure of collagen assembled by three amino acids i.e. glycine, proline, and hydroxyproline [54]. Amide III representation observed at 1249 cm$^{-1}$ is due to coupled C-N stretching and N-H bending motions. The characteristic peaks of both amide and amine vibrations are observed at 603 cm$^{-1}$ [50]. The FTIR spectra (fig.2a) of BG show the absorption

peaks at 1116, 813, and 471 cm$^{-1}$ that is associated with the bending and stretching vibration of Si-O-Si bonds [44]. The appearance of prominent bands at 640 cm$^{-1}$ and 496 cm$^{-1}$ observed for CBG in fig.2(a & b) as compared with collagen (fig.2a) correspond to asymmetrical stretching vibrations of the phosphate group displaying the interaction of BG precursors with collagen protein. The peak at 1047 cm$^{-1}$ in CBG also corresponds to the Si-O-Si asymmetric stretch and confirms the *in-situ* mineralization of the BG network into collagen with the retention of amide I (C=O) peak at 1650 cm$^{-1}$ [44]. The reduction in intensities at amide I and amide II in CBG may be ascribed to the physical interaction of ionic moieties present in the BG network with C=O, C-N, N-H groups of collagen protein suggesting a significant change in orientation of protein structure [55]. In addition, a weak shoulder observed at 1401 cm$^{-1}$ in collagen is shifted to 1404 cm$^{-1}$ with increased intensity in CBG depicting physical interlinkage of the BG network with collagen fibril and forming Si-OH [52]. The association of BG with collagen was further revealed by the shifting of the amide A band from 3414 cm$^{-1}$ (N-H stretching) of collagen to 3262 cm$^{-1}$ for CBG. The aforementioned FTIR findings are supporting the *in-situ* mineralization of the BG network in the collagen matrix. The FTIR spectra is following the XRD pattern indicating the changes in the triple helical structure of collagen due to the incorporation of BG precursors and its mineralization thereby forming the BG network. Fig. 2b depicts the distinctive spectra of dextran. The peak at 3302 cm$^{-1}$ in dextran corresponds to the secondary -OH group [56] and O-H stretching due to intra- & inter-molecular H-bonding between crosslinker glycerol and dextran [57]. It is evident from the FTIR spectra of DCD that there exists a significant van der Waal interaction between dextran and loosely bound Ca$^{2+}$ ions of the BG network in CBG [56]. The characteristic absorption peak of the C-C bond of dextran at 1627 cm$^{-1}$ is shifted to 1633 cm$^{-1}$ in DCD with increased intensity showcasing the physical interaction between CBG and dextran. Also, the peak at 674 cm$^{-1}$ & 521 cm$^{-1}$ in DCD depicts the phosphate group [58] pronouncing the interaction between different layers of films during

its fabrication. In general, the sandwiched film DCD showed the combined peaks of dextran, collagen, and BG.
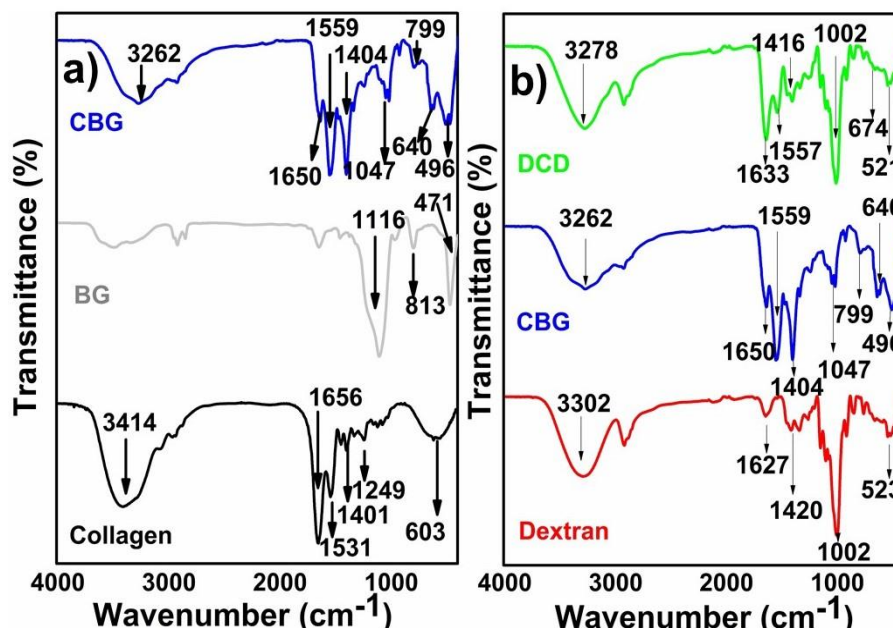


Fig.3.2 a) FTIR spectra of collagen, BG, and CBG (left panel) b) FTIR spectra of Dextran, CBG, and DCD (right panel)

### 3.3.3 *Morphological determination by SEM*

The topographical structure of different film variants was observed using SEM as depicted in Fig. 3. From the images, it was observed that dextran (Fig.3a) has a smooth surface showcasing homogenous distribution of glycerol during film fabrication forming a continuous structure [59]. Glycerol acts as a plasticizer and the hydrogen bonding of glycerol and dextran (shown in FTIR, Fig.2b) resulted in a uniform film structure [60]. Collagen (Fig.3b) showed a continuous arrangement of collagen fibers in the film matrix maintaining structural integrity and forming a patterned assembly of polypeptide chains [61]. Under the influence of metal ions, there exists protein aggregation. Also, peptide chains undergo self-association to form non-covalently linked peptides [62]. *In-situ* mineralization of BG in collagen causes the

intercalated network formation of BG with collagen fibers forming the crosslinked microstructure as shown in CBG (Fig.3c). The physical interaction of ionic constituents of BG within protein molecules as evident by FTIR (Fig.2b) causes the interconnection among collagen fibrils forming a clustered arrangement of polypeptide chains. This physical crosslinking and agglomerated structure of CBG becomes more evident in the cross-sectional view of DCD in Fig. 3d. The presence of Si, P, Ca, and Na elements in CBG and DCD EDAX spectra in Fig.3e & 3f respectively supports the mineralization of BG into collagen protein matrix and stands by FTIR findings. The elemental analysis of the BG network in DCD using EDAX is also shown in Table 1.

**Table 3.1: Elemental analysis of BG in DCD using EDAX spectra. (p-value <0.05)**

| Element | Atomic % EDAX analysis | |
|---------|------------|------------|
| | Observed | Calculated |
| Si | 12.07 | 13.27 |
| Na | 41.50 | 44.44 |
| Ca | 16.90 | 12.03 |
| P | 34.20 | 30.24 |
| Total | 100 | 99.98 |
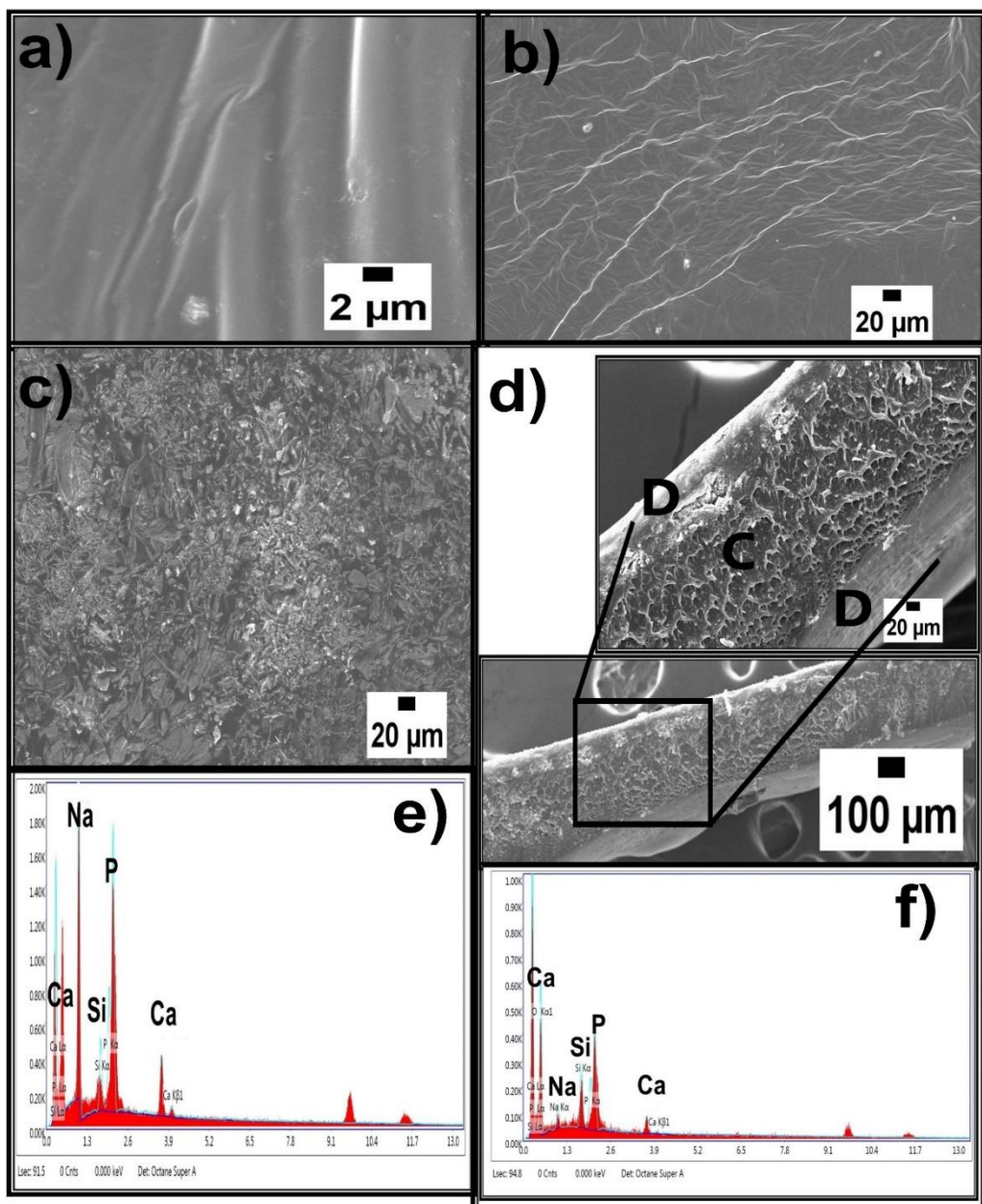
Fig. 3.3 SEM images at an accelerating voltage of 5.0kV a) Dextran b) Collagen c) CBG at 500X d) DCD at 50 X with magnified cross-sectional image at 500 X e) SEM- EDAX spectra of CBG f) SEM- EDAX spectra of DCD

### 3.3.4    TGA

Thermogravimetric analysis was carried out to analyze the weight loss percentage of biomacromolecule-based films dextran, collagen, and its variants. The observed thermal stability of CBG (Fig.4a) is more as compared to collagen. This can be attributed to the mineralization of the BG network with collagen fibrils forming dense aggregation and crosslinked structure as manifested in SEM images (Fig.3c) and depicted in FTIR (Fig.2b). A three-stage thermal degradation was observed in all film samples. In the first stage, the weight loss in the range of 70 °C to 120 °C is attributed to the loss of moisture/ free water during evaporation for all film variants [52]. Major weight loss in collagen and CBG occurs in the second stage in the range of 160 °C to 380 °C, predominantly due to protein degradation [63]. Finally, at 700 °C, approximately 27 % of CBG content remains pertaining to the inorganic content of BG in it. The second degradation step for dextran occurred in the range from 200 °C to 250 °C with a weight loss of about 25 % and is associated with the breaking of glycosidic linkage eventually resulting in the depolymerization of dextran. The third step that occurred in the range between 250 °C to 380 °C is ascribed to the degradation of the dextran chain with approximately 80 % weight loss. At 700 °C, a complete loss of dextran is discerned [60]. In comparison with collagen and dextran, DCD has more thermal stability. Mineralized BG in collagen forming compact agglomerated structure enclosed in a sandwiched layer of dextran as shown in SEM (Fig.3d) and FTIR (Fig.2b) may have imparted more thermal strength to DCD leaving 18 % of inorganic residue near about 700 °C.
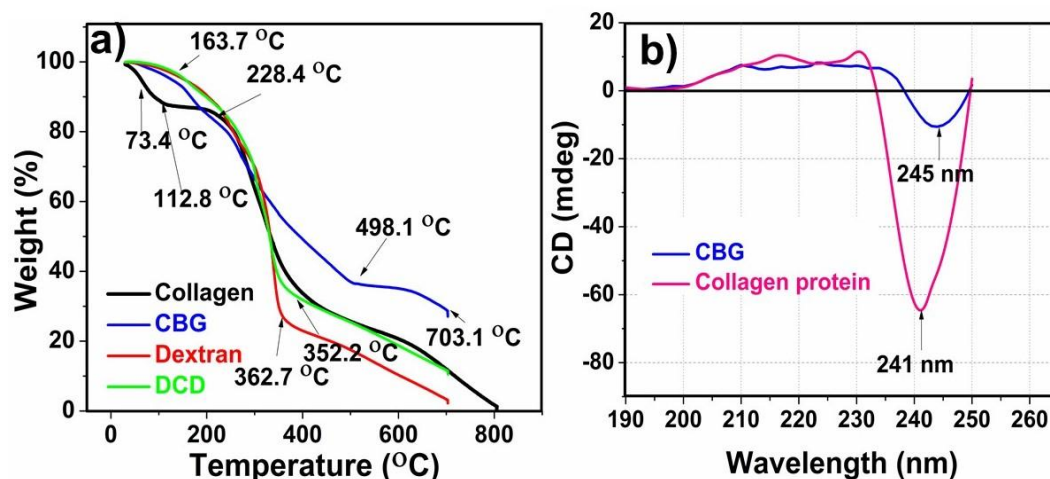
Fig.3.4 a) TGA of collagen, dextran, CBG, and DCD at a heating rate of 10 °C/min in $N_2$ gas flow of 50 ml/min b) Circular Dichroism spectra of collagen protein and CBG

### 3.3.5  CDS

CDS is a potent device for investigating the folding of collagen and other triple helical peptide systems [64]. With the in-situ mineralization of BG in collagen, the protein might have encountered constructional changes. Therefore, CDS is done for CBG only as dextran is only fabricated to protect the CBG film in upper GI tract. There supposed to be no chemical interaction of dextran with collagen as per FTIR (fig.2b). To understand the structural and conformational changes of pure collagen after interaction with precursors of BG, CD spectra of native collagen and with BG were studied. CD spectrum in the far UV region of collagen is shown in Fig. 4b. Pure Type I collagen demonstrates a strong negative ellipticity band between 204 – 210 nm [64]. The collagen protein used in this investigation is marine based with 97 % purity. It contains 380 mg of calcium per 100 g (Table 2). Therefore, due to the presence of calcium in the protein sample, there is a strong negative ellipticity at 241 nm [65]. The negative ellipticity in the range from 210 to 245 nm is ascribed to α-helix and random coil secondary structures of the polypeptide chain [66,67]. With *in-situ* mineralization of BG network in

collagen protein, there exists a reduction in negative ellipticity and a red shift towards 245 nm depicting the change in the α-helical structure of the protein which can also be deduced from XRD (Fig. 1) spectra. Apart from the presence of calcium ions that are already present in the collagen protein sample, the ionic moieties existing in the BG network like $Ca^{2+}$, $PO_4^{3-}$, Si-O-Si linkage, and Si-OH may have been responsible for the physical interaction with collagen protein as demonstrated in FTIR spectra of CBG (Fig 2b) which may have led to the modification in the helical and random coil arrangement of the polypeptide chain of collagen fibrils. These observations validate the conformation changes in the secondary structure of collagen protein during CBG fabrication.

**Table 3.2: Estimation of protein content and Ca in pure collagen protein.**

| S.No. | Test parameters | Test result | Test Method |
|---|---|---|---|
| 1. | Protein (N×6.25), g/100 g | 96.62± 4.83 | IS:7219:1973 |
| 2. | Calcium (as Ca), mg/100 g | 380.60±17.03 | STRC/STP/F129 |

*3.3.6    Rheological Studies*

Rheological properties play an indispensable role in comprehending the stability of both liquid and semi-solid pharmaceutical products. It helps in the fabrication of pharmaceuticals by elucidating the stability of polymer structure. For drug delivery, a drug delivery system (DDS) needs specific flow properties. The rheological interpretation of a semi-solid drug carrier system is an important physical parameter for targeted drug delivery. To determine drug release behavior from DCD in different intestinal fluids (SGF & SIF), an oscillatory frequency sweep and amplitude sweep test were carried out (Fig 5). These measurements can help deduce

information regarding inter- and intramolecular forces in the material [68]. The storage modulus (G') depicts the elastic component of the material and the loss modulus (G") gives information about the viscous property of the material. Initially, an amplitude sweep test was performed to determine the viscoelastic region. Within the viscoelastic region, G' remains constant under applied stress for DCD in SIF whereas there is a dip in storage modulus for DCD in SGF (Fig 5c). For frequency sweep, the measurements were carried out in LVER (linear viscoelastic region) over a frequency range of 0.1 to 100 rad/s. As can be seen from Fig 5b, G' of DCD in SGF is greater than G' of DCD in SIF over the measured frequency range which indicates the presence of a gel-like structure of DCD in gastric (stomach) fluid. The loss factor or damping factor is a ratio of loss modulus to storage modulus and it describes the viscoelastic behavior of the material. From Fig. 5a, it can be seen that the loss factor of DCD in SIF is greater as compared to DCD in SGF. In general, a low value of loss factor depicts the capacity of the material to store more energy/load rather than dissipate it [69]. As the strain % increases, the viscous nature of the DCD in SIF increases, eventually losing its elastic nature. This is attributed to the strain-softening of polymeric chains in SIF. At pH 6.8, deprotonation of the -OH group on dextran forms an alkoxide anion that leads to chain repulsion resulting in dissociation and mobility in polymeric chains. Since the IEP (isoelectric point) of collagen is around 5.5 [70], with the increase in the pH, the zeta potential of collagen becomes negative [19]. Thus, the negative charge density on DCD in SIF pH 6.8 causes instability of the polymer matrix due to anion-anion charge repulsion. This may contribute to the increased mobility among polymeric chains causing chain mobility and escalating the fluid nature of DCD in SIF. It is pertinent to note that at higher angular frequency, G' of DCD in SGF increases indicating material stiffening. In contrast, the elastic modulus for DCD in SIF sharply decreases at higher frequency resulting in a liquid state (viscous) behavior of the film. These observations can be

correlated with loss factor data elucidating the dynamic nature (visco-elastic) of the film at different pHs of the GI tract [32].
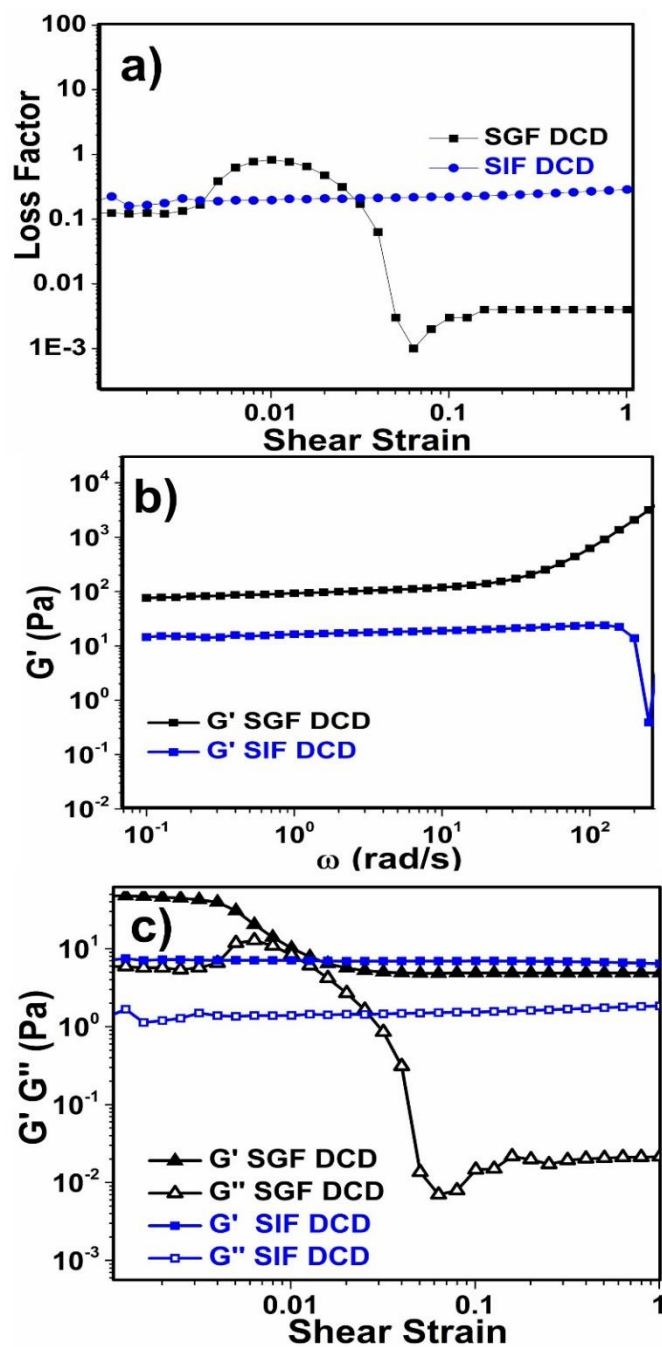


Fig. 3.5. a) Loss factor versus shear strain b) Comparative frequency sweep studies from 0.1 to 100 rad/s at 0.1 % strain variation in storage modulus (G') c) Comparative amplitude sweep profiles at a constant angular frequency of 10 rad/s for strain % 0.01-1000 at 37 °C.

### 3.3.7    Swelling and drug release studies

To determine the swelling behavior, all film variants (dextran, collagen, DCD) were immersed in SGF at pH 1.2 for 3 h followed by SIF at pH 6.8 for another 6 h. It was observed that approximately after 30 min, there was a complete dissolution of stand-alone dextran and collagen due to weaker physical interaction between polymer and glycerol as depicted in FTIR (Fig.2). Therefore, only the swelling data of the functional film DCD is depicted in Fig. 6a. As observed, there was a low account of swelling for DCD at pH 1.2, going maximum up to 38 %. This could be attributed to the presence of $H^+$ ions in an acidic buffer causing the protonation of the -OH group in dextran forming $H_2O$ and making it a leaving group and causing minimal swelling [32,71]. On the other hand, when DCD was placed in SIF at pH 6.8, swelling occurs. The pronounced swelling in SIF is due to the deprotonation of the hydroxyl group in dextran leading to charge repulsion and opening of polymeric chains. Also, the crosslinking BG network in the collagen matrix and physical interaction between loosely bound $Ca^{2+}$ ions of BG with dextran as evidenced by FTIR (Fig 2b) causes the opening of DCD layered structure and thus swelling to reach a maximum of up to 80 %. The aforementioned observation corroborates with rheology data depicting increased loss factor causing molecular mobility in SIF at pH 6.8. After 6 h, there exists a declination in swelling showing disintegration of the film due to anion-anion charge repulsion. Simultaneously, at regular intervals during the swelling experiment, the supernatant solutions from SGF & SIF were taken out and were further subjected to determine the release of Vit D and collagen at wavelength 265 nm and 595 nm respectively. From Fig. 6b, it was observed that the release of Vit D was 4.3 % up to 1 h and 15 % after 3 h. Similarly, collagen release was initially 8.5 % after 1 h and it reaches a maximum of 20 % in SGF after 3 h. When the film was placed in SIF, the release percentage of Vit D increased to 61 % and maintained a sustained release of about 78 % for 9 h. Likewise, collagen release in SIF increased to 75 % at 4 h and reaches a maximum of 95 % at 9 h. It can

be concluded that the release of Vit D and collagen in SGF was minimal due to the acidic pH and protective dextran layer. While in SIF, the release was escalated due to deprotonation, and also the presence of dextranase helped in the degradation of the protective dextran layer, thus releasing the nutrients (collagen & vit D) at the targeted site. These findings justify the objective of swelling to understand the function of film for the controlled and targeted release of the protein at various pH (SGF & SIF) [46]. Analysis from ICP-MS (fig.6c) of the SIF fluid after disintegration showed that the presence of Si has increased and that of P decreased confirming the dissolution of silica network during disintegration and formation of HAP
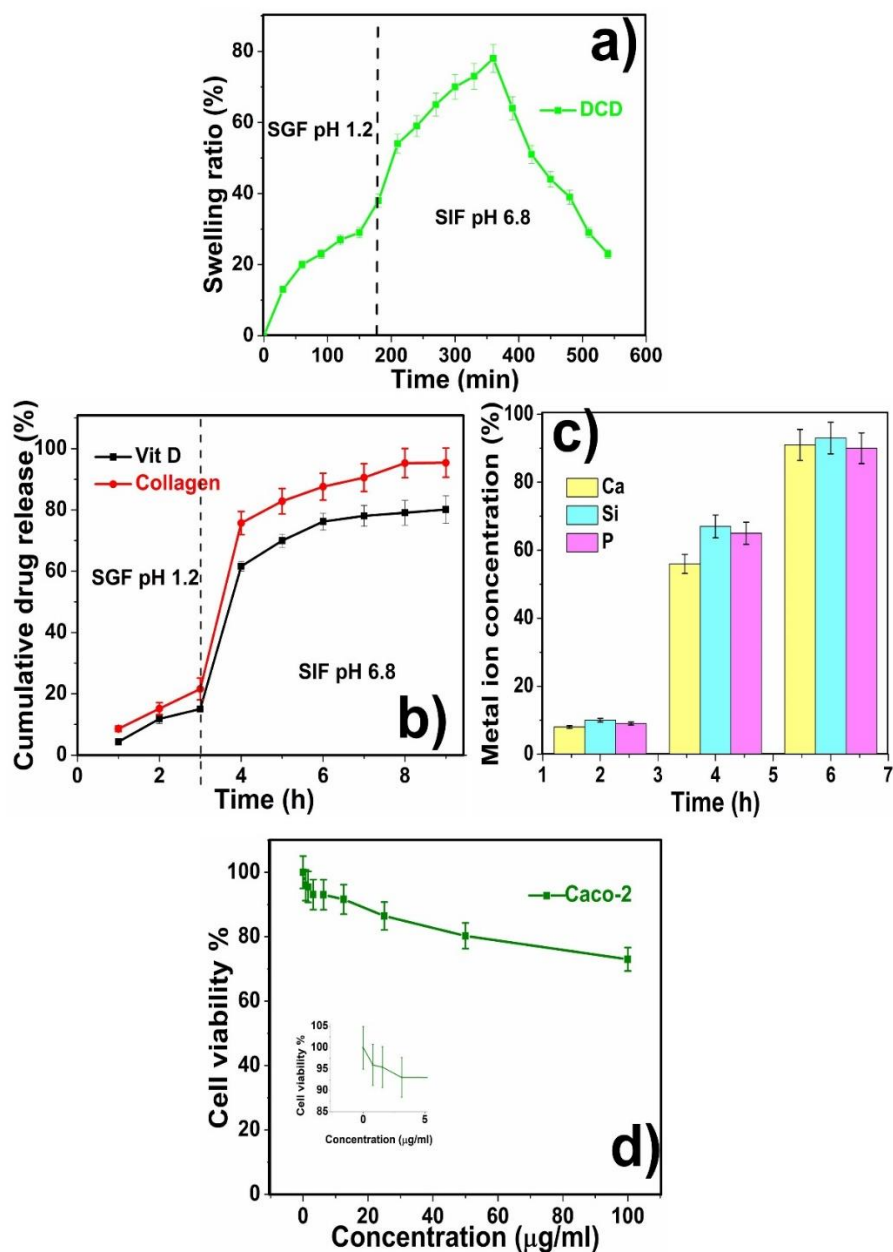
Fig3.6 a) Percentage swelling of DCD as a function of time in SGF at pH 1.2 & in SIF at pH 6.8. b) Cumulative release % with time intervals at pH 1.2 & 6.8 c) Release of metal ions from BG network in DCD with an increase in time interval d) Cytotoxicity test of DCD at different concentrations using Caco-2 cell lines. Each datum point is expressed as the average of triplicate observations and the error bars represent corresponding standard deviations.

*3.3.8    MTT assay*

Cellular viability is a vital tool for an oral delivery system to promote drug delivery and drug dissolution [72]. One of the main intents of this study was to assess the biocompatibility of the BG network on intestinal cells as maximum absorption occurs through the intestinal region. As the aim is to deliver BG particles along with collagen and Vit D, the MTT assay was performed in DCD film at a varying concentration (0.5 µg/ml to 100 µg/ml) on Caco-2 cell lines. The assay was carried out after 24 h exposure of the sample to the cell lines and the results are displayed in Fig 6c. From the fig, it can be seen that the viability of cell lines was above 80 % for the complete concentration range. The inserted graph in the image shows the magnified range from 0.5 µg/ml to 5 µg/ml proclaiming approximately 95 % viability. These results are highly encouraging to employ these films for oral delivery applications and follow earlier reported work [56,73].

*3.3.9    SDS-PAGE for protein analysis*

Dextran is considered to be the promising polymer vehicle for the colon-targeted delivery of proteins. Therefore, to elucidate the role of dextran in the controlled targeted release of collagen at the colon site, two separate gels were run having protein samples released from CBG and DCD respectively at different pH (SGF & SIF). M represents the protein latter in the SDS-PAGE profile (Fig. 7). As depicted in Fig. 7a & 7b, pure collagen designated as C and CBG exhibited a typical collagen protein profile having α1 and α2 chains with a molecular weight of about 100 kDa as a major component. These findings have also been reported earlier that fish collagen comprises two or more different chains (typically α1 & α2) around 97-100 kDa [74–76]. In Fig. 7a, Columns 1 to Column 3 (depicted as numeric 1, 2, & 3) have protein samples released in SGF after consecutive 3 h, and columns 4 to column 7 (numeric depictions 4, 5, 6, & 7) have protein samples released in SIF after consecutive 4 h. Thus, from the SDS

profile, the release of collagen is evident in SGF for CBG samples. But for DCD, the protein bands exist only in SIF samples as shown in Fig. 7b columns 1 to 3. The absence of protein band in SGF in DCD might be attributed due to the feeble amount of protein as depicted in the release assay also (Fig. 6b). Hence, it can be inferred that dextran can be used as the fundamental polysaccharide for colon-targeted protein delivery as colon microflora contain dextranase enzyme that helps in the degradation of dextran [37,77] and thereby resulting in protein release. It is important to note that the released collagen retained its primary structure when compared to native collagen(C ) in harsh GI tract environments.
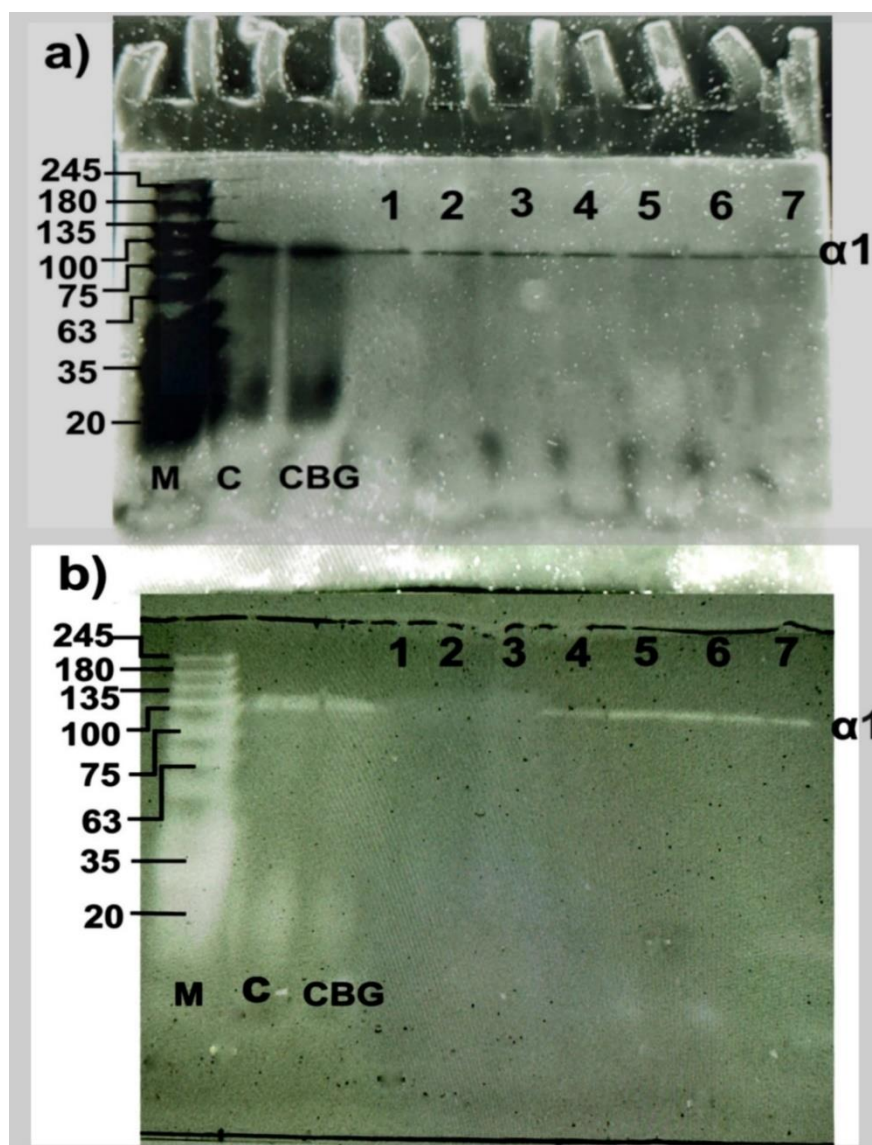
Fig.3.7 a) SDS-PAGE profile in the absence of sandwich layer of dextran b) SDS-PAGE profile in the presence of sandwich layer of dextran

### 3.3.10 Disintegration studies

As depicted in Fig. 8c, major disintegration or erosion of the film started after 6 h and reaches a maximum of 80 % showcasing maximum weight loss of dextran and collagen due to the dissolution of DCD during swelling at intestinal pH and by the enzymatic action of dextranase and proteases respectively. Near about 18 % remains of DCD film show the residence of inorganic matter of the BG network. The surface morphological difference can be seen after soaking and dissolution of the said film in SIF at pH 6.8 in Fig 8a. The formation of an apatite-like crystal can be visualized in SEM. This may correspond to the hydroxyapatite (HAP) formation over the BG network as BG tends to show bioactivity when present in simulated body fluid [19,78]. The elemental presence of Si, P, Ca, and O as depicted in EDAX spectra (inserted in Fig 8a) substantiates the formation of HAP. FTIR spectra (Fig. 8d) also validate the aforementioned findings with new peaks observed at 580 cm$^{-1}$ and 1069 cm$^{-1}$ corresponding to P-O peaks after DCD disintegration in SIF [79]. Also, the peaks at 1465 cm$^{-1}$ and 807 cm$^{-1}$ indicate the formation of carbonate apatite [2]. Therefore, it can be inferred from precedent data that the major organic portion of the film was dissolved in SIF persisting inorganic content of HAP formed during the bioactivity of the BG network. Analysis from ICP-MS (fig.8b) of the SIF fluid after disintegration showed that the presence of Si has increased and that of P decreased confirming the dissolution of silica network during disintegration and formation of HAP [80].
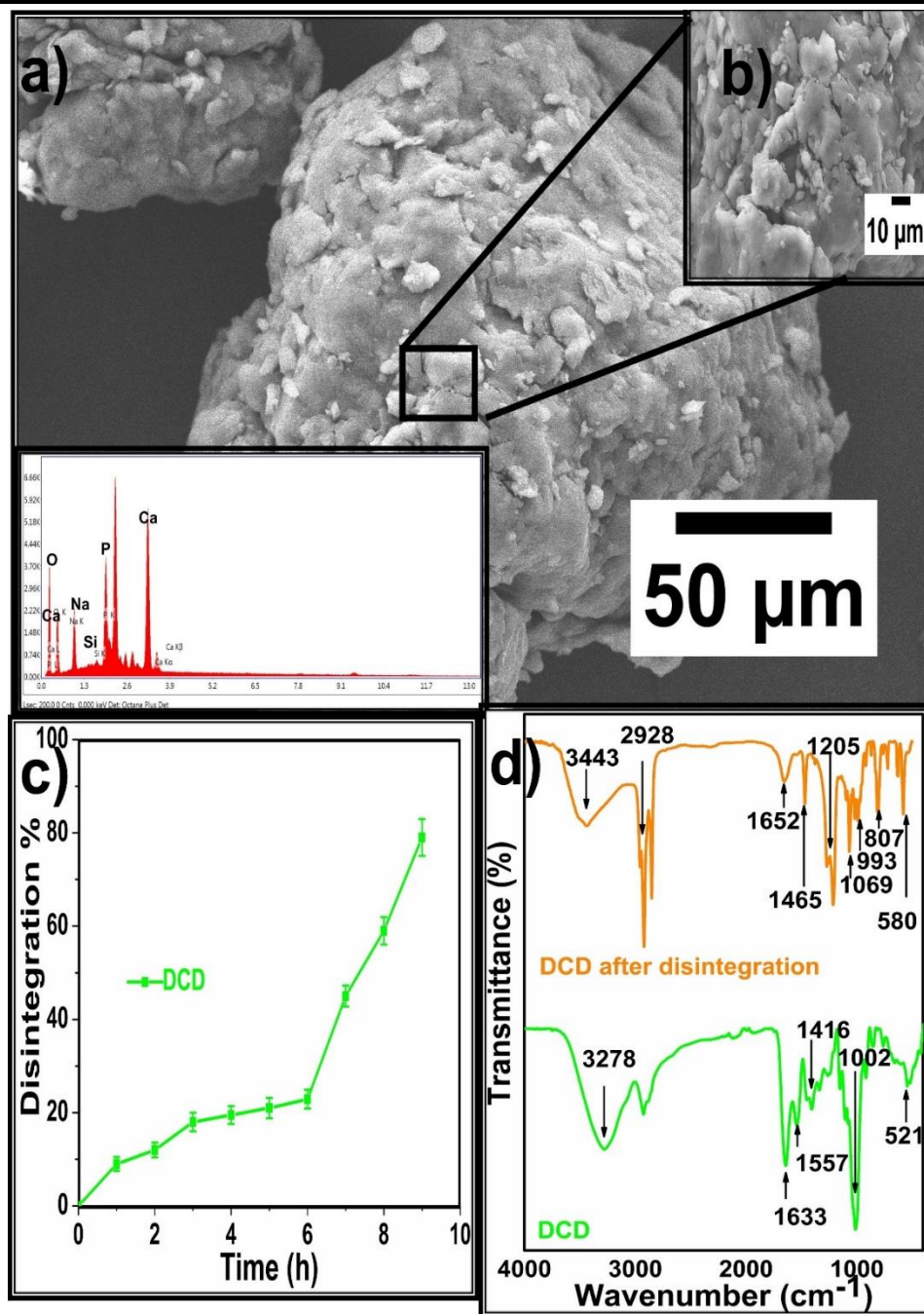
Fig.3.8 a) SEM image of DCD after disintegration at 50 X, along with EDAX spectra c) Disintegration % of DCD with respect to time. d) FTIR spectra of DCD before and after degradation.

## 3.4    Conclusion

This investigation is strongly evident in the delivery of collagen and Vit D to the colon-targeted site using dextran as a controlled drug delivery system. The SDS-PAGE release profile

corroborated with drug release data signifying targeted nutrient delivery. The formed films are found to be visco-elastic. *In-situ* mineralization of the BG network imparts more thermal stability to the sandwiched film due to the intercalation of BG into collagen fibrils. The key features possessed by the film include pH sensitivity, enzyme specificity, biocompatibility, biodegradability, and bioactivity. These attributes thus make it an efficient controlled drug delivery system.

**References:**

[1]     X. Feng, Chemical and Biochemical Basis of Cell-Bone Matrix Interaction in Health and Disease, Curr. Chem. Biol. 3 (2012) 189–196. https://doi.org/10.2174/2212796810903020189.

[2]     R. Florencio-Silva, G.R.D.S. Sasso, E. Sasso-Cerri, M.J. Simões, P.S. Cerri, Biology of Bone Tissue: Structure, Function, and Factors That Influence Bone Cells, Biomed Res. Int. 2015 (2015). https://doi.org/10.1155/2015/421746.

[3]     S.N. Deshmukh, A.M. Dive, R. Moharil, P. Munde, Enigmatic insight into collagen, J. Oral Maxillofac. Pathol. 20 (2016) 276–283. https://doi.org/10.4103/0973-029X.185932.

[4]     M. Yazaki, Y. Ito, M. Yamada, S. Goulas, S. Teramoto, M. aki Nakaya, S. Ohno, K. Yamaguchi, Oral Ingestion of Collagen Hydrolysate Leads to the Transportation of Highly Concentrated Gly-Pro-Hyp and Its Hydrolyzed Form of Pro-Hyp into the Bloodstream and Skin, J. Agric. Food Chem. 65 (2017) 2315–2322. https://doi.org/10.1021/acs.jafc.6b05679.

[5]     R.M. Bielemann, J. Martinez-Mesa, D.P. Gigante, Physical activity during life course and bone mass: A systematic review of methods and findings from cohort studies with young adults, BMC Musculoskelet. Disord. 14 (2013). https://doi.org/10.1186/1471-2474-14-77.

[6]     S.F. Chastin, O. Mandrichenko, D.A. Skelton, The frequency of osteogenic activities and the pattern of intermittence between periods of physical activity and sedentary behaviour affects bone mineral content: The cross-sectional NHANES study, BMC

Public Health. 14 (2014). https://doi.org/10.1186/1471-2458-14-4.

[7]     J.H. Park, J.H. Moon, H.J. Kim, M.H. Kong, Y.H. Oh, Sedentary Lifestyle: Overview of Updated Evidence of Potential Health Risks, Korean J. Fam. Med. 41 (2020) 365–373. https://doi.org/10.4082/KJFM.20.0165.

[8]     A.G.A.G. M, The effect of exercise and nutrition on the mechanostat, J. Musculoskelet. Neuronal Interact. 5 (2005) 239–254. https://doi.org/10.4103/jmsr.jmsr.

[9]     C.T. Price, J.R. Langford, F.A. Liporace, Essential Nutrients for Bone Health and a Review of their Availability in the Average North American Diet, Open Orthop. J. 6 (2012) 143–149. https://doi.org/10.2174/1874325001206010143.

[10]    J.B. Driban, M.S. Harkey, S.-H. Liu, M. Salzler, T.E. McAlindon, Osteoarthritis and Aging: Young Adults with Osteoarthritis, Curr. Epidemiol. Reports. 7 (2020) 9–15. https://doi.org/10.1007/s40471-020-00224-7.

[11]    A. Mobasheri, A. Mahmoudian, U. Kalvaityte, I. Uzieliene, C.E. Larder, M.M. Iskandar, S. Kubow, P.C. Hamdan, C.S. de Almeida, L.J. Favazzo, L.J.C. van Loon, P.J. Emans, P.G. Plapler, M.J. Zuscik, A White Paper on Collagen Hydrolyzates and Ultrahydrolyzates: Potential Supplements to Support Joint Health in Osteoarthritis?, Curr. Rheumatol. Rep. 23 (2021). https://doi.org/10.1007/s11926-021-01042-6.

[12]    D.R. Coates, J.M. Chin, S.T.L. Chung, 基因的改变NIH Public Access, Bone. 23 (2011) 1–7. https://doi.org/10.1002/art.34453.Osteoarthritis.

[13]    T. Sozen, L. Ozisik, N. Calik Basaran, An overview and management of osteoporosis, Eur. J. Rheumatol. 4 (2017) 46–56. https://doi.org/10.5152/eurjrheum.2016.048.

[14]    D.M. Reilly, J. Lozano, Skin collagen through the lifestages: importance for skin

health and beauty, Plast. Aesthetic Res. 2021 (2021). https://doi.org/10.20517/2347-9264.2020.153.

[15]    F. Pouresmaeili, B. Kamalidehghan, M. Kamarehei, Y.M. Goh, A comprehensive overview on osteoporosis and its risk factors, Ther. Clin. Risk Manag. 14 (2018) 2029–2049. https://doi.org/10.2147/TCRM.S138000.

[16]    S. Stevenson, J. Thornton, Effect of estrogens on skin aging and the potential role of SERMs., Clin. Interv. Aging. 2 (2007) 283–297. https://doi.org/10.2147/cia.s798.

[17]    A. Birkenmaier, TRANsPARENCIA DEL sUBcoNscENTE: EscRTURA AUTOMÁTICA, Rev. Iberoam. 74 (2008) 685–701. https://doi.org/10.3945/ajcn.111.031070.1.

[18]    K.J. Loud, C.M. Gordon, Adolescent bone health, Arch. Pediatr. Adolesc. Med. 160 (2006) 1026–1032. https://doi.org/10.1001/archpedi.160.10.1026.

[19]    H. Goel, N. Gupta, D. Santhiya, N. Dey, H.B. Bohidar, A. Bhattacharya, Bioactivity reinforced surface patch bound collagen-pectin hydrogel, Int. J. Biol. Macromol. 174 (2021) 240–253. https://doi.org/10.1016/j.ijbiomac.2021.01.166.

[20]    M.N. Rahaman, X. Liu, B.S. Bal, D.E. Day, L. Bi, L.F. Bonewald, Bioactive glass in bone tissue engineering, Ceram. Trans. 237 (2012) 73–82. https://doi.org/10.1002/9781118511466.ch8.

[21]    N. Al-Harbi, H. Mohammed, Y. Al-Hadeethi, A.S. Bakry, A. Umar, M.A. Hussein, M.A. Abbassy, K.G. Vaidya, G. Al Berakdar, E.M. Mkawi, M. Nune, Silica-based bioactive glasses and their applications in hard tissue regeneration: A review, Pharmaceuticals. 14 (2021) 1–20. https://doi.org/10.3390/ph14020075.

[22]    H. Goel, D. Santhiya, Role of Trigonella foenum-graecum leaf extract in tailoring the

synthesis and properties of bioactive glass nanoparticles, Sustain. Mater. Technol. 33 (2022) e00485. https://doi.org/10.1016/j.susmat.2022.e00485.

[23] M.M. Abeer, P. Rewatkar, Z. Qu, M. Talekar, F. Kleitz, R. Schmid, M. Lindén, T. Kumeria, A. Popat, Silica nanoparticles: A promising platform for enhanced oral delivery of macromolecules, J. Control. Release. 326 (2020) 544–555. https://doi.org/10.1016/j.jconrel.2020.07.021.

[24] N. Sreeharsha, M. Philip, S.S. Krishna, V. Viswanad, R.K. Sahu, P.N. Shiroorkar, A.H. Aasif, S. Fattepur, S.M.B. Asdaq, A.B. Nair, M. Attimarad, K.N. Venugopala, Multifunctional Mesoporous Silica Nanoparticles for Oral Drug Delivery, Coatings. 12 (2022). https://doi.org/10.3390/coatings12030358.

[25] X. Sun, J. Zhang, Z. Wang, B. Liu, S. Zhu, L. Zhu, B. Peng, Licorice isoliquiritigenin-encapsulated mesoporous silica nanoparticles for osteoclast inhibition and bone loss prevention, Theranostics. 9 (2019) 5183–5199. https://doi.org/10.7150/thno.33376.

[26] T. Kokubo, H. Takadama, How useful is SBF in predicting in vivo bone bioactivity?, Biomaterials. 27 (2006) 2907–2915. https://doi.org/10.1016/j.biomaterials.2006.01.017.

[27] A.L.B. Maçon, T.B. Kim, E.M. Valliant, K. Goetschius, R.K. Brow, D.E. Day, A. Hoppe, A.R. Boccaccini, I.Y. Kim, C. Ohtsuki, T. Kokubo, A. Osaka, M. Vallet-Regí, D. Arcos, L. Fraile, A.J. Salinas, A. V. Teixeira, Y. Vueva, R.M. Almeida, M. Miola, C. Vitale-Brovarone, E. Verné, W. Höland, J.R. Jones, A unified in vitro evaluation for apatite-forming ability of bioactive glasses and their variants, J. Mater. Sci. Mater. Med. 26 (2015) 1–10. https://doi.org/10.1007/s10856-015-5403-9.

[28] A.M. El-Kady, M.M. Farag, Bioactive Glass Nanoparticles as a New Delivery System

for Sustained 5-Fluorouracil Release: Characterization and Evaluation of Drug Release Mechanism, J. Nanomater. 2015 (2015). https://doi.org/10.1155/2015/839207.

[29]  G.B. Wasilewski, M.G. Vervloet, L.J. Schurgers, The Bone—Vasculature Axis: Calcium Supplementation and the Role of Vitamin K, Front. Cardiovasc. Med. 6 (2019) 1–16. https://doi.org/10.3389/fcvm.2019.00006.

[30]  K. Galior, S. Grebe, R. Singh, Development of vitamin d toxicity from overcorrection of vitamin D deficiency: A review of case reports, Nutrients. 10 (2018). https://doi.org/10.3390/nu10080953.

[31]  M.E. Cam, S. Yildiz, H. Alenezi, S. Cesur, G.S. Ozcan, G. Erdemir, U. Edirisinghe, D. Akakin, D.S. Kuruca, L. Kabasakal, O. Gunduz, M. Edirisinghe, Evaluation of burst release and sustained release of pioglitazone-loaded fibrous mats on diabetic wound healing: An in vitro and in vivo comparison study, J. R. Soc. Interface. 17 (2020). https://doi.org/10.1098/rsif.2019.0712.

[32]  M. Gautam, D. Santhiya, In-situ mineralization of calcium carbonate in pectin based edible hydrogel for the delivery of protein at colon, J. Drug Deliv. Sci. Technol. 53 (2019) 101137. https://doi.org/10.1016/j.jddst.2019.101137.

[33]  K. Lampropoulou-Adamidou, E. Karlafti, C. Argyrou, K. Makris, G. Trovas, I.A. Dontas, S. Tournis, I.K. Triantafyllopoulos, Effect of Calcium and Vitamin D Supplementation With and Without Collagen Peptides on Volumetric and Areal Bone Mineral Density, Bone Geometry and Bone Turnover in Postmenopausal Women With Osteopenia, J. Clin. Densitom. 25 (2022) 357–372. https://doi.org/10.1016/j.jocd.2021.11.011.

[34]  S. Mende, M. Peter, K. Bartels, T. Dong, H. Rohm, D. Jaros, Concentration dependent

effects of dextran on the physical properties of acid milk gels, Carbohydr. Polym. 98 (2013) 1389–1396. https://doi.org/10.1016/j.carbpol.2013.07.072.

[35]   P. K. Shrivastava, S. K. Shrivastava, Dextran Carrier Macromolecule for Colon Specific Delivery of Celecoxib, Curr. Drug Deliv. 7 (2010) 144–151. https://doi.org/10.2174/156720110791011828.

[36]   N. van der Wielen, P.J. Moughan, M. Mensink, Amino acid absorption in the large intestine of humans and porcine models, J. Nutr. 147 (2017) 1493–1498. https://doi.org/10.3945/jn.117.248187.

[37]   S. Amidon, J.E. Brown, V.S. Dave, Colon-Targeted Oral Drug Delivery Systems: Design Trends and Approaches, AAPS PharmSciTech. 16 (2015) 731–741. https://doi.org/10.1208/s12249-015-0350-9.

[38]   S. Bourgeois, R. Harvey, E. Fattal, Polymer colon drug delivery systems and their application to peptides, proteins, and nucleic acids, Am. J. Drug Deliv. 3 (2005) 171–204. https://doi.org/10.2165/00137696-200503030-00003.

[39]   J.M. Maurer, R.C.A. Schellekens, H.M. Van Rieke, C. Wanke, V. Iordanov, F. Stellaard, K.D. Wutzke, G. Dijkstra, M. Van Der Zee, H.J. Woerdenbag, H.W. Frijlink, J.G.W. Kosterink, Gastrointestinal pH and transit time profiling in healthy volunteers using the IntelliCap system confirms ileo-colonic release of ColoPulse tablets, PLoS One. 10 (2015) 1–17. https://doi.org/10.1371/journal.pone.0129076.

[40]   R. Naomi, H. Bahari, P.M. Ridzuan, F. Othman, Natural-Based Biomaterial for Skin Wound Healing ( Gelatin vs . Collagen ): Expert Review, (2021) 1–20.

[41]   D.U. Tulyaganov, E. Fiume, A. Akbarov, N. Ziyadullaeva, S. Murtazaev, A. Rahdar, J. Massera, E. Verné, F. Baino, In Vivo Evaluation of 3D-Printed Silica-Based Bioactive

Glass Scaffolds for Bone Regeneration, J. Funct. Biomater. 13 (2022). https://doi.org/10.3390/jfb13020074.

[42]    R.T. Rosen, R.D. Hiserodt, E.K. Fukuda, R.J. Ruiz, Z. Zhou, J. Lech, S.L. Rosen, T.G. Hartman, Determination of allicin, S-allylcysteine and volatile metabolites of garlic in breath, plasma or simulated gastric fluids, J. Nutr. 131 (2001) 968–971. https://doi.org/10.1093/jn/131.3.968s.

[43]    S.G. Nugent, D. Kumar, D.S. Rampton, D.F. Evans, Intestinal luminal pH in inflammatory bowel disease: Possible determinants and implications for therapy with aminosalicylates and other drugs, Gut. 48 (2001) 571–577. https://doi.org/10.1136/gut.48.4.571.

[44]    N. Gupta, D. Santhiya, In situ mineralization of bioactive glass in gelatin matrix, Mater. Lett. 188 (2017) 127–129. https://doi.org/10.1016/j.matlet.2016.11.045.

[45]    J. Cihlář, Hydrolysis and polycondensation of ethyl silicates. 1. Effect of pH and catalyst on the hydrolysis and polycondensation of tetraethoxysilane (TEOS), Colloids Surfaces A Physicochem. Eng. Asp. 70 (1993) 239–251. https://doi.org/10.1016/0927-7757(93)80298-S.

[46]    N. Ahmad, M.C.I.M. Amin, S.M. Mahali, I. Ismail, V.T.G. Chuang, Biocompatible and mucoadhesive bacterial cellulose-g-poly(acrylic acid) hydrogels for oral protein delivery, Mol. Pharm. 11 (2014) 4130–4142. https://doi.org/10.1021/mp5003015.

[47]    M. Gautam, D. Santhiya, N. Dey, Zein coated calcium carbonate nanoparticles for the targeted controlled release of model antibiotic and nutrient across the intestine, Mater. Today Commun. 25 (2020) 101394. https://doi.org/10.1016/j.mtcomm.2020.101394.

[48]    H. Peng, S. Chen, M. Luo, F. Ning, X. Zhu, H. Xiong, Preparation and self-assembly

mechanism of bovine serum albumin-citrus peel pectin conjugated hydrogel: A potential delivery system for Vitamin C, J. Agric. Food Chem. 64 (2016) 7377–7384. https://doi.org/10.1021/acs.jafc.6b02966.

[49]    R. pour Nouroozi, Determination of Protein Concentration Using Bradford Microplate Protein Quantification Assay, Int. Electron. J. Med. 4 (2015) 11–17. https://doi.org/10.31661/iejm158.

[50]    D. Dhinasekaran, S. Vimalraj, A.R. Rajendran, S. Saravanan, B. Purushothaman, B. Subramaniam, Bio-inspired multifunctional collagen/electrospun bioactive glass membranes for bone tissue engineering applications, Mater. Sci. Eng. C. 126 (2021) 111856. https://doi.org/10.1016/j.msec.2020.111856.

[51]    S. Kamiloglu, G. Sari, T. Ozdal, E. Capanoglu, Guidelines for cell viability assays, Food Front. 1 (2020) 332–349. https://doi.org/10.1002/fft2.44.

[52]    M. Kaur, D. Santhiya, Fabrication of soy film with in-situ mineralized bioactive glass as a functional food for bone health, Food Biosci. 47 (2022) 101767. https://doi.org/10.1016/j.fbio.2022.101767.

[53]    E. Teodor, S.C. Liţescu, C. Petcu, M. Mihalache, R. Somoghi, Nanostructured biomaterials with controlled properties synthesis and characterization, Nanoscale Res. Lett. 4 (2009) 544–549. https://doi.org/10.1007/s11671-009-9278-x.

[54]    S. El Moujahed, F. Errachidi, H. Abou Oualid, A.V. Botezatu-Dediu, F. Ouazzani Chahdi, Y. Kandri Rodi, R.M. Dinica, Extraction of insoluble fibrous collagen for characterization and crosslinking with phenolic compounds from pomegranate byproducts for leather tanning applications, RSC Adv. 12 (2022) 4175–4186. https://doi.org/10.1039/d1ra08059h.

[55]     R.I. Litvinov, D.A. Faizullin, Y.F. Zuev, J.W. Weisel, The α-helix to β-sheet transition in stretched and compressed hydrated fibrin clots, Biophys. J. 103 (2012) 1020–1027. https://doi.org/10.1016/j.bpj.2012.07.046.

[56]     P. Nikpour, H. Salimi-kenari, F. Fahimipour, S. Mahmood, Dextran hydrogels incorporated with bioactive glass-ceramic : Nanocomposite sca ff olds for bone tissue engineering, Carbohydr. Polym. 190 (2018) 281–294. https://doi.org/10.1016/j.carbpol.2018.02.083.

[57]     E. Fathi, N. Atyabi, M. Imani, Z. Alinejad, Physically crosslinked polyvinyl alcohol-dextran blend xerogels: Morphology and thermal behavior, Carbohydr. Polym. 84 (2011) 145–152. https://doi.org/10.1016/j.carbpol.2010.11.018.

[58]     M. Mozafari, M. Rabiee, M. Azami, S. Maleknia, Biomimetic formation of apatite on the surface of porous gelatin/bioactive glass nanocomposite scaffolds, Appl. Surf. Sci. 257 (2010) 1740–1749. https://doi.org/10.1016/j.apsusc.2010.09.008.

[59]     S. Singh, B. Gupta, Physicochemical characteristics of glycerol-plasticized dextran / soy protein isolate composite membranes, 43847 (2016) 1–9. https://doi.org/10.1002/app.43847.

[60]     M. Gordic, G. Cabrera-barjas, A. Nesic, Dextran-Based Edible Coatings to Prolong the Shelf Life of Blueberries, (2021).

[61]     Z. Wang, S. Hu, H. Wang, Scale-Up Preparation and Characterization of Collagen / Sodium Alginate Blend Films, 2017 (2017).

[62]     R. John, J. Mathew, A. Mathew, C.T. Aravindakumar, U.K. Aravind, Probing the Role of Cu(II) Ions on Protein Aggregation Using Two Model Proteins, ACS Omega. 6 (2021) 35559–35571. https://doi.org/10.1021/acsomega.1c05119.

[63]    A. Pourjavadi, M. Kurdtabar, Collagen-based highly porous hydrogel without any porogen: Synthesis and characteristics, Eur. Polym. J. 43 (2007) 877–889. https://doi.org/10.1016/j.eurpolymj.2006.12.020.

[64]    K.E. Drzewiecki, D.R. Grisham, A.S. Parmar, V. Nanda, D.I. Shreiber, Circular Dichroism Spectroscopy of Collagen Fibrillogenesis: A New Use for an Old Technique, Biophys. J. 111 (2016) 2377–2386. https://doi.org/10.1016/j.bpj.2016.10.023.

[65]    J. Turnay, N. Olmo, M. Gasset, I. Iloro, J.L.R. Arrondo, M. Antonia Lizarbe, Calcium-dependent conformational rearrangements and protein stability in chicken annexin A5, Biophys. J. 83 (2002) 2280–2291. https://doi.org/10.1016/S0006-3495(02)73988-X.

[66]    D. Corrêa, C. Ramos, The use of circular dichroism spectroscopy to study protein folding, form and function, African J Biochem Res. 3 (2009) 164–173. http://www.academicjournals.org/AJBR/PDF/Pdf2009/May/Special Issue/Corrêa  and Ramos.pdf.

[67]    Y. Wei, A.A. Thyparambil, R.A. Latour, Protein helical structure determination using CD spectroscopy for solutions with strong background absorbance from 190 to 230 nm, Biochim. Biophys. Acta - Proteins Proteomics. 1844 (2014) 2331–2337. https://doi.org/10.1016/j.bbapap.2014.10.001.

[68]    A. Lippacher, R.H. Müller, K. Mäder, Preparation of semisolid drug carriers for topical application based on solid lipid nanoparticles, Int. J. Pharm. 214 (2001) 9–12. https://doi.org/10.1016/S0378-5173(00)00623-2.

[69]    S.A.A. Aziz, S.A. Mazlan, U. Ubaidillah, N. Mohamad, M. Sedlacik, N.A. Nordin, N. Nazmi, Loss factor behavior of thermally aged magnetorheological elastomers,

Materials (Basel). 14 (2021). https://doi.org/10.3390/ma14174874.

[70]   W.J. Znidarsic, I.W. Chen, V.P. Shastri, ζ-potential characterization of collagen and bovine serum albumin modified silica nanoparticles: A comparative study, J. Mater. Sci. 44 (2009) 1374–1380. https://doi.org/10.1007/s10853-008-2998-y.

[71]   R. Shah, N. Saha, P. Saha, Influence of temperature, pH and simulated biological solutions on swelling and structural properties of biomineralized (CaCO3) PVP–CMC hydrogel, Prog. Biomater. 4 (2015) 123–136. https://doi.org/10.1007/s40204-015-0043-1.

[72]   M. Vedhanayagam, S. Anandasadagopan, B.U. Nair, K.J. Sreeram, Polymethyl methacrylate (PMMA) grafted collagen scaffold reinforced by PdO–TiO2 nanocomposites, Mater. Sci. Eng. C. 108 (2020). https://doi.org/10.1016/j.msec.2019.110378.

[73]   L. Musilová, E. Achbergerová, L. Vítková, R. Kolaˇ, M. Martínková, A. Mráˇ, Cross-Linked Gelatine by Modified Dextran as a Potential Bioink Prepared by a Simple and Non-Toxic Process, (2022) 1–16.

[74]   M.J. Seixas, E. Martins, R.L. Reis, T.H. Silva, Extraction and Characterization of Collagen from Elasmobranch Byproducts for Potential Biomaterial Use, Mar. Drugs. 18 (2020) 1–18. https://doi.org/10.3390/md18120617.

[75]   V. Shanmugam, Extraction, structural and physical characterization of type I collagen from the outer skin of Sepiella inermis (Orbigny, 1848), African J. Biotechnol. 11 (2012). https://doi.org/10.5897/ajb12.444.

[76]   C.G. Sotelo, M.B. Comesaña, P.R. Ariza, R.I. Pérez-Martín, Characterization of Collagen from Different Discarded Fish Species of the West Coast of the Iberian

Peninsula, J. Aquat. Food Prod. Technol. 25 (2016) 388–399.

https://doi.org/10.1080/10498850.2013.865283.

[77]   V.R. Sinha, R. Kumria, Polysaccharides in colon-specific drug delivery, Int. J. Pharm.

224 (2001) 19–38. https://doi.org/10.1016/S0378-5173(01)00720-7.

[78]   Z. Tabia, K. El Mabrouk, M. Bricha, K. Nouneh, Mesoporous bioactive glass

nanoparticles doped with magnesium: Drug delivery and acellular: In vitro bioactivity,

RSC Adv. 9 (2019) 12232–12246. https://doi.org/10.1039/c9ra01133a.

[79]   C. Wu, W. Fan, J. Chang, Functional mesoporous bioactive glass nanospheres:

Synthesis, high loading efficiency, controllable delivery of doxorubicin and inhibitory

effect on bone cancer cells, J. Mater. Chem. B. 1 (2013) 2710–2718.

https://doi.org/10.1039/c3tb20275e.

[80]   N. Rocton, H. Oudadesse, B. Lefeuvre, H. Peisker, K. Rbii, Fine analysis of interaction

mechanism of bioactive glass surface after soaking in SBF solution: AFM and ICP-

OES investigations, Appl. Surf. Sci. 505 (2020) 144076.

https://doi.org/10.1016/j.apsusc.2019.144076.

# Chapter 4

# Fabrication of soy film with in-situ mineralized bioactive glass as a functional food for bone health
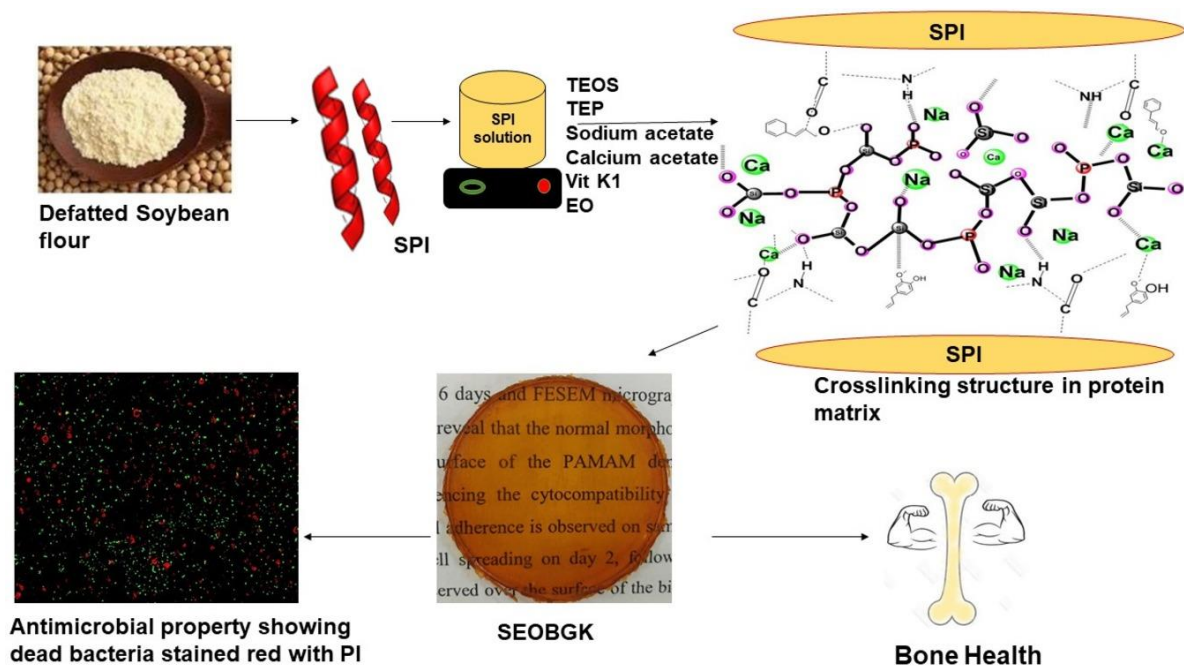
# Chapter 3

# Fabrication of soy film with *in-situ* mineralized bioactive glass as a functional food for bone health

**4.1 Introduction**:

Bone health plays a vital role in the overall well-being of our life. Bones not just help in movement and locomotion but also supports our body infrastructure by protecting internal organs. For a jovial and healthful lifestyle, bones need to be strong, flexible, and healthy. With the increase in bone health issues including low bone mass density, Osteoporosis (OP), and Osteomalacia, by 2030, the number of individuals affected by OP and low bone density will increase to 71.2 million (a 29% increase from 2010) [1]. Various health supplements such as Calcium (Ca), vitamin D, etc. are available in the market for bone well-being. Besides Ca and vitamin D, there exist other micro-and macronutrients that are considered essential for bone health. These include Magnesium (Mg), Phosphorous (P), Silicon (Si), vitamin K, and proteins [2]. Proteins are considered as building blocks of our body and bone mass loss may be influenced by the protein diet. After the approval of the US Food & Drug Administration (FDA) claiming cholesterol-lowering properties of soy protein in 1999 [3,4], similar health petitions for soy protein were approved by other countries including Malaysia, the United Kingdom, Brazil, etc. [5]. Therefore, Soy protein (plant-based protein) is considered a complete protein as it contains all the essential amino acids required in a balanced diet to promote good health [6]. This protein also contains various types of isoflavones which are known to be plant-based phytoestrogens [3]. The amount of isoflavones present in soy protein isolate after its extraction from soybean flour accounts to be approximately 26% namely genistein, daidzein, etc.[7]. Inquisitive findings show that soy protein and its isoflavones have a positive effect on bone

mass density [8]. When it comes to fat-soluble vitamin K, some shreds of evidence suggest a key role of it in keeping up bone health as it is associated with carboxylation of the bone-related protein osteocalcin [9]. Bones are made of both organic and inorganic portions i.e. proteins and minerals. To have a grip on bone disorders and bone-related issues, not just a protein diet is to be restored but also bone mineralization is to be considered. Bone mineralization is the process of filling calcium phosphate nanocrystals into the organic segment of the bone matrix [10]. Osteo-malacia often called soft bones is associated with decreased mineralization of bones. A bone framework is a reserve of minerals including Ca, P, Mg, Si (Ca being the most abundant). With senescence, bone mineral content decreases causing various bone-related problems. In recent advancements in biomaterials, bioactive glass (BG) being osteo-inductive and osteoconductive, has received great attention for treating bone defects. Investigation shows that the dissolution of BG particles enhances osteoblast attachment and bone mineralization [11]. First introduced in 1969, this FDA-approved BG [12] has revolutionized the biomaterial research and healthcare sector for its potential to support new bone tissue growth, to show cellular attachment to surrounding soft and hard tissues, and to form hydroxyapatite-like material in *in-vitro* and *in-vivo* conditions showing bioactivity. These attributes make BG worthy for treating bone-related ailments [13].

Taking into account all the possible ways to provide nutrition to the bone for overall good bone health in the form of food supplements, the present work aims to fabricate protein film that can act as a functional food to provide nourishment to the bone. According to International Food Information Council (IFIC), functional foods can be defined as the foods or dietary components that may provide a health benefit to an individual beyond providing basic nutrition [14–16]. The incorporation of vitamins, probiotics, bioactive compounds, antioxidants, etc. within the food system can offer great benefits. Functional foods and food supplements reinforced with nutraceutical compounds are found to be effective in preventing various chronic diseases such

as diabetes, obesity, cardiovascular disorder, cancer, inflammation, etc. [15]. To the best of our knowledge, it is the first time that soy films have been fabricated as a functional food along with *in-situ* mineralized BG network and vitamin K1 for bone growth. The purpose of formulating these protein films is to provide all the essential minerals i.e., Ca, P, Si to the bone along with soy protein that promises a positive effect on bone metabolism. To avoid microbial contamination to chewy films, essential oils (EOs), herein cinnamon oil and clove oil have been incorporated. EOs are classified as GRAS (Generally considered as Safe) [17]. These are secondary plant metabolites comprising volatile compounds that exhibit elemental properties including antibacterial, antiviral, antifungal, anti-inflammatory, antioxidant, analgesic, etc. Furthermore, the presence of eugenol and cinnamaldehyde present in clove oil and cinnamon oil contributes to osteoblastogenesis [18,19] and have been known to show inhibitory effects against osteoclast activity, subsequently leading to an increase in bone mineral density [20]. For the film formation, soy protein is extracted from soybean flour and protein identification is carried out using LC-MS. Also, the protein estimation is performed using the Kjeldahl method. The nutritional analysis of the soy film formed is done by standard test methods (AOAC- Association of Official Analytical Chemists, IS test methods) followed by thorough characterizations including XRD, TGA, and FTIR. The mineralization of the BG network in the soy films is confirmed by SEM/ EDAX. The microstructure and the mechanical stability of soy-based films under stress are studied through rheological studies and dynamic mechanical analyzer (DMA) respectively. The swelling capacity of the films is studied which plays an important role to study the diffusion of nutrients. Further, the films are subjected to *in-vitro* antimicrobial testing using fluorescent microscopy and disk diffusion assay.

**4.2 Experimental Section**

*4.2.1   Materials*

For the preparation of the film, defatted soybean flour in powder form with 97 - 99% purity, essential oils (EOs) (Cinnamon oil, product number-W229105 and clove oil, product number-C8392), glycerol, precursors for *in-situ* mineralization of BG particles namely triethyl orthosilicate (TEOS), triethyl phosphate (TEP), sodium acetate, calcium acetate monohydrate, and vitamin K1 were purchased from Sigma-Aldrich, USA. Live/Dead Baclight bacterial viability kit for the antimicrobial assay was purchased from Thermo Fischer Scientific. Test microorganisms, namely *Escherichia coli* (*E. coli*) and *Staphylococcus aureus* (*S.aureus*) were obtained from National Centre for Microbial Resource, Pune, India. Milli Q water was used for all the experimental work and all other reagents used in this study were of analytical reagent (AR) grade *of high purity.*

*4.2.2   Methods*

*4.2.2.1 Extraction of soy protein isolate (SPI) from soybean flour*

Defatted soybean flour was suspended in 0.1N NaOH solution (1:20 w/v) and kept for stirring for 30 min at room temperature i.e. 25 °C. The suspension was then centrifuged at 10,000 × g for 10 min. The supernatant was then adjusted to pH 4.5 for isoelectric precipitation of the soy protein by adding 0.1 N HCl. Finally, the suspension containing protein precipitate was centrifuged at 10,000 × g for 10 min. The protein thus obtained was washed with Milli Q water and the pH was adjusted to 7 and was freeze-dried. This extracted freeze-dried protein sample was named SPI.

*4.2.2.2 Characterization techniques for extracted protein sample*

*4.2.2.2.1 Protein Determination:*

The protein content from the SPI extract was determined using the Kjeldahl method using the nitrogen conversion factor of 6.25 for protein determination. The detailed procedure can be found in ESI S3. The extracted protein percentage may be expressed as equation 1:

% protein = N × F    (where N is % $N_2$ and F is the protein factor i.e. 6.25)               (1)

% $N_2$ = [(T – B) ×N×14×100]/ weight of sample in mg               (2)

Where T= Volume of HCl consumed in sample titration

B= Volume of HCl consumed blank titration

N= Normality of HCl

Molecular weight of $N_2$= 14 g

### 4.2.2.2.2 *Sodium dodecyl sulfate-polyacrylamide gel electrophoresis (SDS-PAGE):*

SPI was characterized by SDS-PAGE to analyze its molecular weight (k Da) based on the method of Laemmli [21]. Reducing SDS-PAGE was performed on a discontinuous buffered system using 12% resolving gel and 5% stacking gel. The SPI solution (2 mg/ml) was prepared with SDS sample buffer (1.5 M Tris-HCl, pH 8.8), 20% (v/v) glycerol, 10% (w/v) 2-mercaptoethanol, 4% Sodium dodecyl sulfate) 0.004% (w/v) Bromophenol blue. An aliquot (15μl) of the sample solution was loaded per well after incubating with the loading buffer at 95 ° C for 5 min. The gel was stained with Coomassie Brilliant Blue R-250 for 1 h and destained into 20% methanol and 10% acetic acid mixed solution. The gel was scanned and analyzed by iBright CL750 Imaging System (Thermo Fischer Scientific). Before running the gel electrophoresis, the SPI solution was dialyzed (using dialysis tubing cellulose membrane D9277, Sigma Aldrich) in dialysis buffer for 48 h at 4 °C.

*4.2.2.2.3 Protein Identification by LC-MS (Liquid Chromatography-Mass Spectrometry):*

20 µg of the extracted protein sample was analyzed on an Orbitrap Fusion™ Tribrid™ Mass Spectrometer coupled to a Thermo EASY-nLC 1200 system. The following test parameters were used for the analysis: Trypsin enzyme, peptide mass tolerance 10 ppm monoisotopic, fragment mass tolerance 0.6 Da, maximum of 2 missed cleavages, carbamidomethylation of a cysteine residue as a fixed modification. The data were confronted with the database NCBIprot20180818. The detailed procedure can be found in ESI S4.

*4.2.2.3 Film Fabrication*

Soy film was obtained by dissolving 5% SPI (w/v) in TRIZMA buffer at pH 8 with constant stirring at 45 °C for 60 min. After complete hydration and dissolution of SPI, BG precursors namely TEOS, TEP, sodium acetate, and calcium acetate monohydrate were sequentially added dropwise with an interval of 30 min with constant stirring and kept in a silicon oil bath for 24 h at 37 °C to synthesize bioglass as reported [22]. After 24 h, glycerol was added dropwise to the solution (SPI/glycerol weight ratio 5:1) and stirred continuously until a homogenous mixture was obtained. Subsequently, before adding EOs into the mixture, the o/w emulsion was prepared to have a 3:3:4 ratio of EOs i.e. clove oil & cinnamon oil in water respectively and then 120 µl of this mixture was added simultaneously to the homogenous solution of SPI followed by the dropwise addition of 20 µl of 0.1% of vitamin K1 stock solution. The mixture was continued to stir for 45 min and the film was prepared by solvent cast method and was named SEOBGK. This film was dried overnight in a hot air oven at 45 °C and was peeled off after complete drying. To elucidate the mechanism for the film formation and to study the effect of different constituents in the soy protein matrix, soy-based films were prepared at each successive step. These were named SF (containing SPI + glycerol), SEO (containing SPI + Glycerol + EOs), and the functional film SEOBGK (containing SPI + Glycerol + EOs + BG

network + Vitamin K1) while maintaining the weight percent of SPI in each film. The thickness (measured by precision micrometer) of SF and SEO films was $0.215 \pm 0.011$ mm each and for SEOBGK, it was $0.261 \pm 0.013$ mm. Differences were observed in thickness despite using the same weight percentage of SPI. This difference may have been due to the *in-situ* mineralization of the BG network in functional film SEOBGK.

*4.2.3 Characterization of the film*

*4.2.3.1. XRD*

XRD was performed on various soy-based films and SPI. Measurements were carried out with Rikagu Miniflex-II operating at 20 kV and a current of 10 mA using Cu-Kα radiations with a scanning range 2θ of $5^{\circ}$ to $90^{\circ}$ at 0.2 $^{\circ}$/min. A glass substrate was used to record the data.

*4.2.3.2. FTIR*

Dried samples of films were ground and mixed thoroughly with potassium bromide at the ratio of 1:100 and pelleted. The IR spectra of pellets were then recorded using the NICOLET 380 FTIR operating in the range of 4000-400 $cm^{-1}$ with a resolution of 4 $cm^{-1}$.

*4.2.3.3. TGA*

The thermal stability of the film samples was performed using TGA (TGA 4000, Perkin Elmer, USA). The samples were weighed approximately 5 mg and heated from 0 $^{\circ}$C to 700 $^{\circ}$C at a heating rate of 10 $^{\circ}$C/min in an $N_2$ gas flow of 50 ml/min.

*4.2.3.4. SEM*

The surface morphology of the film samples was studied with SEM (ZESIS EVO MA15). The samples were gold coated and then observed at an accelerating voltage of 5.0 kV at 10,000 magnifications.

*4.2.3.5. Rheological Properties*

The elaborated rheological analysis for SF and SEOBGK was carried out with an MCR 702, advanced rheometer, Anton Paar, Austria, loaded with Rheoplus Software using parallel plate (PP-40) geometry at a measuring distance of 1 mm at 37 °C. Shear viscosity was measured as a function of shear rate in the range of 0-1000 s$^{-1}$. Amplitude sweep studies were performed from 0.01 to 1000 strain % at 10 rad/s to find out the crossover point of storage (G') and loss (G") moduli that signify the sol-gel transition of the film. The mechanical deformation and flow behavior were measured by frequency sweep experiments which yielded storage modulus (G') and loss modulus (G") as a function of angular frequency ($\omega$) in the range of 0.1 to 100 rad/s at 0.1% strain to demonstrate the stability of the soy-based films. For each measurement, a freshly prepared soy film suspension was used and then degassed before pouring it into a parallel plate geometry instrument. The experiments were performed in triplicates.

*4.2.3.6 DMA*

Stress-strain measurements for SF and SEOBGK in the transient mode were studied using Q800 from TA instruments (USA) equipped with a DMA-RH attachment. The temperature was maintained at 23 °C – 25 °C and RH (relative humidity) at $50 \pm 4\%$. The films were conditioned before testing. Film strips were carefully mounted into a film tension clamp with a gauge length set at 15 mm and equilibrated at desired temperature and RH. A static force of 1 N/min was applied until breaking. For each film, 3 strips were tested and Young's Modulus (MPa) was taken as the initial slope of the stress-strain curve, the tensile strength, TS (MPa) was taken as the point of maximum stress on the curve and the elongation at break, EB (%) was taken as the strain when the film ruptured.

*4.2.3.7 Swelling studies*

The swelling studies on SF and SEOBGK were carried out by immersing both soy films (square-shaped, 5 cm× 5 cm) into SGF pH 1.2 for 3 h. After 3 h, samples were washed and transferred to SIF, pH 6.0, and the swelling experiment was continued in the same way for the next 3 h. Further, the swelling studies were carried out at SIF pH 6.8 depicting colonic pH for 3 h. Additionally, dynamic swelling of the films was carried out (alternatively 1 h in each solution) by immersing the films in SGF pH 1.2, and SIF pH 6.8. This procedure was repeated for 9 h. In all these studies, the swelling ratio was calculated gravimetrically [23]. The *in-vitro* disintegration studies for the SF and SEOBGK were examined in SIF pH 6.8 at 37 °C for 48 h. Herein, equal-sized soy film strips were sliced under aseptic conditions into a square shape (5 cm × 5 cm), were accurately weighed, and placed in 10 ml of SIF, pH 6.8. Samples were taken out at the required time interval (every 1 h up to 48 h), washed with water, dried, and weighed by refreshing the medium every 2 h. The percentage of dispersion was calculated from the dry weight before and after the immersion [24]. The experiment was conducted in triplicate.

*4.2.3.8  In-vitro antimicrobial activity of films*

  Disk diffusion method: Antimicrobial activity of films (5 cm in diameter) was conducted by using agar disc diffusion method against Gram-negative *E. coli* ATCC 25922 and Gram-positive *S. aureus* ATCC 29213 as test microorganisms to check the antimicrobial activity of EOs. Two film samples were made: one having EOs and the other film having no EOs (SEOBGK & SBGK respectively). The overnight cultures of bacteria were prepared in nutrient broth at 37 °C using 10 % inoculum at the late log phase. For antimicrobial tests, agar plates were made, three for each of the test microorganisms. After this, 20 µl of bacterial inoculums were spread over the agar plates. Disks from each film were prepared under aseptic conditions of approximately 0.5 cm in diameter. They were placed over those agar plates and were

incubated at 37 $^{\circ}$C for 14-16 h and the areas of the fully formed zones (ffz) were determined by measuring the zone diameter with the digital caliper.

Live/ Dead Baclight Bacterial Viability kit was used for monitoring the viability of the bacterial population in presence of SEOBGK as a function of membrane integrity of the bacterial cell. Cells with a compromised membrane that are considered to be dead or dying stain red whereas cells with intact cell membrane stain green. The detailed procedure can be found in ESI S5.

### 4.2.3.9 *Nutritional analysis and nutrition facts*

Nutritional analysis of SEOBGK was conducted to determine the nutritional content of the food by standard test methods (Table 2).

### *. Statistical analysis*

Data are expressed as mean ± SD. Statistical analysis was carried out through Origin Pro 8.6 32-bit software using two-way ANOVA, (least significant difference) at the significance level of p-value <0.05

## 4.3 Results and discussion

### 4.3.1 Protein determination by Kjeldahl method and SDS-PAGE

The protein percentage present in SPI as determined by the Kjeldahl method was found to be 66.9%. Details can be found in ESI S3. Protein electrophoresis is commonly used to elucidate the protein profile, including the concentration of proteins [25]. As depicted in SDS-PAGE, the extracted SPI sample exhibited a typical soy protein profile and agrees with [26], indicating the excellent quality of the SPI sample. As shown in Fig.1 (M depicts protein ladder), lane 2 depicting SPI under the reducing conditions (with 2-mercaptoethanol), illustrates a typical

SDS-PAGE profile of soy protein consisting of subunits of glycinin polypeptide and subunits of β-conglycinin. β-conglycinin (7S) has a trimeric structure and is composed of three major subunits, namely α, α', and β with masses of about 70 (α & α' subunits) and 48 kDa (β-subunit) respectively. On the other hand, the glycinin component (11S) is composed of acidic polypeptide subunits (AS) and a basic polypeptide subunit (BS) joined by a disulfide linkage. The mass of acidic polypeptide is about 38 kDa and the basic polypeptide is about 20 kDa. These results stand in good agreement with various researchers [27,28].
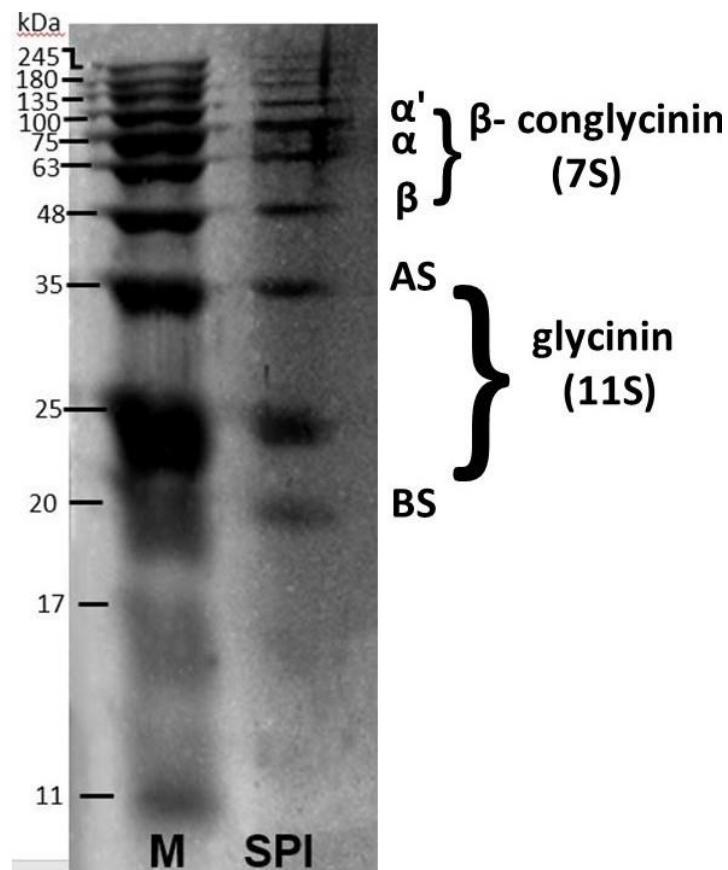


Fig. 4.1 SDS-PAGE for SPI

*4.3.2. Protein identification by LC-MS*

Protein identifications were performed by using liquid chromatography coupled to mass spectrometry (LC-MS/MS). The identified proteins were classified using the software

MASCOT DAEMON VER 2.6.0, NCBIprot 20180818 NCBI database. Then a total of 24 proteins have been identified in SPI. (Table 1) The overall protein score for the 7S glycine max (β-conglycinin) subunit and glycinin subunit are 108 and 90 respectively as depicted in Table 1. This number reflects the combined scores of all observed mass spectra that can be matched to the amino acid sequence within that protein. A high score indicates a more confident match [29]. These findings conclude the presence of 7S β-conglycinin and 11S glycinin subunits in SPI and corroborate SDS-PAGE data.

**Table 4.1: Description of proteins identified in an extracted sample of SPI**

| Accession | Score | Mass | emPAI | Description |
|---|---|---|---|---|
| AAB03390.1 | 108 | 47006 | 0.19 | 7S seed globulin precursor [Glycine max] |
| KHN10744.1 | 90 | 56410 | 0.16 | Glycinin G1 [Glycine soya] |
| AAF05723.1 | 71 | 56142 | 0.08 | sucrose binding protein homolog S-64 [Glycine max] |
| Q04672.1 | 51 | 60884 | 0.07 | RecName: Full=Sucrose-binding protein; Short=SBP; Flags: Precursor |
| KHN07145.1 | 44 | 104649 | 0.04 | Alpha-1,4 glucan phosphorylase L isozyme, chloroplastic/amyloplastic [Glycine soja] |
| XP_021832445.1 | 41 | 147671 | 0.03 | putative disease resistance RPP13-like protein 1 [Prunus avium] |
| XP_022766826.1 | 38 | 37012 | 0.12 | 4-hydroxy-tetrahydrodipicolinate reductase 2, chloroplastic-like [Durio zibethinus] |
| CAD43279.1 | 37 | 30010 | 0.15 | lectin [Helicotropis linearis var. linearis] |
| ADG03093.1 | 33 | 94605 | 0.04 | lipoxygenase 1 [Glycine max] |
| AAQ94293.1 | 31 | 14125 | 0.33 | Gcyc, partial [Gasteranthus sp. Amaya & Smith 515] |
| POE63159.1 | 31 | 104704 | 0.04 | putative u3 small nucleolar rna-associated protein 13 [Quercus suber] |
| XP_021628792.1 | 30 | 17612 | 0.26 | pectinesterase inhibitor 10-like [Manihot esculenta] |
| PNX77932.1 | 27 | 20359 | 0.22 | magnesium-dependent phosphatase 1-like protein [Trifolium pratense] |
| XP_022721997.1 | 26 | 81303 | 0.05 | probable xyloglucan glycosyltransferase 12 [Durio zibethinus] |

| | | | | |
|---|---|---|---|---|
| **AIU50438.1** | 22 | 44637 | 0.1 | **pectin lyase-like superfamily protein, partial [Setaria italica]** |
| **XP_011082032.1** | 22 | 90719 | 0.05 | **ubiquitin carboxyl-terminal hydrolase 18 [Sesamum indicum]** |
| **XP_022757165.1** | 21 | 43147 | 0.1 | **peroxisome biogenesis protein 16-like isoform X1 [Durio zibethinus]** |
| **XP_011078223.2** | 20 | 82700 | 0.05 | **wall-associated receptor kinase-like 8 [Sesamum indicum]** |
| **KHN18640.1** | 18 | 64531 | 0.07 | **Bromodomain and PHD finger-containing protein 3 [Glycine soja]** |
| **XP_006293894.1** | 17 | 61946 | 0.07 | **chaperonin CPN60-like 1, mitochondrial [Capsella rubella]** |
| **XP_020172805.1** | 17 | 28674 | 0.15 | **ethylene-responsive transcription factor 5-like [Aegilops tauschii subsp. tauschii]** |
| **XP_002872839.1** | 17 | 76442 | 0.06 | **L-type lectin-domain containing receptor kinase IV.4 [Arabidopsis lyrata subsp. lyrata]** |
| **XP_021729232.1** | 15 | 32216 | 0.14 | **transcription factor Pur-alpha 1-like isoform X1 [Chenopodium quinoa]** |
| **KHN20042.1** | **15** | **12818** | **0.37** | **Lysine-specific demethylase PHF2 [Glycine soja]** |

### *4.3.3 XRD*

XRD patterns were employed to examine the structure of 7S and 11S globulin of SPI and soy-based films. In Fig. 2a, diffraction domains at $2\theta \approx 9.4$ ° and $19.94$ ° of pure SPI represent the α-helix and β-pleated secondary structure of soy protein [30–32]. These aforementioned

diffractions depict the domain structure of 7S and 11S globulin from soy protein respectively [33]. As shown in XRD, the presence of glycerol, EOs, and BG network along with vitamin K1 influenced the XRD pattern of the α-helix structure of 7S globulin but does not affect the 11S globulin domain. This phenomenon may have occurred due to the intercalation of added entities with the helical structure of SPI. In all film variants, the intensity of both the peaks was less than SPI confirming that the helical structure of the protein matrix was weakened during the fabrication process. The average distance between particles ($d_{hkl}$) for 7S globulin at $2\theta \approx$ 20° for SPI was 0.44 nm, similar to the soy-based films. This depicted the intact β-sheet structure of the protein. On the contrary, it can be observed that at $2\theta \approx$ 10°, the mean distance ($d_{hkl}$) for 7S globulin for SPI was less (0.94 nm) than SEO (1.04 nm). This increase in d-spacing can be due to the intercalation of functional groups in the interlayer spacing of protein. This causes more ordered arrangements leading to the polycrystalline nature of the films showing sharp diffracting domains with $2\theta$ angles at 31.7°, 45.5°, and 56.5° for all the films. The sharp peaks got intensified in SEOBGK due to the *in-situ* mineralization of the BG network. The ion contents of the BG network might have assembled the macromolecules in a regular fashion thus aiding the crystallization of soy protein. It is worth mentioning that metals have been observed to form crystal contacts thus aiding in the crystallization of protein. [34]. Fig.2b portrays that after successive swelling of SEOBGK in SIF at pH 6.8, the XRD pattern depicts the amorphous nature of the film maintaining broad diffraction at $2\theta \approx$ 21.3°. This could be attributed to the opening of the polymeric chains during water uptake. The transformation of crystalline form into amorphous form is considered to be the most favorable formulation approach for the poorly water-soluble nutrient molecules. Since the amorphous form provides a considerable solubility advantage over its crystalline counterpart [35]. Therefore, this transition from the crystalline to amorphous nature of SEOBGK in SIF can play a very crucial role in site-specific diffusion and absorption of bioactive compounds and nutrients.
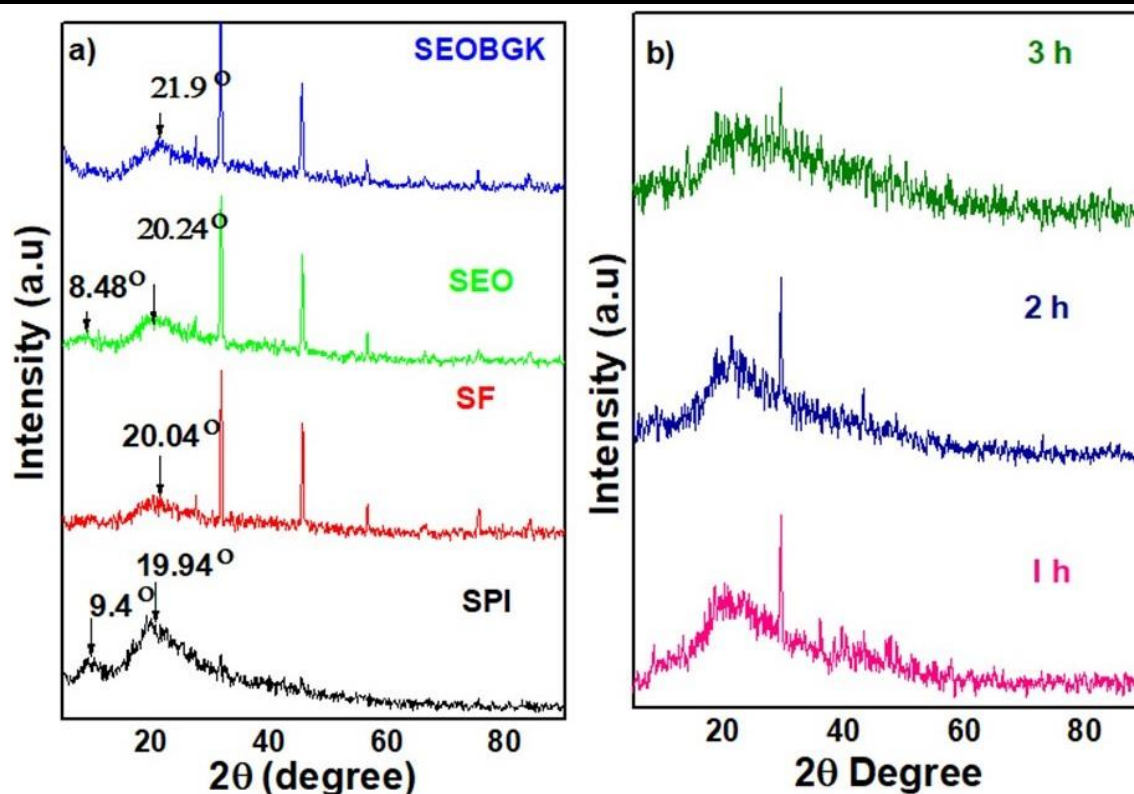
Fig. 4.2 a) XRD pattern of SPI, SF, SEO, and SEOBGK (left panel) b) XRD pattern of SEOBGK

after swelling in SIF at pH 6.8 (right panel) with scanning range $2\theta$ of $5^\circ$ to $70^\circ$ at $0.2°$/min.

*4.3.4  FTIR*

To study the effect of EOs, BG precursors, and vitamin K1 on the molecular level interactions

with SPI among film components, functional groups in the films were analyzed by their IR

spectra (Fig. 3a). The absorption band of Amide A is used to study the interaction of $-NH_2$

groups between peptide chains. [36] The conformational structure of the protein is directly

related to the Amide I band and the shape of the Amide I band is characteristic of the secondary

structure ($\alpha$-helix $1660 – 1650$ cm$^{-1}$ & $\beta$-pleated sheet $1637-1614$ cm$^{-1}$) [37]. For SPI, the

absorption band related to C=O stretching at 1648 cm$^{-1}$ (amide I), N-H stretching at 1541 cm$^{-1}$

(amide II), and C-N stretching, and N-H bending (amide III) vibration at 1240 cm$^1$ is shown.

The broad absorption band observed at 3418 cm$^{-1}$ (Amide A) is ascribed to the stretching

vibration of free and bonded O-H and N-H groups[26,38]. In the case of SEO, Amide I at 1625

cm$^{-1}$ is higher than Amide II at 1540 cm$^{-1}$ indicating that the N-H group in SPI, O-H group present in glycerol, and EOs are surely able to form intra- and intermolecular hydrogen bonding[39,40]. In Fig. 3b, BG spectra show the characteristic peaks at 1411 cm$^{-1}$ depicting Si-OH, peaks between 1100 cm$^{-1}$ to 805 cm$^{-1}$ correspond to asymmetric Si-O-Si stretching vibration. Further peaks detectable at 662 cm$^{-1}$ and 468 cm$^{-1}$ are related to P-O bond bending vibration [41,42]. Reduction of intensities at Amide I and Amide II in SEOBGK are ascribed to the interaction of Ca$^{2+}$ metal ions present in the BG network with C=O, C-N, and N-H groups of the protein that suggest a significant decrease in the α-helix structure of the protein due to metal ion interaction [37,43]. In addition (Fig. 3a), a weak shoulder observed at 1401 cm$^{-1}$ of SPI due to -COO$^{-}$ symmetric stretching is slightly shifted to 1411 cm$^{-1}$ in SEOBGK. The observed changes in -C=O, -COO$^{-}$, and -OH peaks of SEOBGK can be attributed to the interaction of ions of the BG network as well as with vitamin K1 molecules with SPI. The binding interaction of Ca$^{2+}$ ions with SPI proteins was further revealed by the shifting of the Amide A band from 3418 cm$^{-1}$ (N-H stretch) of SPI to 3428 cm$^{-1}$ for SEOBGK. These FTIR findings are following XRD spectra showing the α-helical conformational changes in SPI during film formation.
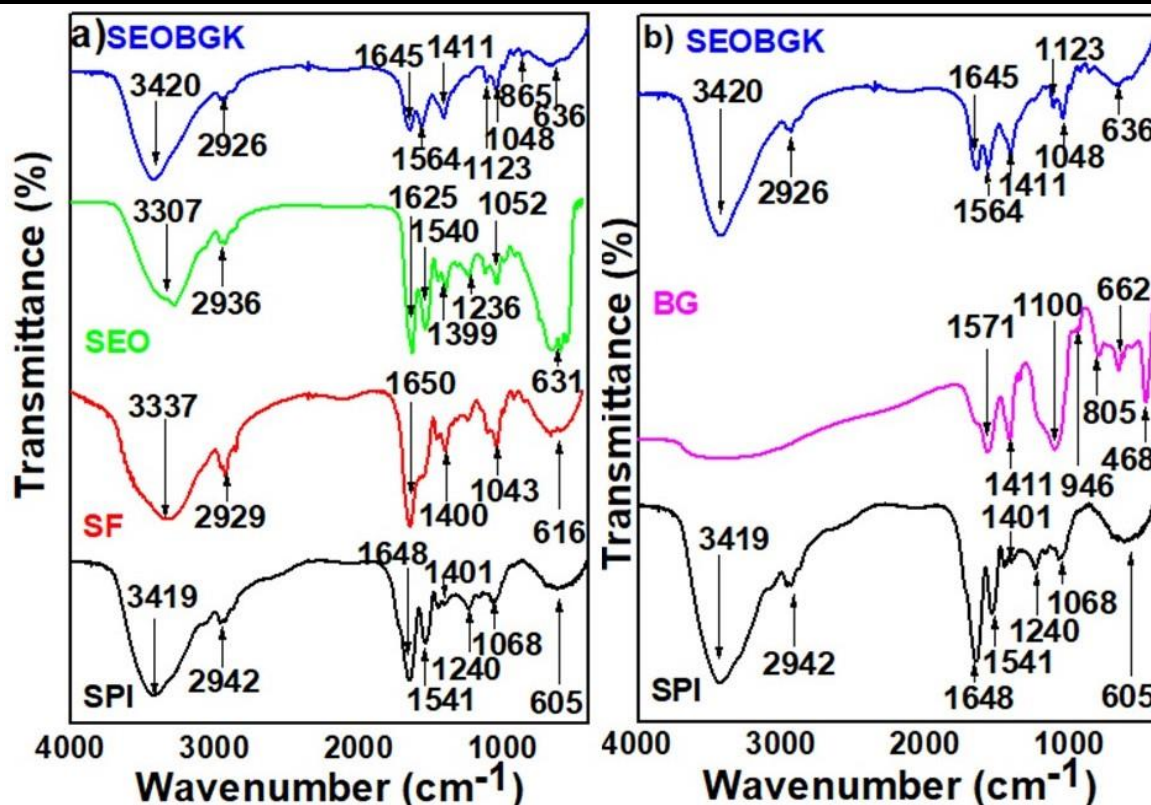
Fig. 4.3 a) FTIR spectra of SPI, SF, SEO, and SEOBGK (left panel) b) FTIR spectra of SPI, BG, and SEOBGK (right panel)

*4.3.5 TGA*

Thermogravimetric analysis was carried out to analyze the weight loss of SPI and soy-based films as a function of temperature. The thermal stability of SPI and its film variants is depicted in Fig. 4. The observed thermal stability of SPI was higher than all soy-based films due to its intact α-helix structure as evident by XRD (Fig.2a) The weight loss occurred in three stages. In the first stage, weight loss of 3%-5% occurring in the range of 25° C to 120° C was due to the evaporation of water [44,45]. In the second stage, weight loss was observed between 120° C to 200° C is accounted to the vaporization of glycerol [46]. Major weight loss occurs in the third stage from 200 °C to 470 °C because of the thermal degradation of the protein [47]. The reported final weight loss in SEOBGK was 72.96% at 601.1 °C leading to the existence of 27% of residue due to the presence of inorganic contents of the BG network [26] as shown in Fig.

4b. It is pertinent to note that the onset of major weight loss for SEOBGK started at 161 °C (in contrast to SPI = 200 °C). This could be due to the disruption of the secondary structure of protein causing a decrease in thermal stability of the film. These results validate XRD and FTIR findings (Fig 2 & 3).
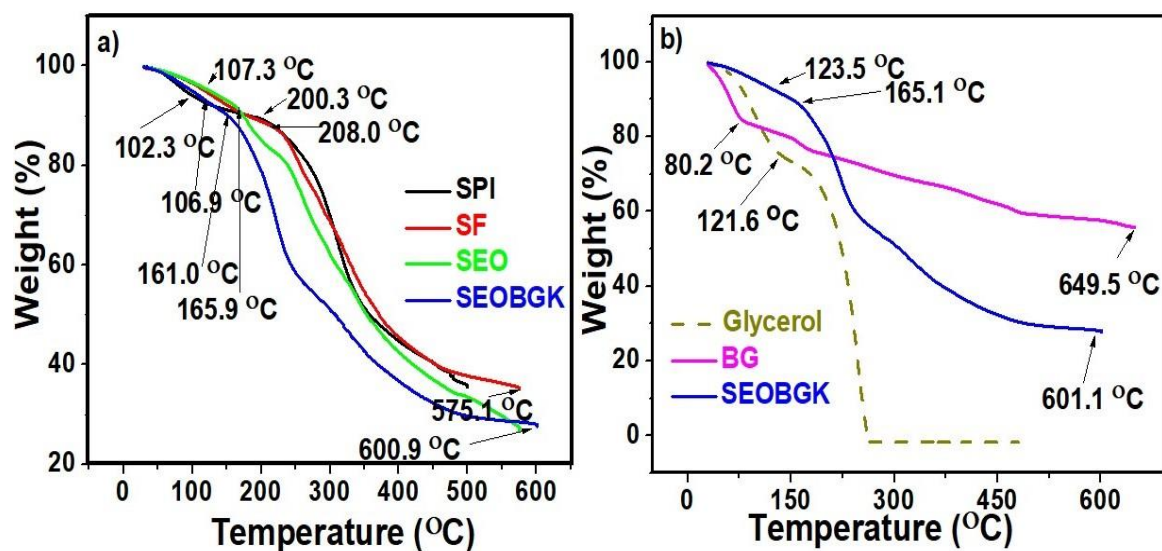


Fig. 4.4 a) TGA of SPI, SF, SEO, and SEOBGK (b) TGA of glycerol, BG, and SEOBGK at a heating rate of 10 °C/min in $N_2$ gas flow of 50 ml/min.

### 4.3.6 Morphological determination by SEM

The microstructure of SPI and soy-based films was observed using SEM as depicted in Fig.5. From the images, it was observed that SPI (Fig.5a) shows an irregular rough surface [48]. With the reinforcement of other additives for film fabrication, a more dense and continuous structure is formed (Fig. 5c) [49]. Due to the presence of the BG network (Fig.5d), a more agglomerated solid 3D structural surface is seen due to the crosslinking of the BG network in SEOBGK sculpting a compact network arrangement. This can be assigned to the loss of the α-helix content of the protein during physical interaction with the BG network, causing them to lose their secondary structure and exposing hydrophobic residues to the surface. The same observation can be obtained from the cross-sectional view of the SEOBGK where crosslinking

can be viewed between the BG network with the entire protein matrix (Fig.5f). It is evident from EDAX spectra (Fig.5e) the existence of Si, P, Na, and Ca elements in SEOBGK. These observations confirmed the mineralization of the BG network in the soy protein matrix and stand in accordance with the FTIR findings (Fig. 3a & 3b).
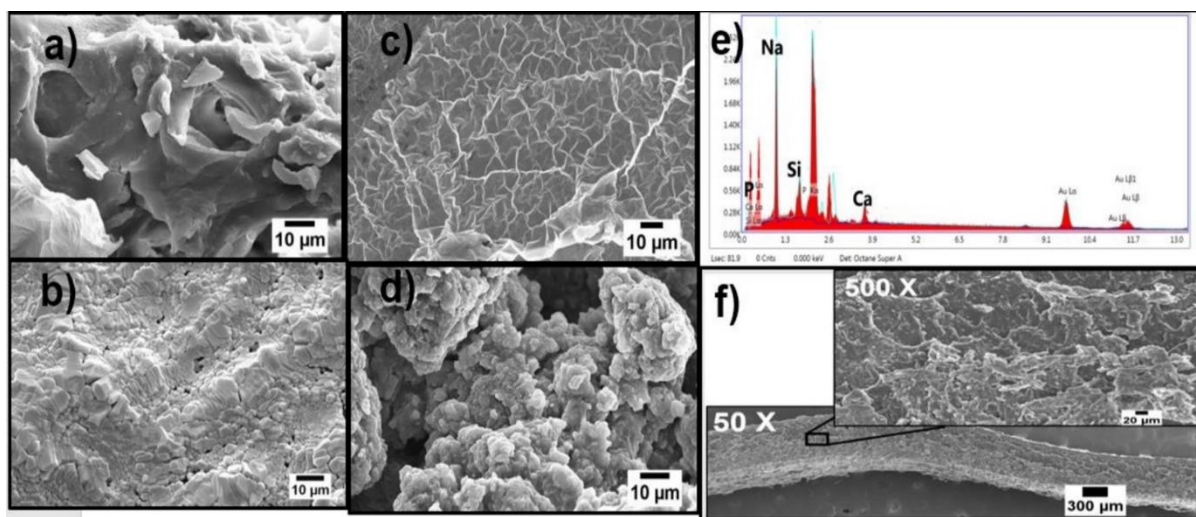


Fig. 4.5 SEM images at an accelerating voltage of 5.0 kV a) SPI b) SF c) SEO d) SEOBGK at 10k X e) SEM-EDAX spectra of SEOBGK f) Cross-sectional image of SEOBGK

### 4.3.7 Rheological measurements

Analysis of rheological properties of food plays an important role in food science as it helps to know about the processing operations and sensory properties [50]. It helps gather information regarding the microstructure of the food material. When the food is ingested, it undergoes deformation following mastication of food content. Thus, flow properties play an important role in understanding the interaction of different food components with each other and their dynamic stability to maintain food quality. To elucidate the microstructure of chewy soy-based films, the rheological property was monitored through a parallel plate rheometer. For this, SF and SEOBGK were characterized to deduce their respective flow behavior. The

oscillatory frequency sweep measurement showed a clear influence of interaction between the BG network and the soy protein matrix. From Fig. 6a, it can be seen that G' (storage modulus) for SEOBGK increases with an increase in angular frequency showing that the elastic nature of the film is maintained. For SF, G' decreases showing the transition of elastic nature to viscous behavior of the film. The elastic nature of SEOBGK can be due to the intercalation of the BG network with protein strands causing the unfolding of protein structure and imparting elasticity. Amplitude sweep is crucial to determine the LVE region (Linear Viscoelastic Region). From Fig.6b storage modulus (G') of SEOBGK decreases continuously after leaving the LVE region thus depicting a gradual breakdown of the microstructure bearing flow point at 20% shear strain. The LVE region of SF is larger than SEOBGK having a yield point at 50% shear strain and 10% shear strain respectively. But the storage modulus of SEOBGK is 1000 times more than SF. This shows that SEOBGK has exhibited viscoelastic gel-like properties. This property of SEOBGK is assigned to the BG network that acts as fillers in-between protein chains. BG network tend to unfold the protein when adsorbed over their surface during the incubation time in the reaction mixture for 24 h. Nanoparticles are known to unfold proteins over their surface [51–53]. SF tends to be a viscous fluid depicting a larger value of loss modulus (G") over storage modulus (G'). The steady shear flow curves of freshly prepared suspensions of SPI-based films are presented in fig.6c. Both the films exhibited shear-thinning behavior within the shear rate range from 0.1-1000 $s^{-1}$. The phenomenon showed that both film suspensions were typical non-newtonian fluids depicting Bingham pseudoplastic-like behavior (data not shown). SEOBGK showed more viscosity as compared to SF. The crosslinking between SPI and BG network could have been responsible for the high apparent viscosity. Similar results were reported where the rheological properties of waxy corn starch with SPI were studied [54]. These findings were also manifested through FTIR and XRD where the BG network crosslinks with soy protein matrix and uncoil α-helix structure, thus transmitting resilience to SEOBGK.
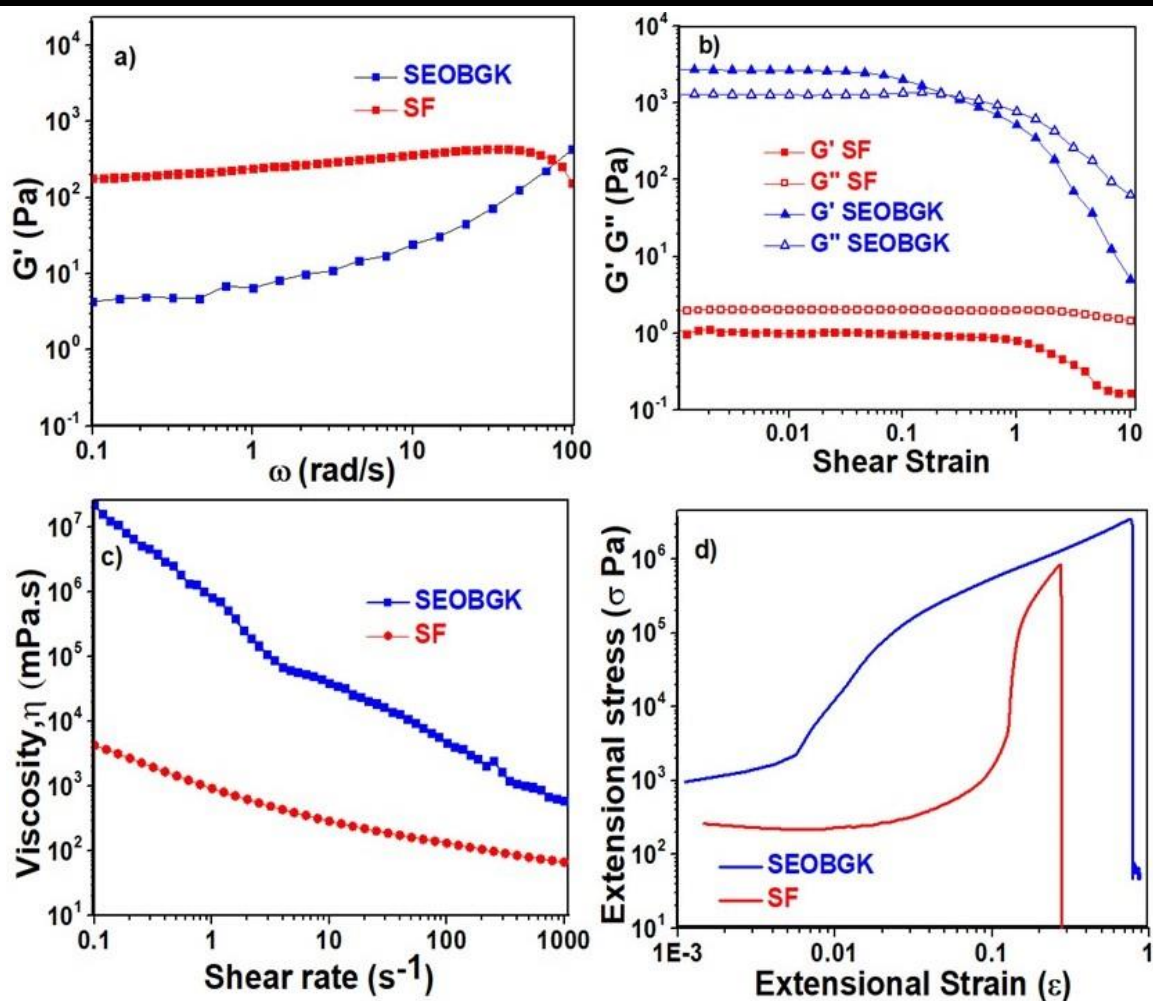
Fig.4.6 a) Rheology data showing comparative frequency sweep studies from 0.1 to 100 rad/s at 0.1% strain variation in storage modulus (G') b) Comparative amplitude sweep profiles at a constant angular frequency of 10 rad/s for strain % 0.01-1000 at 37 °C. c) Viscosity versus shear rate from range 0.1 to 1000 s$^{-1}$ d) Mechanical performance of the film using DMA

### 4.3.8 DMA

Mechanical properties were evaluated by TS, EB, and Young's modulus from the stress-strain curve of SF and SEOBGK. As observed from Fig. 6d, the TS value increased significantly from 0.819 ± 0.04MPa for SF to 3.46 ± 0.17 MPa for SEOBGK. These results were found to be as per other researchers [55]. It can be credited to the presence of the BG network that acts as a reinforcing material. Also, the presence of EOs caused intra- and intermolecular hydrogen

bonding with protein matrix (depicted in FTIR) contributed to a stronger network. The cinnamaldehyde and eugenol present in essential oils bond with protein network forming a crosslinking structure through physical interactions thus increasing the mechanical strength [39]. Also, the improvement in the mechanical properties in SEOBGK can be related to the lipid nature of the EOs that might introduce flexibility to the film structure [56]. The BG network's uniform distribution in the soy protein matrix during its *in-situ* mineralization also shows a synergistic effect on the mechanical strength of SEOBGK. Further supporting evidence can be seen in SEM micrographs (Fig.5d & 5f) where distribution and crosslinking of BG network can be viewed in entire soy protein matrix. The intermolecular interaction of BG network with protein matrix leads to modification of film microstructure and act as reinforcement depicting higher tensile strength as compare to SF. Similar observations were obtained where soy protein films were made using cinnamaldehyde and zinc oxide nanosheets [57]. Furthermore, EB for SEOBGK increased to $77 \pm 3.8\%$ (strain %) in comparison to SF ($27 \pm 1.3\%$, strain%). Nucleation of BG networking uniformly in soy protein matrix delays the break or crack propagation in SEOBGK. The increase in Young's modulus of SEOBGK ($4.52 \pm 0.23$ MPa) indicates that the film became strong rubbery with the *in-situ* mineralization of the BG network causing inter-ionic interaction between various constituents in soy protein film suspension.

### 4.3.9 Swelling studies on soy-based films

The fabricated films would follow the oral route. Therefore, *in-vitro* swelling experiments were carried out at different pH conditions mimicking those of the stomach (using SGF 1.2), intestine (using SIF pH 6.0), and colon (using SIF pH 6.8) as shown in Fig. 7. The swelling of SEOBGK in SGF, pH 1.2 was minimal i.e.$37 \pm 1.8\%$ and for SF, it was $27 \pm 1.3\%$ (Fig. 7a). The carboxylic group on soy protein was converted to the protonated acid form which is related to the breaking of hydrogen bonding with the environment and resulted in decreased swelling at acidic pH. It

is relevant to note that the zeta potential of soy protein above its isoelectric point i.e. 4.5 is negative [58]. Also, the zeta potential of the BG network is negative [59]. As the pH increased, carboxylate groups were ionized and electrostatic repulsion between negatively charged species resulted in enhancement of the swelling capacity of SEOBGK ($300 \pm 15\%$) as compared to SF ($205 \pm 10.2\%$). It is pertinent to recall that the absence of the BG network in SF is responsible for lower swelling capacity due to a lack of crosslinking. At pH 6.8, the maximal swelling ratio is obtained as most of the carboxylate ions interact with ion content of the BG network such as $Ca^{2+}$, $Na^+$ causing maximum swelling for SEOBGK compared to SF. These observations stand in good agreement with FTIR and XRD results where prominent interaction between soy protein and BG network has been depicted (Fig. 2 & 3). The flexible structure of SEOBGK having BG network as fillers in-between protein chain justifies the swelling behavior of the film in On-Off switching swelling -deswelling (Fig.7b) behaviors of the film at acidic and alkaline pH. As depicted by rheological studies also, the viscoelastic nature of SEOBGK resulted in its pronounced swelling. As seen in Fig. 7b, after 9 h, swelling in SEOBGK became constant and for SF, it started decreasing. Therefore the disintegration studies were carried out at colonic pH 6.8 for 48 h since the residence time for food content in the colon is approximately 5 days [60]. It was observed (ESI S7, Fig. S2) that SF completely disintegrates after 45 h and more than 90% of SEOBGK disintegrated at 48 h. The minimal and maximal swelling behavior of SEOBGK in acidic and intestinal pH respectively can serve as an advantage for the release of drugs and micronutrients at the intestinal surface thus protecting the same in a harsh acidic environment [40]. These studies proved that SEOBGK can play a significance in oral delivery applications.
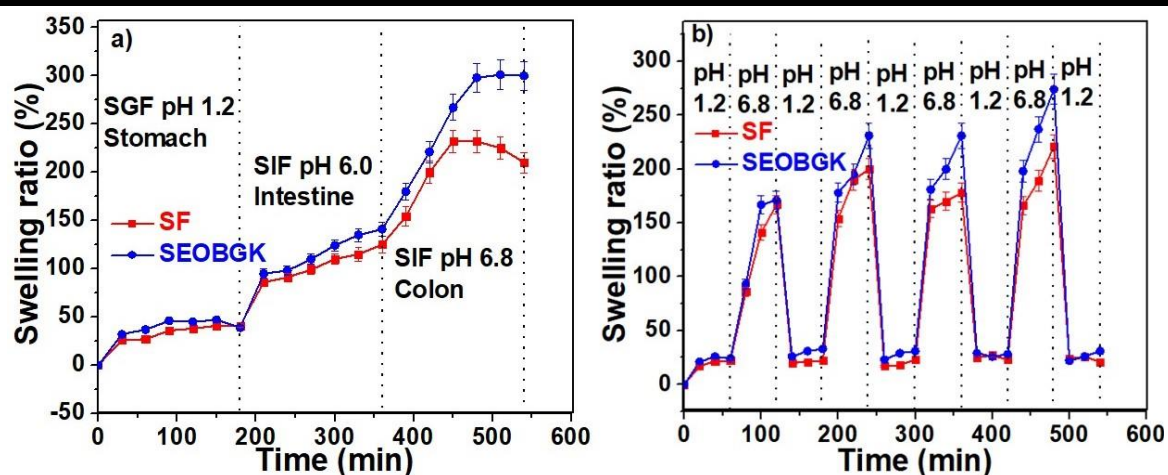
Fig. 4.7 Percentage (a) Swelling (b) On-Off-switching swelling of SF and SEOBGK as a function of time in SGF at pH 1.2, SIF at pH 6.0, and SIF at pH 6.8. Each datum point is expressed as the average of triplicate observations and the error bars represent corresponding standard deviations.

### 4.3.10 Antibacterial activity

The *in-vitro* antibacterial activity against two common food-borne pathogens is presented in Fig.8. As expected, SBGK didn't show any antibacterial activity but with the addition of EOs, SEOBGK exerted an obvious inhibitory effect on both *E. coli* and *S. aureus*. (Disk diffusion assay results shown in ESI S6, Fig. S1). The antimicrobial characteristic is imparted due to the presence of EOs as reported by various other researchers [36,42,61,62]. After seeing the results of the disk diffusion assay, SEOBGK film was tested against Live/ Dead Bac light Bacterial viability kit for monitoring the viability of the bacterial population. In fluorescent microscopic images (Fig. 8), bacterial strains were exposed to SEOBGK film for 0 h, 1 h, and 12 h. As observed at 0 h (Fig. 8a & 8d), both bacterial strains were seen alive maintaining their morphology and mobility (stained green with SYTO 9). With the incubation period of 1 h, the bacteriostatic effect was seen. The bacteria instead of being mobile, clustered and became static. (Fig. 8b & 8e).

As the incubation period increased to 12 h, a major proportion of bacteria were dead (stained red with PI) since PI cannot permeate live cells due to their intact cell membrane depicting the bactericidal effect of EOs present in SEOBGK (Fig. 8c & 8f). Thus, the fabricated film SEOBGK showed notable antimicrobial characteristics.
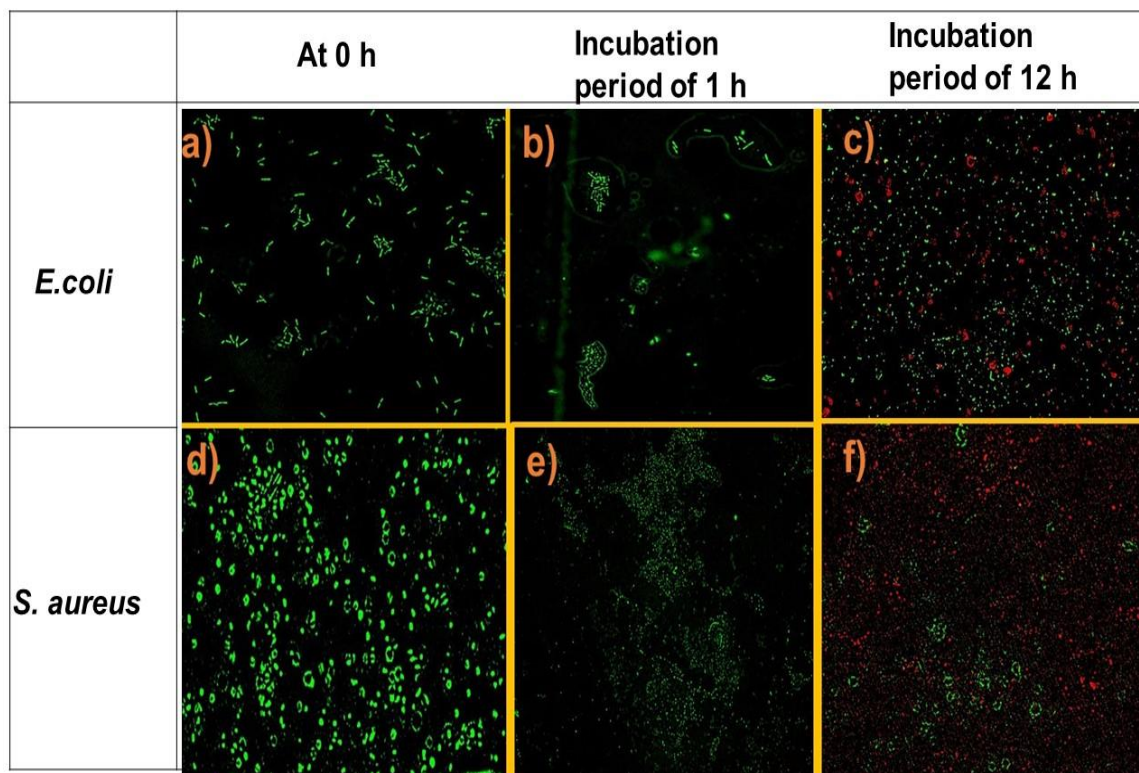


Fig. 4.8 Antimicrobial activity:(Lane 1-Left to right) a), b), & c) *E.coli* exposed to SEOBGK after an incubation period of 0 h, 1 h, and 12 h respectively. (Lane 2-Left to right) d), e), & f) *S.aureus* exposed to SEOBGK after an incubation period of 0 h, 1 h, and 12 h respectively.

### 4.3.11  Nutritional analysis and nutrition facts

Nutritional analysis of SEOBGK was conducted to determine the nutritional content of the food by standard test methods (Table 2). From the table, it can be inferred that SEOBGK has the highest protein content and this result lies in sync with the Kjeldahl assay. The nutritional

inspection of SEOBGK shows that these can serve as a good source of nutrition as well as energy.

**Table 4.2: Nutritional analysis of SEOBGK**

| S.No. | Test Parameters | Unit | Test Result | Test Method |
|---|---|---|---|---|
| A. | Nutritional Parameters | | | |
| A.1. | Protein (N×6.38) | g/100g | 69.71 | IS: 7219:1973 |
| A.2. | Fat | g/100g | Nil | AOAC 922.06 |
| A.3. | Carbohydrate | g/100g | 12.85 | IS: 1656: 2007 |
| A.4. | Dietary Fibre | g/100g | 2.82 | AOAC 985.29 |
| B. | Minerals | | | |
| B.1. | Phosphorus (as P) | mg/100g | 26.09 | AOAC 965.17 |
| B.2. | Sodium (as Na) | mg/100g | 194.30 | AOAC 966.16 |
| B.3. | Calcium (as Ca) | % by mass | 0.56 | By AAS |
| C. | Energy | Kcal/100g | 330.24 | STRC/STP/F073 |

**4.4 Conclusion**

This manuscript successfully describes the extraction of soy protein from defatted soybean flour and the functionalization of soy films with BG and vitamin K1. The formed films have intrinsic antimicrobial properties due to the presence of EOs. The nutritional analysis depicts it to be a rich source of protein and essential nutrients like P, Ca, and Si for the healthy bone. *In-situ* mineralization of the BG network in the soy protein matrix enhances the mechanical

properties of the film, forming it a viscoelastic material. Thus, SEOBGK can stand to be used

as a nutritional functional food for bone health showing nourishing and antibacterial properties.

**References**

[1]     N. Wright, A. Looker, K. Saag, J. Curtis, E. Delzel, S. Randall, M. Dawson-Hughes, The recent prevalence of osteoporosis and low bone mass in the United States, J. Bone Miner. Res. 29 (2014) 2520–2526. https://doi.org/10.1002/jbmr.2269.The.

[2]     C.T. Price, J.R. Langford, F.A. Liporace, Essential Nutrients for Bone Health and a Review of their Availability in the Average North American Diet, Open Orthop. J. 6 (2012) 143–149. https://doi.org/10.2174/1874325001206010143.

[3]     B. Dawson-Hughes, Interaction of dietary calcium and protein in bone health in humans, J. Nutr. 133 (2003) 63–68. https://doi.org/10.1093/jn/133.3.852s.

[4]     G. Rizzo, L. Baroni, Soy, soy foods and their role in vegetarian diets, 2018. https://doi.org/10.3390/nu10010043.

[5]     W.X. Chao, Health effects of soy protein and isoflavones in humans, J. Nutr. 138 (2008) 4–9. https://doi.org/10.1093/jn/138.6.1244s.

[6]     P. V. Paulsen, Isolated soy protein usage in beverages, Woodhead Publishing Limited, 2009. https://doi.org/10.1533/9781845695569.3.318.

[7]     C. Wang, Q. Ma, S. Pagadala, M.S. Sherrard, P.G. Krishnan, Changes of isoflavones during processing of soy protein isolates, JAOCS, J. Am. Oil Chem. Soc. 75 (1998) 337–341. https://doi.org/10.1007/s11746-998-0050-7.

[8]     A.J. Lanou, Soy foods: Are they useful for optimal bone health?, Ther. Adv. Musculoskelet. Dis. 3 (2011) 293–300. https://doi.org/10.1177/1759720X11417749.

[9]     S.L. Booth, K.E. Broe, D.R. Gagnon, K.L. Tucker, M.T. Hannan, R.R. McLean, B.

Dawson-Hughes, P.W.F. Wilson, L.A. Cupples, D.P. Kiel, Vitamin K intake and bone mineral density in women and men, Am. J. Clin. Nutr. 77 (2003) 512–516. https://doi.org/10.1093/ajcn/77.2.512.

[10]   X. Feng, Chemical and Biochemical Basis of Cell-Bone Matrix Interaction in Health and Disease, Curr. Chem. Biol. 3 (2012) 189–196. https://doi.org/10.2174/2212796810903020189.

[11]   S. Kargozar, F. Baino, S. Hamzehlou, R.G. Hill, M. Mozafari, Bioactive Glasses: Sprouting Angiogenesis in Tissue Engineering, Trends Biotechnol. 36 (2018) 430–444. https://doi.org/10.1016/j.tibtech.2017.12.003.

[12]   F. Baino, S. Hamzehlou, S. Kargozar, Bioactive glasses: Where are we and where are we going?, J. Funct. Biomater. 9 (2018). https://doi.org/10.3390/jfb9010025.

[13]   L. Bi, S. Jung, D. Day, K. Neidig, V. Dusevich, D. Eick, L. Bonewald, Evaluation of bone regeneration, angiogenesis, and hydroxyapatite conversion in critical-sized rat calvarial defects implanted with bioactive glass scaffolds, J. Biomed. Mater. Res. - Part A. 100 A (2012) 3267–3275. https://doi.org/10.1002/jbm.a.34272.

[14]   C.J. Henry, Functional foods, Eur. J. Clin. Nutr. 64 (2010) 657–659. https://doi.org/10.1038/ejcn.2010.101.

[15]   M.N. Vella, L.M. Stratton, J. Sheeshka, A.M. Duncan, Functional food awareness and perceptions in relation to information sources in older adults, Nutr. J. 13 (2014) 1–12. https://doi.org/10.1186/1475-2891-13-44.

[16]   K. Gul, A.K. Singh, R. Jabeen, Nutraceuticals and Functional Foods: The Foods for the Future World, Crit. Rev. Food Sci. Nutr. 56 (2016) 2617–2627. https://doi.org/10.1080/10408398.2014.903384.

[17]   S. Sharma, S. Barkauskaite, A.K. Jaiswal, S. Jaiswal, Essential oils as additives in active food packaging, Food Chem. 343 (2021) 128403. https://doi.org/10.1016/j.foodchem.2020.128403.

[18]   H.M. Abuohashish, D.A. Khairy, M.M. Abdelsalam, A. Alsayyah, M.M. Ahmed, S.S. Al-Rejaie, In-vivo assessment of the osteo-protective effects of eugenol in alveolar bone tissues, Biomed. Pharmacother. 97 (2018) 1303–1310. https://doi.org/10.1016/j.biopha.2017.11.068.

[19]   Z. Wu, S. Weng, D. Yan, Z. Xie, Q. Zhou, H. Li, B. Bai, V. Boodhun, Z. Shen, J. Tang, L. Zhou, Z. Tao, L. Yang, Administration of cinnamaldehyde promotes osteogenesis in ovariectomized rats and differentiation of osteoblast in vitro, J. Pharmacol. Sci. 138 (2018) 63–70. https://doi.org/10.1016/j.jphs.2018.09.002.

[20]   C. Chircov, I.I. Miclea, V. Grumezescu, A.M. Grumezescu, Essential oils for bone repair and regeneration—mechanisms and applications, Materials (Basel). 14 (2021). https://doi.org/10.3390/ma14081867.

[21]   Pak, K.S. , William L.; Grossfield, Joseph; Arnold, © 1970 Nature Publishing Group, Nat. Publ. Gr. 228 (1970) 726–734. http://www.mendeley.com/research/discreteness-conductance-chnge-n-bimolecular-lipid-membrane-presence-certin-antibiotics/.

[22]   N. Gupta, D. Santhiya, A. Aditya, K. Badra, Dendrimer templated bioactive glass-ceramic nanovehicle for gene delivery applications, RSC Adv. 5 (2015) 56794–56807. https://doi.org/10.1039/c5ra04441c.

[23]   N. Ahmad, M.C.I.M. Amin, S.M. Mahali, I. Ismail, V.T.G. Chuang, Biocompatible and mucoadhesive bacterial cellulose-g-poly(acrylic acid) hydrogels for oral protein delivery, Mol. Pharm. 11 (2014) 4130–4142. https://doi.org/10.1021/mp5003015.

[24]  E. Teodor, S.C. Liţescu, C. Petcu, M. Mihalache, R. Somoghi, Nanostructured biomaterials with controlled properties synthesis and characterization, Nanoscale Res. Lett. 4 (2009) 544–549. https://doi.org/10.1007/s11671-009-9278-x.

[25]  W. Ma, F. Xie, S. Zhang, H. Wang, M. Hu, Y. Sun, M. Zhong, J. Zhu, B. Qi, Y. Li, Characterizing the structural and functional properties of soybean protein extracted from full-fat soybean flakes after low-temperature dry extrusion, Molecules. 23 (2018). https://doi.org/10.3390/molecules23123265.

[26]  S. Tansaz, M. Schulte, U. Kneser, D. Mohn, W. Stark, J.A. Roether, I. Cicha, A.R. Boccaccini, Soy protein isolate/bioactive glass composite membranes: Processing and properties, Eur. Polym. J. 106 (2018) 232–241. https://doi.org/10.1016/j.eurpolymj.2018.07.003.

[27]  N. Chen, M. Zhao, C. Chassenieux, T. Nicolai, Data on the characterization of native soy globulin by SDS-Page, light scattering and titration, Data Br. 9 (2016) 749–752. https://doi.org/10.1016/j.dib.2016.10.016.

[28]  W. Xia, S. Pan, Z. Cheng, Y. Tian, X. Huang, High-intensity ultrasound treatment on soy protein after selectively proteolyzing glycinin component: Physical, structural, and aggregation properties, Foods. 9 (2020). https://doi.org/10.3390/foods9060839.

[29]  C. Lou Chepanoske, B.E. Richardson, M. Von Rechenberg, J.M. Peltier, Average peptide score: A useful parameter for identification of proteins derived from database searches of liquid chromatography/tandem mass spectrometry data, Rapid Commun. Mass Spectrom. 19 (2005) 9–14. https://doi.org/10.1002/rcm.1741.

[30]  C. Xia, L. Wang, Y. Dong, S. Zhang, S.Q. Shi, L. Cai, J. Li, Soy protein isolate-based films cross-linked by epoxidized soybean oil, RSC Adv. 5 (2015) 82765–82771.

https://doi.org/10.1039/c5ra15590h.

[31]  A. González, C.I. Alvarez Igarzabal, Nanocrystal-reinforced soy protein films and their application as active packaging, Food Hydrocoll. 43 (2015) 777–784. https://doi.org/10.1016/j.foodhyd.2014.08.008.

[32]  K. Li, S. Jin, X. Liu, H. Chen, J. He, J. Li, Preparation and characterization of chitosan/soy protein isolate nanocomposite film reinforced by Cu nanoclusters, Polymers (Basel). 9 (2017) 1–11. https://doi.org/10.3390/polym9070247.

[33]  J. Chen, X. Chen, Q. Zhu, F. Chen, X. Zhao, Q. Ao, Determination of the domain structure of the 7S and 11S globulins from soy proteins by XRD and FTIR, J. Sci. Food Agric. 93 (2013) 1687–1691. https://doi.org/10.1002/jsfa.5950.

[34]  R.P. Hegde, G.C. Pavithra, D. Dey, S.C. Almo, S. Ramakumar, U.A. Ramagopal, Can the propensity of protein crystallization be increased by using systematic screening with metals?, Protein Sci. 26 (2017) 1704–1713. https://doi.org/10.1002/pro.3214.

[35]  D. Novakovic, A. Isomäki, B. Pleunis, S.J. Fraser-Miller, L. Peltonen, T. Laaksonen, C.J. Strachan, Understanding Dissolution and Crystallization with Imaging: A Surface Point of View, Mol. Pharm. 15 (2018) 5361–5373. https://doi.org/10.1021/acs.molpharmaceut.8b00840.

[36]  F. Xue, Y. Gu, Y. Wang, C. Li, B. Adhikari, Encapsulation of essential oil in emulsion based edible films prepared by soy protein isolate-gum acacia conjugates, Food Hydrocoll. 96 (2019) 178–189. https://doi.org/10.1016/j.foodhyd.2019.05.014.

[37]  R.I. Litvinov, D.A. Faizullin, Y.F. Zuev, J.W. Weisel, The α-helix to β-sheet transition in stretched and compressed hydrated fibrin clots, Biophys. J. 103 (2012) 1020–1027. https://doi.org/10.1016/j.bpj.2012.07.046.

[38] H. Wang, D. Hu, Q. Ma, L. Wang, Physical and antioxidant properties of flexible soy protein isolate films by incorporating chestnut (Castanea mollissima) bur extracts, LWT - Food Sci. Technol. 71 (2016) 33–39. https://doi.org/10.1016/j.lwt.2016.03.025.

[39] M. Kaur, D. Santhiya, UV-shielding antimicrobial zein films blended with essential oils for active food packaging, J. Appl. Polym. Sci. 138 (2021) 1–10. https://doi.org/10.1002/app.49832.

[40] M. Gautam, D. Santhiya, In-situ mineralization of calcium carbonate in pectin based edible hydrogel for the delivery of protein at colon, J. Drug Deliv. Sci. Technol. 53 (2019) 101137. https://doi.org/10.1016/j.jddst.2019.101137.

[41] N. Gupta, D. Santhiya, A. Aditya, Tailored smart bioactive glass nanoassembly for dual antibiotic: In vitro sustained release against osteomyelitis, J. Mater. Chem. B. 4 (2016) 7605–7619. https://doi.org/10.1039/c6tb01528j.

[42] I. Unalan, T. Fuggerer, B. Slavik, A. Buettner, A.R. Boccaccini, Antibacterial and antioxidant activity of cinnamon essential oil-laden 45S5 bioactive glass/soy protein composite scaffolds for the treatment of bone infections and oxidative stress, Mater. Sci. Eng. C. 128 (2021) 112320. https://doi.org/10.1016/j.msec.2021.112320.

[43] H.A. Alhazmi, FT-IR spectroscopy for the identification of binding sites and measurements of the binding interactions of important metal ions with bovine serum albumin, Sci. Pharm. 87 (2019). https://doi.org/10.3390/scipharm87010005.

[44] P. Guerrero, K. De La Caba, Thermal and mechanical properties of soy protein films processed at different pH by compression, J. Food Eng. 100 (2010) 261–269. https://doi.org/10.1016/j.jfoodeng.2010.04.008.

[45] C. Li, J. Luo, Z. Qin, H. Chen, Q. Gao, J. Li, Mechanical and thermal properties of

microcrystalline cellulose-reinforced soy protein isolate-gelatin eco-friendly films, RSC Adv. 5 (2015) 56518–56525. https://doi.org/10.1039/c5ra04365d.

[46]    A. Gómez-Siurana, A. Marcilla, M. Beltrán, D. Berenguer, I. Martínez-Castellanos, S. Menargues, TGA/FTIR study of tobacco and glycerol-tobacco mixtures, Thermochim. Acta. 573 (2013) 146–157. https://doi.org/10.1016/j.tca.2013.09.007.

[47]    X. Liu, R. Song, W. Zhang, C. Qi, S. Zhang, J. Li, Development of eco-friendly soy protein isolate films with high mechanical properties through HNTs, PVA, and PTGE synergism effect, Sci. Rep. 7 (2017) 1–9. https://doi.org/10.1038/srep44289.

[48]    X. Zhao, J. Chen, Q. Zhu, F. Du, Q. Ao, J. Liu, Surface characterization of 7S and 11S globulin powders from soy protein examined by X-ray photoelectron spectroscopy and scanning electron microscopy, Colloids Surfaces B Biointerfaces. 86 (2011) 260–266. https://doi.org/10.1016/j.colsurfb.2011.03.044.

[49]    Y. Xiao, Y. Liu, S. Kang, K. Wang, H. Xu, Development and evaluation of soy protein isolate-based antibacterial nanocomposite films containing cellulose nanocrystals and zinc oxide nanoparticles, Food Hydrocoll. 106 (2020) 105898. https://doi.org/10.1016/j.foodhyd.2020.105898.

[50]    Q. Zhong, C.R. Daubert, Food Rheology, Elsevier Inc., 2013. https://doi.org/10.1016/B978-0-12-385881-8.00015-X.

[51]    H. Pan, M. Qin, W. Meng, Y. Cao, W. Wang, How do proteins unfold upon adsorption on nanoparticle surfaces?, Langmuir. 28 (2012) 12779–12787. https://doi.org/10.1021/la302258k.

[52]    S. Ashrafpour, T. Tohidi Moghadam, Interaction of silver nanoparticles with Lysozyme: Functional and structural investigations, Surfaces and Interfaces. 10 (2018)

216–221. https://doi.org/10.1016/j.surfin.2017.09.010.

[53] A. Ostafin, Nanotechnology: Nanoparticle Characterization and Application in Pharmacology and Toxicology, J. Nanomed. Nanotechnol. 10 (2019). https://doi.org/10.35248/2157-7439.19.10.533.

[54] C. Qiu, X. Li, N. Ji, Y. Qin, Q. Sun, L. Xiong, Rheological properties and microstructure characterization of normal and waxy corn starch dry heated with soy protein isolate, Food Hydrocoll. 48 (2015) 1–7. https://doi.org/10.1016/j.foodhyd.2015.01.030.

[55] M. Mikus, S. Galus, A. Ciurzyńska, M. Janowicz, Development and characterization of novel composite films based on soy protein isolate and oilseed flours, Molecules. 26 (2021). https://doi.org/10.3390/molecules26123738.

[56] N. Vahedikia, F. Garavand, B. Tajeddin, I. Cacciotti, S.M. Jafari, T. Omidi, Z. Zahedi, Biodegradable zein film composites reinforced with chitosan nanoparticles and cinnamon essential oil: Physical, mechanical, structural and antimicrobial attributes, Colloids Surfaces B Biointerfaces. 177 (2019) 25–32. https://doi.org/10.1016/j.colsurfb.2019.01.045.

[57] J. Wu, Q. Sun, H. Huang, Y. Duan, G. Xiao, T. Le, Enhanced physico-mechanical, barrier and antifungal properties of soy protein isolate film by incorporating both plant-sourced cinnamaldehyde and facile synthesized zinc oxide nanosheets, Colloids Surfaces B Biointerfaces. 180 (2019) 31–38. https://doi.org/10.1016/j.colsurfb.2019.04.041.

[58] M.L.F. Freitas, K.M. Albano, V.R.N. Telis, Characterization of biopolymers and soy protein isolate-high-methoxyl pectin complex, Polimeros. 27 (2017) 62–67.

https://doi.org/10.1590/0104-1428.2404.

[59]   A. Doostmohammadi, A. Monshi, R. Salehi, M.H. Fathi, Z. Golniya, A.U. Daniels, Bioactive glass nanoparticles with negative zeta potential, Ceram. Int. 37 (2011) 2311– 2316. https://doi.org/10.1016/j.ceramint.2011.03.026.

[60]   S. Amidon, J.E. Brown, V.S. Dave, Colon-Targeted Oral Drug Delivery Systems: Design Trends and Approaches, AAPS PharmSciTech. 16 (2015) 731–741. https://doi.org/10.1208/s12249-015-0350-9.

[61]   G. Sara, H.S.J. Nasrin, M. Mehran, K.D. Kianoush, Application of zein antimicrobial edible film incorporating Zataria multiflora boiss essential oil for preservation of Iranian ultrafiltered Feta cheese, African J. Biotechnol. 14 (2015) 2014–2021. https://doi.org/10.5897/ajb2014.13992.

[62]   D. Konuk Takma, F. Korel, Active packaging films as a carrier of black cumin essential oil: Development and effect on quality and shelf-life of chicken breast meat, Food Packag. Shelf Life. 19 (2019) 210–217. https://doi.org/10.1016/j.fpsl.2018.11.002.

# Chapter 5

# UV-shielding antimicrobial zein films blended with essential oils for active food packaging
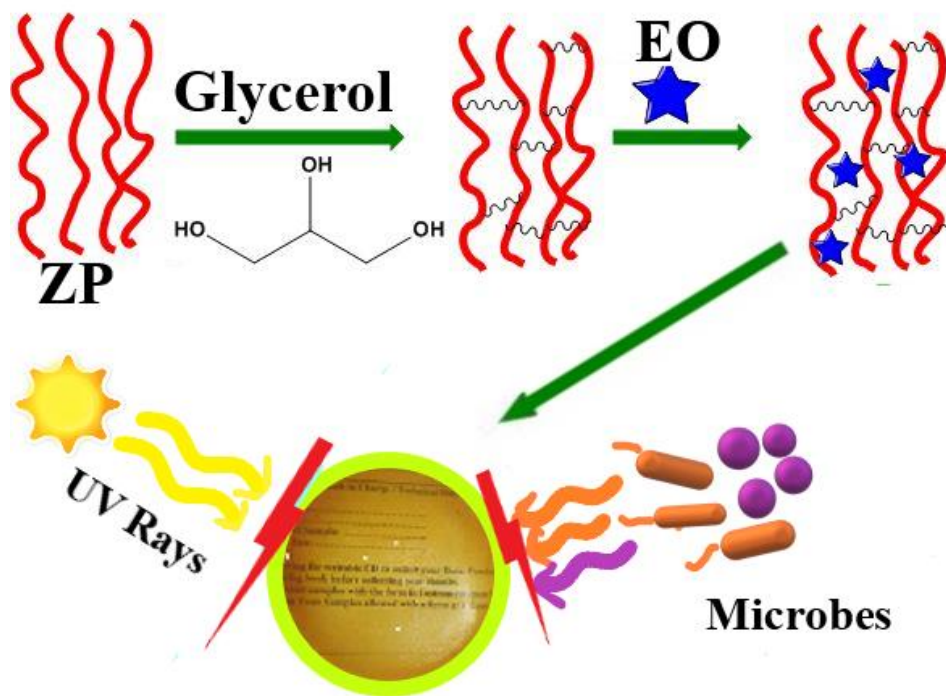


UV Shielding Antimicrobial ZEO Film

<div align="center">

**Chapter 5**

# UV-Shielding Antimicrobial Zein Films Blended with Essential Oils for Active Food Packaging

</div>

## 5.1 INTRODUCTION

The Packaging industry is growing rapidly and nearly all other industries are directly or indirectly depending on it. When viewed in terms of packaging, the global share of flexible plastic packaging is 42 %. [1] As reported by FICCI (The Federation of Indian Chambers of Commerce and Industry) 1/3$^{rd}$ of plastic products used by the packaging industry are petroleum-based non-biodegradable and environmentally unfriendly. Out of the total global share, 24 % of flexible packaging is needed in the food packaging industry.[2] These plastics used for the packaging purpose are often discarded and barely reprocessed.[3] In this regard, in December 2018, Great Britain's Royal Statistical Society conducted the study and stated that only 9 % of the plastic is being recycled.[4] The conventional packaging materials like HDPE (high-density polyethylene), polypropylene (PP), polyethylene terephthalate (PET), etc. though have excellent mechanical and barrier properties [5] but are unhealthy to the environment. They do not have active properties, causing the growth of spoilage and pathogenic microorganisms over the fruits and vegetables packaged into it. [6-8] Traditional packaging also have poor resistance to UV. [9] They may undergo photo-oxidation leading to polymeric structural degradation [10-11] and release of free radicals. [12] These free radicals may enter into food materials packaged into it and the human body. This can exert a detrimental effect on the food quality as well as human health. [13] To curb this problem and to provide a shield against UV radiation, various UV blockers, UV stabilizers like carbon black, titanium dioxide, benzophenones, benzonitriles, etc. are added to plastics. IARC (International Agency for

Research on Cancer) has reported titanium dioxide as a possible carcinogen to humans and studies showed that the increase in lung tumors in rats is associated with titanium oxide inhalation. [14]

Thus, with such a downside of synthetic polymers, its associated health concerns, and the rapid increase in plastic waste, extensive studies are conducted to produce active packaging materials. For this purpose, various food-grade polymers like proteins, polysaccharides, lipids [15] have gathered attraction and are being explored for the same purpose. Various natural antimicrobial active agents such as essential oils containing eugenol, cinnamaldehyde [16, 24] are incorporated to make these active packaging. The usage of such bio-based materials for antimicrobial packaging can reduce ecological waste and eliminate undesirable changes in food quality. [15, 16] They can also act as a nutrient carrier. [17] These edible biodegradable polymers can be used as films and may be directly applied onto the surface of the food product. [18, 19] In food industries and medical sectors, the use of natural polymers and food-grade additives have been steadily increasing as coating materials over a drug, candies, fruits, etc. [20, 23]

In this investigation, zein, a class of alcohol-soluble prolamine hydrophobic storage protein found in corn attracts the interest because of its film-forming ability, biodegradability, and biocompatibility. [21, 24] FDA (Food and Drug Administration) has approved it 'as one of the safe materials' for pharmaceutical coatings because of its non-toxic nature. [22] Zein has been used in the food packaging industry as a coating material due to its ability to provide a moisture barrier. [21] But the classical brittleness and flexibility problems of zein films [25] limit their use as a free-standing film.

 Hence, to monitor limitations regarding flexibility, active zein film packaging bearing UV shielding and antimicrobial properties have been fabricated using essential oils (EOs) and glycerol as crosslinker and plasticizer. [16, 24, 27] EOs are biological substances produced by

some plants as secondary metabolites and are distinguished by their volatile nature.[26] These EOs generally constitute terpenes and terpenoids comprising as main group, aromatic and aliphatic constituents comprising the other group, all characterized by low molecular weight. [28] They act as active agents having germicidal antimicrobial property because of the presence of major aromatic compounds (e.g., thymol, carvacrol, and eugenol) present in concentrations of as much as 85% [26, 29, 28] and help in reducing, retarding, or even inhibiting the growth of spoilage and pathogenic microorganisms. [30, 31] Herein, cinnamon oil and clove oil are used, having major constituents as cinnamaldehyde and acetyl eugenol respectively. [29] These major constituents of chosen EOs are not only expected to be natural crosslinkers but also provide natural aroma [32] along with antimicrobial properties to zein based food packaging material. More importantly these aromatic compounds are expected to be efficient in UV screening [33] and attracted our attention towards UV shielding edible packaging.

This work aims to the development of novel flexible zein based food packaging material. Importantly, this zein based film is expected to be functioning as a guard against UV radiation without the addition of any kind of UV blockers, stabilizers, etc. along with antimicrobial property. The attempt of making these protein packaging materials by simple solvent cast method using glycerol and essential oils is beneficial both to the ecosystem and human health. Further, the fabrication of these films requires no unhealthy chemicals and its processing produce no malodorous toxic gases. The films formed have thoroughly been characterized by standard characterization techniques including their surface morphology. Also, the barrier properties of the films are tested through a water vapor permeability test (WVP) and oxygen transmission rate (OTR) test along with their mechanical strength. Further, the films are subjected to *in-vitro* antimicrobial testing using the disk diffusion method.

## 5.2 EXPERIMENTAL SECTION

### 5.2.1 Materials

For the preparation of the film, zein protein in powder form with 97 % - 99 % purity (ZP, MW= 38 kDa), essential oils (EOs) (Cinnamon oil, product number-W229105 and clove oil, product number- C8392) and glycerol were purchased from Sigma-Aldrich, Gallarate, Italy. Milli Q water was used for all the experimental work and all other reagents used in this study were of analytical reagent (AR) grade of high purity.

### 5.2.2 Methods

### 5.2.2.1 Fabrication of Zein film

Zein films (ZF) were obtained by dissolving 0.5 g of zein protein (w/v) in 80 % ethanol with constant stirring at 45 °C followed by drop-wise addition of glycerol (Zein/glycerol weight ratio 5:1) to the solution and stirred continuously for 30 min until a homogenous mixture was obtained followed by cooling and casting onto polypropylene petri-plates having 5 cm diameter. So obtained ZF films were used as control. Subsequently, 150 µl of the emulsion was prepared using EOs (clove oil and cinnamon oil) and water by mixing 45 µl of cinnamon oil and clove oil each and 60 µl of water. After the preparation, 120 µl of that emulsion was added simultaneously to the homogenous mixture of Zein/glycerol (as prepared for ZF) with constant stirring for 30 min and cast after cooling the mixture. The films obtained were named as ZEO (Zein with essential oil). These ZF and ZEO films obtained using the solvent cast method were dried at 45 °C in hot air oven overnight for 18 h, and peeled off after complete drying. In this way, zein based films with an average thickness of 0.296 ± 0.015 mm were obtained using a precision micrometer.

*5.2.3 Characterization of the film*

*5.2.3.1 FTIR*

Dried samples of films were ground and mixed thoroughly with potassium bromide at the ratio of 1:100 and pelleted. The IR spectra of pellets were then recorded using the NICOLET 380 FTIR operating in the range of 4000-400 cm$^{-1}$ with a resolution of 4 cm$^{-1}$.

*5.2.3.2 XRD*

XRD was performed on various zein films and pure zein protein. Measurements were carried out with Rikagu Miniflex-II operating at 20 kV and a current of 10 mA using Cu-K$\alpha$ radiations with scanning range 2$\theta$ of 5$^\circ$ to 70$^\circ$ at 0.2 $^\circ$/min. A glass substrate was used to record the data.

*5.2.3.3 TGA*

The thermal stability of the film samples was performed using TGA (TGA 4000, Perkin Elmer, USA). The samples were weighed approximately 5 mg and heated from 0 $^\circ$C to 600 $^\circ$C at a heating rate of 10 $^\circ$C/min in an N$_2$ gas flow of 50 ml/min.

*5.2.3.4 DSC*

Thermal analysis was performed in a differential scanning calorimeter (Perkin Elmer DSC 8000, USA). The sample of approximately 3 mg was weighed inside an Aluminium sample holder with a cover that was hermetically sealed. For the experiment, heat flow was kept at 3 $^\circ$C/min at a temperature range from 0 $^\circ$ to 350 $^\circ$C with N$_2$ as a purging gas at a flow rate of 50 ml/min and with a cooling gas line at a flow rate of 2 ml/min, which used an empty Aluminium sample holder as a reference. Glass transition temperature (Tg) was determined as a point of intersection of the tangent drawn at the point of greatest slope on the transition curve with the extrapolated baseline before the transition.

*5.2.3.5 UV- visible spectroscopy (UV-Vis)*

 To check the shielding effect of the film against UV radiations, the transmittance of polyethylene (PE) (conventional packaging), zein film (ZF), and ZEO was observed in the wavelength range 200 nm-800 nm using UV-Vis Spectrophotometer (Cary 300 UV-Vis-Agilent). Each film was assessed in five replicates

 *5.2.3.6 Scanning electron microscopy (SEM)*

The surface morphology of the film samples was studied with SEM (ZESIS EVO MA15). The samples were gold coated and then observed at an accelerating voltage of 5.0 kV at 10,000 magnifications.

*5.2.3.7 Mechanical properties of the film (Breaking Strength)*

 Mechanical testing was done as per ASTM D618-61(1990) standards using Instron Micro Tensile Tester Model 5848, Singapore,  with film dimension (2.5 cm × 5 cm), load cell of 10 N, speed of elongation (5 mm/min) film thickness 0.296 ± 0.015 mm. The temperature of the laboratory was constantly maintained at 23 °C -25 °C and relative humidity (RH) was 50 ± 4% and films were conditioned before testing. Film strips were mounted on cardboard grips with initial grip separation of 50 mm. Tensile strength was calculated by dividing the maximum load that the film could withstand by the initial cross-section area of the strip. Elongation at break (E %) was expressed by as

$$E = 100 \times (L_1 - L_o)/L_o \qquad (1)$$

 *5.2.3.8 Water vapor permeability (WVP)*

 Water vapor permeability was determined gravimetrically according to standard method E 95-96 (ASTM, 1994) by water vapor permeability tester (L-80-5000, Switzerland). The films were inserted between the two chambers. The lower chamber was filled with distilled de-ionized water and the upper chamber was containing the sensor for controlling the temperature and

relative humidity (25 $^{\circ}$C and 15 % RH). Silica gel was used as a desiccant for the adsorption of water vapors. The moisture adsorbed by the silica gel was detected periodically until a stationary state was reached. For each measurement, three replications were made. The final measurement was done after incubation for two days (48 h). The slope of the weight versus time plot was divided by an effective film area to obtain the water vapor transmission rate (WVTR). This was multiplied by the film thickness and divided by the pressure difference to obtain the water vapor permeability (WVP) [34] and water vapor permeability coefficient (WVPC) which indicates the amount of water vapor that permeates per unit of area and time in packaging material.

WVTR= slope/film area $\qquad$ (g/m$^2$)

WVP= WVTR× thickness/ΔP $\qquad$ (g.mm/m$^2$.kPa)

WVPC= ΔW × X / AΔT×ΔP $\qquad$ (g.mm/m$^2$.h.kPa) $\qquad$ (2)

ΔW= weight gain by desiccant (g)

X= Film thickness (mm)

A= Area of exposed film (m$^2$)

ΔT= incubation period (h)

ΔP= difference in partial pressure (k Pa)

*5.2.3.9 Oxygen Transmission Rate*

Oxygen transmission rate (OTR) was measured according to the ASTM F1927-14, (2014) standard using an oxygen permeation instrument (OXTRAN model 2/20 Mocon, Minneapolis, MN, USA). OTR of the film was determined under control conditions (23 $^{\circ}$C and R.H = 0 %). The film was placed between two sides of the test chamber, one side was exposed to carrier gas containing 98 % $N_2$ and 2 % $H_2$ while the other side was exposed to the test gas (pure $O_2$),

and the sensor present monitored the exit port of the carrier gas measuring the amount of transmission of oxygen. OTR was calculated according to the following equation. [35]

$$OTR = V(O_2)/t.a \qquad\qquad (3)$$

$V(O_2)$ = measured volume of oxygen

t= time required for reaching the stationary state (h)

a= exposed area of the film ($m^2$)

*5.2.3.10 In-vitro antimicrobial activity of films*

*a)* <u>Disk diffusion method</u>: Antimicrobial activity of films (5 cm in diameter) was conducted by using agar disc diffusion method [36] against Gram-negative *Escherichia coli* ATCC 25922 and Gram-positive *Staphylococcus aureus* ATCC 29213 as test microorganisms. The overnight cultures of bacteria were prepared in nutrient broth at 37 °C. For antimicrobial tests, agar plates were made, three for each of the test microorganisms. After this, the bacterial inoculums were spread over the agar plates. Disks from each film were prepared under aseptic conditions of approximately 0.5 cm in diameter. They were placed over those agar plates and were incubated at 37 °C for 14-16 h and the areas of the fully formed zones (ffz) were determined by measuring the zone diameter with the digital caliper. *b)* <u>Food sample testing</u>: Fresh fruits samples of pear were sliced (2.5 cm in length approximately), kept on glass petri-plate having 5 cm diameter, and were covered with the fabricated film (ZEO) and transparent polyethylene poly-film having 150 μm thickness (PE) to carry out the relative study regarding the pace of spoilage of food. Also, one petri-plate having the fruit sample was remained uncovered. All the test samples were kept at standard temperature (25 °C). With regular intervals from one day up to one-week, samples were examined. After every regular interval, food samples from each petri-plate were taken and diluted in the nutrient broth. This followed the spreading of that nutrient broth over the agar plates to see the growth of micro-organisms over food sample which can't

be seen with naked eyes. All experiments were done at ambient conditions at a standard temperature at 25 °C.

*Statistical analysis*

Data are expressed as mean ± SD. Student's t-test was used for the analysis of the test results (least significant difference) at the significance level of p-value <0.05

## 5.3 RESULTS AND DISCUSSION:

At the macroscopic level, homogenous solvent-cast films were obtained having a thickness of 0.296 ±0.015 mm and a diameter of 5 cm having see-through ability showing the transparency of the film (fig.1).
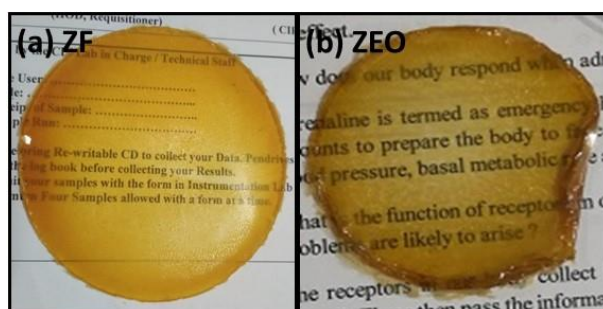


Fig. 5.1 Images of fabricated zein based films (a) ZF and (b) ZEO.

### 5.3.1 FTIR

FTIR spectra of films ZF and ZEO along with native zein protein (ZP) are shown in fig.2. For native ZP, amide A band appearing between 2860 cm$^{-1}$ and 3500 cm$^{-1}$ belongs to the stretching of N-H and O-H bond of the amino acids. The amide I band appearing at 1660 cm$^{-1}$ belongs to the stretching of the carbonyl C=O of the amide group of the peptide. Amide II band at 1536 cm$^{-1}$ corresponds to the angular deformation vibration of the N-H bond and C-H stretching vibration. Also,−COO$^{-}$ symmetrical stretching is observed at 1450 cm$^{-1}$. Moreover, the amide III band at 1246 cm$^{-1}$ belongs to the axial deformation vibration of the C-N bond and C=O

bending vibration. The observed FTIR peaks of ZP are in good agreement with Yingling *et. al.* [37] In the case of ZF, it is noteworthy that the absorption band appearing at 1660 cm$^{-1}$ (amide I) in ZP is shifted to lower wavenumber at 1644 cm$^{-1}$ indicating the existence of hydrogen bonding between O-H of glycerol and C=O of zein protein. Similarly, a shift ($\approx$ 7 to 10 cm$^{-1}$) in amide II, amide III, and $-$COO$^-$ peaks of ZP is also observed towards lower wavenumber for ZF. Fewer changes were observed in the case of ZEO in the range of 2000 to 400 compared to ZF. Peak at 1039 cm$^{-1}$ for ZF corresponds to -C-O-H bond. It is pertinent to note the shortening of a peak at 1038 cm$^{-1}$ for ZEO might be indicating distortion of -C-O-H bond. Interestingly, intermolecular hydrogen bonding between cinnamaldehyde (-CHO) content of EOs with –NH$_2$ of protein in ZEO is evident by -NH stretching at 3437 cm$^{-1}$.[38] In general, the observed peak shifts towards lower wavenumbers confirm the existence of inter- and intramolecular physical forces including ionic, hydrogen bonding, and hydrophobic between zein and glycerol molecules in ZF as well as zein and glycerol/EOs in ZEO. A similar type of interaction is recently reported between pectin and PEG. [39]
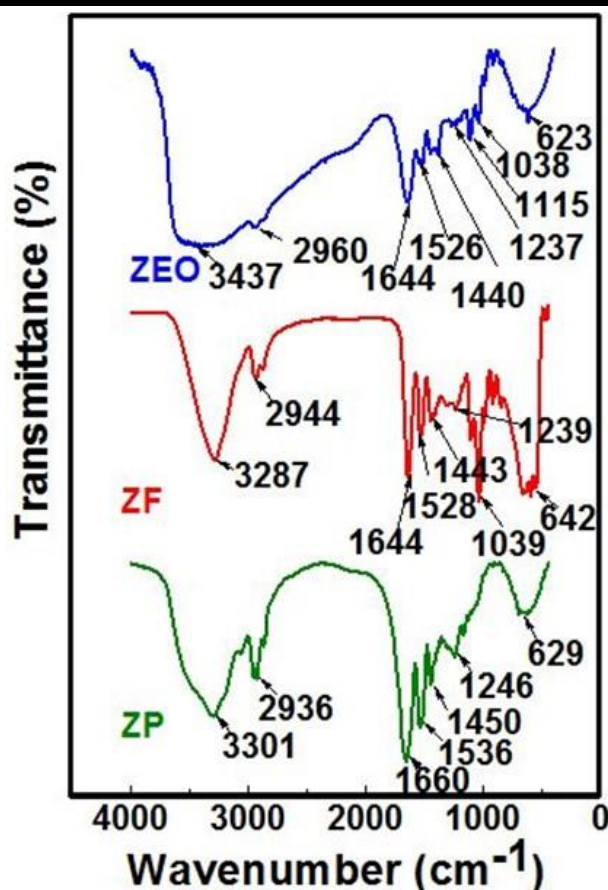
Fig. 5.2 FTIR spectra of ZP, ZF, and ZEO.

*5.3.2 XRD*

X-ray diffraction patterns of various zein films along with ZP are reported in fig. 3. XRD pattern of ZP indicated two broad peaks centered at 9.2° and 20.3°. The reported 9.2° and 20.3° peaks of ZP confirm the intermolecular intervals of 4.6 º and 8.96 º due to the average distance of skeleton in the α-helical structure of protein and distance of α-interhelix peaks in zein respectively. [40, 41] Similarly, in the case of ZF also, these peaks appeared with noticeable intensity reduction in addition to lower 2θ shift for α-helix as well as higher 2θ shift for α-interhelix peaks in comparison with the XRD pattern of ZP. On the other hand, XRD spectrum ZEO film shows an increase in the intensity of both the peaks with lower 2θ shift compared to ZF, but the intensity of both the peaks are still less in comparison with ZP. These observations

confirm that in general both helical structure, as well as molecular accumulation of the protein matrix was weakened in both the films ZF and ZEO. This is due to the existence of inter- and intramolecular physical forces between glycerol-native protein and glycerol/EO molecules-native protein in ZF and ZEO films respectively. Herein, XRD results very well corroborate with the FTIR findings (fig.2)
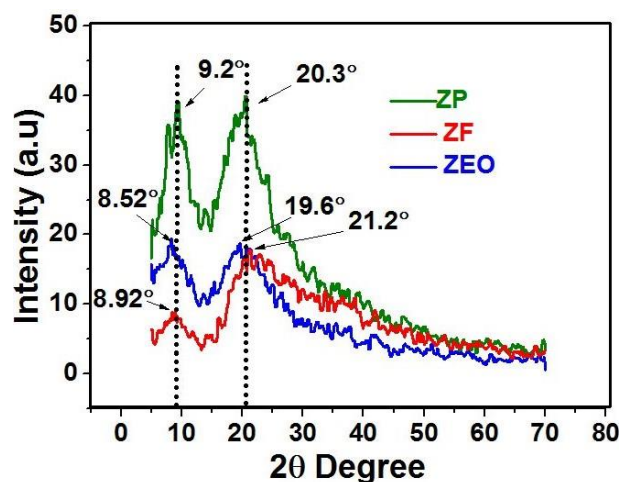


Fig. 5.3 XRD pattern of ZP, ZF, and ZEO with scanning range 2θ of 5° to 70° at 0.2°/min.

*5.3.3 TGA*

Thermogravimetric analysis was carried out to analyze the weight loss of ZP and various films as a function of temperature. The Thermal stability of ZP in its native form (powder), ZF, and ZEO film was determined. The TGA curves are shown in fig.4 (a). The observed thermal stability of ZP was higher than ZF and ZEO due to its intact α-helix structure as evident by XRD (fig. 3). The initial weight loss of 3 % to 5 % occurring in the range of 25 $^{\circ}$C to 120 $^{\circ}$C was due to the evaporation of water. [42] Between 120 $^{\circ}$C to 200 $^{\circ}$C, weight loss observed is accounted for the vaporization of glycerol. This is due to the glycerol decomposition temperature, which is analyzed in isolation reported around 210 $^{\circ}$C. [43] The major thermal degradation and major weight loss of biopolymer of various samples (ZP, ZF, and ZEO) was observed from 220 $^{\circ}$C to 370 $^{\circ}$C having 65.7 % weight loss. The onset of major weight loss for

ZF starts from 187.3 $^\circ$C leading to 7.5 % weight loss. For ZEO, this temperature increased to 231.8 $^\circ$C having weight loss near about 9 %. The reported final weight loss was 83-85% at 574 $^\circ$C leading to the existence of 15-17 % of residue and is in good agreement with various researchers. [40, 42, 44] It should be noted that, as revealed by the derivative curve fig.4(b), there was a slight shift of degradation peak towards higher temperatures for the ZEO film. Specifically, this peak was centered at 318 $^\circ$C for ZF and ZEO it was at 326 $^\circ$C. These findings reveal that degradation temperature of ZEO film is slightly higher compared to ZF indicating the existence of additional crosslinking interaction of EO contents with zein molecules as evident by FTIR and XRD (fig.2 and3).
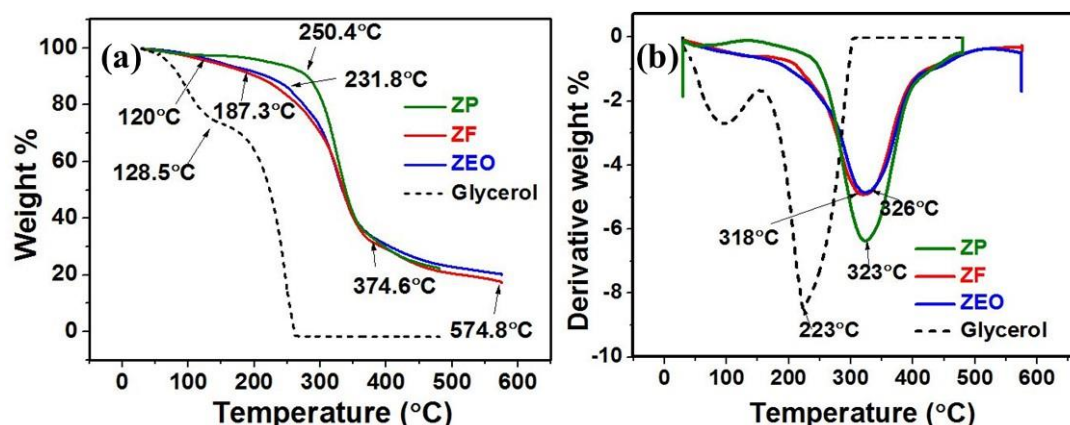


Fig.5.4 Thermogravimetric analysis of glycerol, ZP, ZF, and ZEO at a heating rate of 10 $^\circ$C/min in N$_2$ gas flow of 50 ml/min (a) TGA (b) dTGA thermograms.

*5.3.4 DSC*:

Thermograms of the films (ZF & ZEO) produced by the casting method are portrayed in fig.5. The melting point (Tm) of ZF was obtained as 228.6 $^\circ$C, fig 5(a) which is lower than the ZEO (254.4 $^\circ$C), fig 5(b). Due to the amorphous nature of the Zein protein, instead of a sharp melting peak, the broad range was obtained showing the melting range of the tested films. It is important to note that the increase in Tm of ZEO is ascribed to more ordered zein molecules due to the

cross-linking interaction with the added EOs. This is supported by the XRD pattern of ZEO film, which shows an increase in the intensity of peaks correspond to α-helix as well as α-interhelix compared to ZF (fig.3). The glass transition temperature of films is important as this aspect limits the use of the material under required / extreme temperature conditions and also provides information regarding structural organizations like cross-linking, crystalline nature, etc. Glass transition temperature (Tg) was determined by estimating the midpoint in the proximity of the change in specific heat (ΔCp). Lines tangential to $Cp_{solid}$ to $Cp_{liquid}$ and transient in between were drawn and the intersection between $Cp_{solid}$, $Cp_{liquid,}$ and transient was defined and designated as Tg. [45] The glass transition temperature of ZEO came out to be 47.7 $^{\circ}$C, fig. 5(d) which is much lower to the ZF (77.6 $^{\circ}$C), fig.5(c), similar to which is reported by other researchers. [40, 42] It is thought that depression in Tg could be attributed to the additional crosslinking provided by acetyl eugenol present in clove oil as well as cinnamaldehyde content of cinnamon oil with zein molecule. The decrease in Tg is due to the plasticization of zein protein fibers by the EOs in ZEO film. ZEO contains both glycerol and EOs leading to larger amount of plasticizer and lowering of Tg.[46]
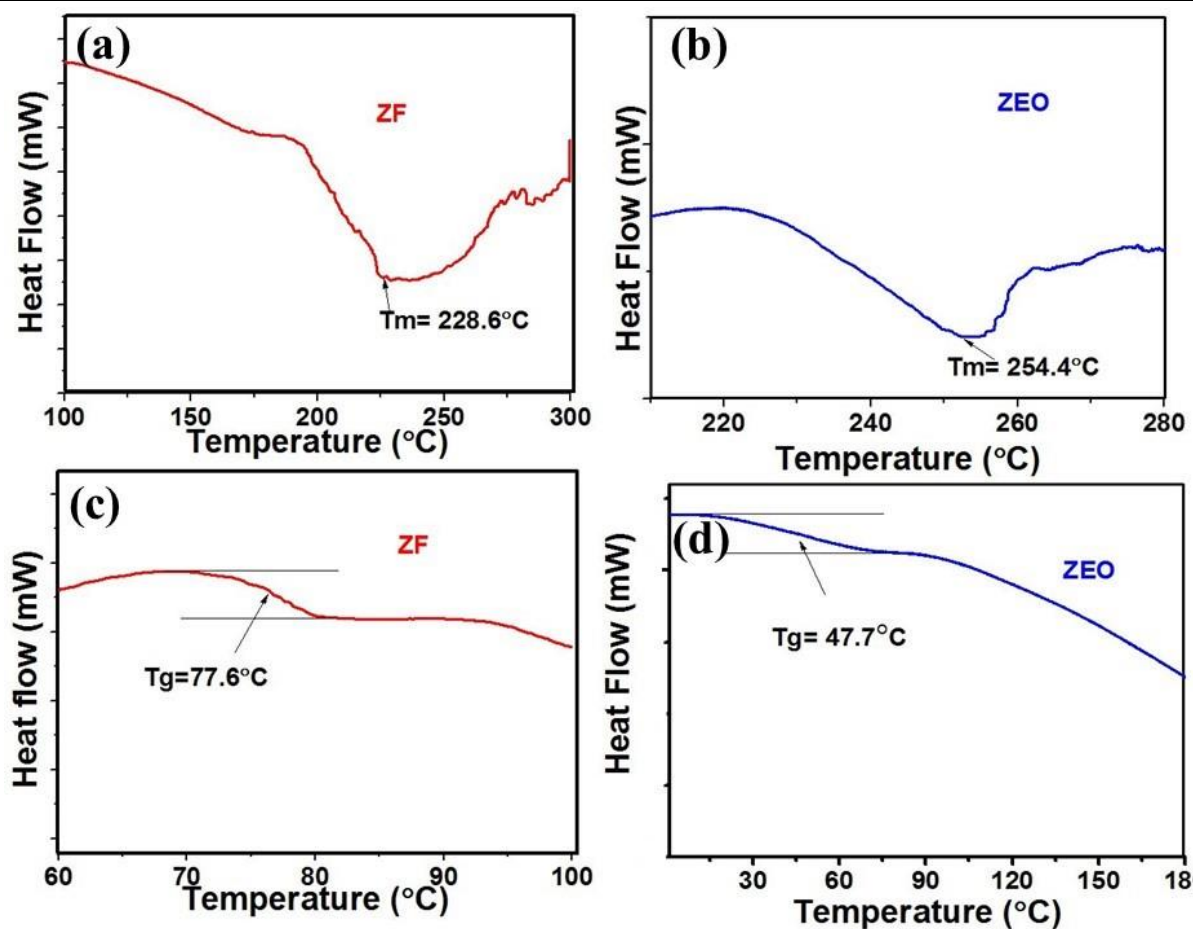
Fig. 5.5 DSC thermograms of ZF and ZEO films at heat flow $3°$C/min and with $N_2$ as a purging gas at a flow rate of 50 ml/min (a) & (b) Tm, (c) & (d) Tg.

*5.3.5 UV Visible Spectroscopy*

UV-Visible spectroscopy was conducted to check the ability of the fabricated film to shield UV radiation and comparing it with conventional packaging (PE) (polyethylene poly-film). It was evident from the graph in fig.6 that PE did not absorb the wavelength in the UV region leading to transmission of UV radiations from 40 % to 80 % in the range of 200-400 nm. The UV transmittance of ZEO and ZF is almost zero increasing up to 1.56 % at 432 nm for ZF and 0.69% at 446 nm for ZEO film which proves it to be UV protecting. This is attributed to the protein nature of the film. [47] Also, ZEO has a little more shielding effect against UV radiations because of the presence of aromatic compounds present in the essential oils that have been incorporated into it. [48] If we compare our data with other biobased films as quoted by

Vilela C. *et. al.* chitosan/ellagic acid films, ZEO films show remarkable UV protection behavior as compare to chitosan/ellagic films that showed approximately 20-30 % of UV transmittance. [49] The addition of essential oils considerably decreased the UV transmittance which is in agreement with Martin *et. al*. where it was quoted that protection against UV is increased by increasing the active components. [48, 50] Thus suggesting ZEO films to be good UV absorbers and can help in preventing photo-oxidation of the photo-sensitive food or pharmaceuticals.
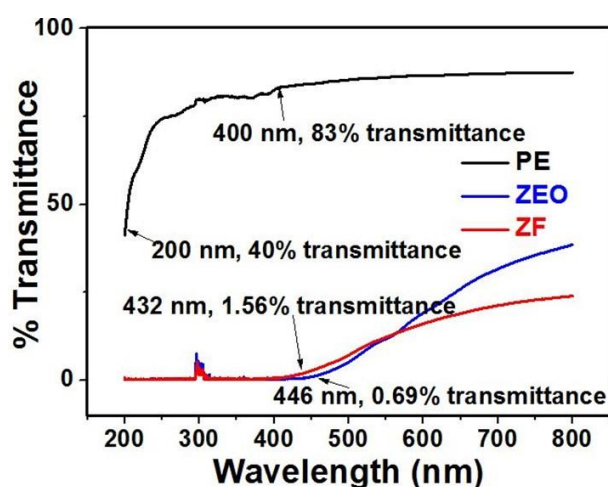


Fig. 5.6  UV transmittance of PE, ZF, and ZEO.

### 5.3.6 Morphological determination by SEM

The microstructure of ZF and ZEO films was observed using SEM depicted in fig.7. From the images, it was observed that ZF fig. 7(a) at magnification 10000X & 7(b) at 1000X magnification has a rough bumpy surface as a result of pure zein and glycerol association which is in agreement with Khalil *et. al.* [51] and as per Ming Zeng. [52] With the addition of EO, it leads to the formation of a smoother ZEO surface as in fig.7(c) at 10000X & 7(d) at 1000X having homogenous nature [42] due to the interaction between EO and protein fibers. It seemed that acetyl eugenol and cinnamaldehyde contents of EOs have good affinity with zein protein

driven by physical interactions and increasing the film networking making it homogenous and smooth.[46]
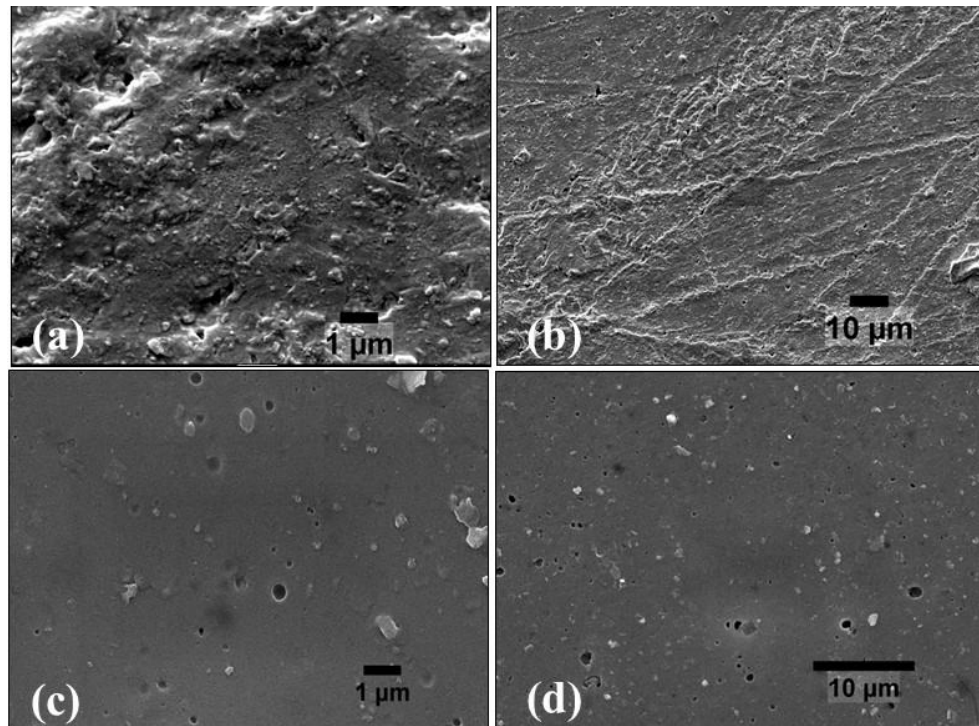


Fig. 5.7  SEM micrographs of films at an accelerating voltage of 5.0 kV (a)10000X & (b)1000X - ZF, (c)10000X & (d) 1000X – ZEO

*5.3.7 Tensile testing*

In table 1, it is depicted that ZF has shown poor mechanical properties having a tensile strength of 0.94 ± 0.047 MPa and elongation at break (E %) at 3.72 ± 0.015%. After the addition of EOs, a higher value of tensile strength 1.21 ± 0.054 MPa, E% 4.93±0.24 % was obtained due to the additional crosslinking provided by EO contents as explained by FTIR and XRD findings (fig.2 & 3) and agrees with earlier reported work. [41] In detail, cinnamaldehyde and acetyl eugenol (present in EOs) interact with zein network along with glycerol through physical forces. This leads to stabilization and alignment of protein fibers in a compact form which could be the reason for the enhancement of the mechanical properties of the ZEO film.

The breaking force of the ZEO of width approximately 25 mm also came out to be $46.0 \pm 2.07$ N slightly greater that ZF ($38.4 \pm 1.53$ N). The data showed no significant difference.

**Table 5.1: Mechanical properties of zein based films as per ASTM D618-61(1990) standards.**

| Film | Tensile strength (MPa) | Elongation at break (%) |
|------|------------------------|--------------------------|
| ZF | 0.94±0.04 | 3.72 ± 0.01 |
| ZEO | 1.21±0.05 | 4.93±0.24 |

ZF= zein film, ZEO= Zein film with EO. Values are mean ± standard deviation and they were not statistically different (p<0.05).

*5.3.8 Water vapor permeability of fabricated films*

It is well known that water vapor barrier property of packaging material is an important factor in determining the shelf life of food products. Water vapor permeability values (g mm/kPa.h.m$^2$) of ZEO and ZF were calculated. From the calculation, as indicated in table 2, water vapor permeability for ZF is higher ($5.47 \pm 0.27$ g.mm/kPa.h.m$^{2)}$ as compare to ZEO ($4.31 \pm 0.21$ g.mm/kPa.h.m$^2$) showing no such significant difference in data and found in agreement with Vahedikia *et. al.* [41] Hydrophobic Zein proteins bonds with EO contents via hydrogen bonding and thus impeding the bond formation with water molecules and reducing the absorption of water.[53] Due to the presence of essential oils, permeability is influenced by the hydrophobic nature of the EO. [41]

**Table 5.2: Barrier properties of zein based films -Water vapor permeability (ASTM E 95-96, 1994) and Oxygen transmission rate (ASTM F1927-14, 2014).**

| Film | WVP (g.mm/kPa.h.m$^2$) | OTR (cm$^3$/m²/day) |
|------|------------------------|---------------------|
| ZF   | 5.47±0.27              | 0.0965±0.0048       |
| ZEO  | 4.31±0.21              | 0.0705±0.0035       |

WVP= Water vapor permeability, OTR= Oxygen transmission rate, ZF= Zein film, ZEO= Zein film with EO. Values are mean ± standard deviation and they were not statistically different (p<0.05).

*5.3.9 Oxygen transmission rate*

Shelf life of food products is enhanced when the oxygen barrier property of the film is high. The Oxygen Transmission Rate (OTR) of both films was measured at 23º C & 0% RH (Relative Humidity) and results are shown in Table 2. Zein film has a lower value of OTR and shows greater gas barrier property than LDPE (Lower Density Polyethylene), HDPE (High-Density Polyethylene), PS (Polystyrene), PVC (Poly Vinyl Chloride). [46, 54] In our study, the OTR value of ZEO came out to be (0.0705±0.0035 cm$^3$/m²/day) which is better than the OTR value of ZF (0.0965±0.0048 cm$^3$/m²/day). The observed trend could be due to homogenizing effect of EOs [46] along with glycerol entrapped in the polymer matrix before drying and is in agreement with the data quoted by Tilminlioglu *et. al*. [55] having GLY/50 (Plasticizer type/Concentration) & 95/5 (Ethanol % (v/v)/Corn-Zein(w/v) concentration. The data showed no significant difference.

*5.3.10 In-vitro* studies

The antimicrobial activity of the films was performed using the disk diffusion method. It can be observed from fig. 8 (1) (c) & (2) (c) that ZEO showed pronounced antibacterial activity against both *E. coli* and *S. aureus* by showing a significant zone of inhibition approximately 20±1 mm in diameter. The antimicrobial activity of this active packaging is credited to the presence of EO. [51] ZF as shown in fig. 8 (1) (b) & (2) (b), didn't show any antimicrobial activity. After observing these results, ZEO film was tested as packaging material over a food sample, and results were compared with conventional packaging material PE poly-film. From fig. 9, we can see that the fruit samples were kept covered by ZEO film, PE, and one without any covering. The film testing over the food sample showed prominent results for the ZEO films exhibiting delayed deterioration of the food sample packaged into it. This was made evident by culturing the food samples over the agar plates to see any growth of micro-organisms. From fig.10 it can be observed that on 3$^{rd}$ day, there was no microbial growth in ZEO film samples and after 7$^{th}$ day of examination of food samples, one bacterial colony was observed in ZEO film packaging unlike PE poly-film and uncovered food sample where the bacterial growth can be seen from 3$^{rd}$ day itself. All these results indicate ZEO as a potential packaging material and EOs as natural ingredients in active packaging material to provide antimicrobial characteristics to the packaging films.
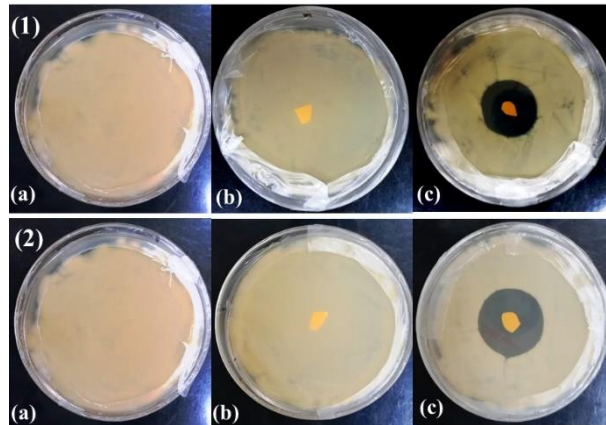
Fig. 5.8  Disk diffusion test for antimicrobial activity at 37 ºC against- Lane (1) (Left to right) E. coli (a) Blank, (b) ZF and (c) ZEO. Lane (2) (Left to right) S. aureus (a) Blank, (b) ZF and (c) ZEO.
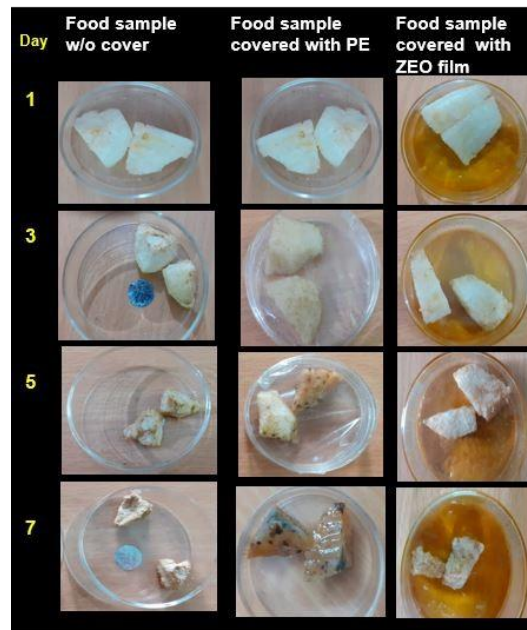


Fig. 5.9 Antimicrobial testing over food sample at 25 ℃ without cover (w/o) and covered with PE and ZEO (Left to Right) respectively on days 1, 3, 5 and 7
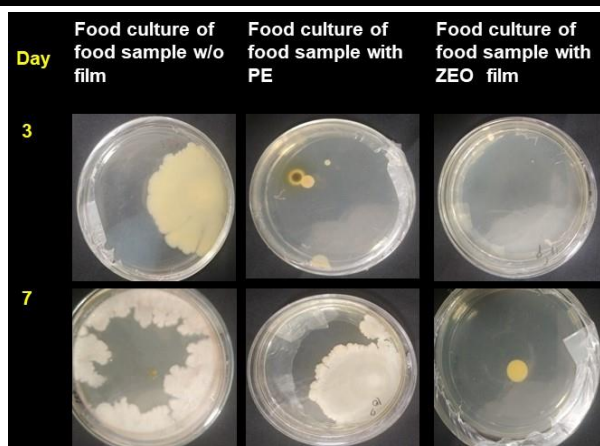
Fig. 5.10  Microbial growth over food sample without cover (w/o) and covered with PE and ZEO (Left to right) respectively on days 3 and 7 at 25 $^\circ$C.

## 5.4 Conclusion:

This manuscript successfully presents a simple fabrication of zein film incorporated with essential oils with zero UV transmittance and antimicrobial property by forming a strong zone of inhibition. Due to added EOs in addition to glycerol, there increases the thermal and mechanical stability of ZEO as compare to ZF. Water vapor permeability and oxygen transmission rate on these active films showed substantially significant barrier properties and increases the shelf life of the packaged food. Lower mechanical resistance of these edible films as compare to conventional poly-film directs their usage as coating materials over food, drugs, etc. and for unit packaging and laminates. These findings promise not only cost-effective and healthy food packages but also can decrease the usage of toxic plastics.

**References:**

[1] Plastic Pollution by Hannah Ritchie and Max Roser, September 2018, https://ourworldindata.org/plastic-pollution

[2] 3$^{rd}$ National Conference on "Sustainable Infrastructure for plastics", Knowledge paper on plastic industry for infrastructure, FICCI, February 2017.

[3] Jeya Jeevahan and M. Chandrasekaran, J.Mater. Sci, 2019, 54, 12290–12318.

[4] https://www.nationalgeographic.com/news/2018/05/plastics-facts-infographics-ocean-pollution/ by Laura Parker.

[5] Khaliq Majeed, Reza Arjmandi, Azman Hassan, Journal of Physical Science, 2018, 29(1), 43-58.

[6] Raquel Fernández, Sebastian Bonardd, Itxaso Algar, Irati Barandiaran, Galder Kortaberria, Junkal Gutierrez, Agnieszka Tercjak, European Polymer Journal, 2019, 122, 109373.

[7] Marina P. Arrieta, Juan López, Alberto Hernández, Emilio Rayón, European Polymer Journal, 2014, 50, 255-270.

[8] Lorenzo Siroli, Francesca Patrignani, Diana I. Serrazanetti, Cristiana Chiavari, Marzia Benevelli, Luigi Grazia, Rosalba Lanciotti, Front. Microbiol., 2017, 8, 2606.

[9] Xiuping Yin, Yuhao Zhang & Jun Zhang Plastics, Rubber and Composites, 2017, 46, 375–380.

[10] Kenichi Shimizu, Yuuki Tokuta, Akihiro Oishi, Takashi Kuriyama, and Masao Kunioka, Journal of Polymers, 2016, 2016, 1-14.

[11] Jan P. Eubeler, Marco Bernhard, Thomas P. Knepper, Trends in Analytical Chemistry, 2010, 29, 84-100.

[12] Yousif and Haddad, SpringerPlus, Springer Plus, 2013, 2, 398.

[13] Subhas C. Shit and Pathik M. Shah, Journal of Polymers, 2014, 2014, 1-13.

[14] Janusz Bogdan, Agnieszka Jackowska-Tracz, Joanna Zarzyńska, and Joanna Pławińska-Czarnak, Nanoscale Research Letters, 2015, 10,57.

[15] Tanja Radusin, Sergio Torres-Giner, Alena Stupar, Ivan Ristic, Aleksandra Miletic, Aleksandra Novakovic, Jose Maria Lagaron, Food Packaging and Shelf Life, 2019, 21 100357.

[16] D. Konuk Takma, F. Korel, Food Packaging and Shelf Life, 2018, 19, 210-217.

[17] John W. Lamppa, Greg Horn, David Edwards, Journal of Controlled Release, 2014, 190, 201-209.

[18] 14th Report on Carcinogens, National Toxicology Program, U.S. Department of Health and Human Services, 2016, http://ntp.niehs.nih.gov.

[19] Jinhe Bai, Victorine Alleyne, Robert D. Hagenmaier, James P. Mattheis, Elizabeth A. Baldwin, Postharvest Biology and Technology, 2003, 28, 259-268.

[20] Ernesto Oregel- Zamudio, M.Valentina Angoa- Perez, Guadalupe Oyoque-Salcedo, Cristobal Noe Aguilar-Gonzaler, Hortencia Gabriela Mene- Violante, Scientia Horticulturae, 2017, 214, 273-279.

[21] Kashiri, M., Cerisuelo, J.P., Domínguez, I., López-Carballo, G., Muriel-Gallet, V., Gavara, R., Hernández-Muñoz, P., Food Hydrocolloids, 2017, 70, 260-268.

[22] Lena Vogt, Liliana Liverani, Judith A. Roether and Aldo R. Boccaccini, Nanomaterials, 2018, 8, 150.

[23] Bilal Hassan, Shahzad Ali Shahid Chatha, Abdullah Ijaz Hussain, Khalid Mahmood Zia, Naseem Akhtar, International Journal of Biological Macromolecules, 2018, 109, 1095-1107.

[24] Ilke Uysal U Nalan, Figen Korel & Ahmet Yemeniciog lu, International Journal of Food Science and Technology, 2011, 46, 1289–1295.

[25] Jun Liang, Qiuyang Xia, Simon Wang, Ji Li, Qingrong Huang, Richard D. Ludescher Food Hydrocolloids, 2015, 44, 94-100.

[26] Caio G. Otoni, Paula J.P. Espitia, Roberto J. Avena-Bustillos, Tara H.McHugh, Food Research International, 2016, 83, 60–73.

[27] Valentina Siracusa, Santina Romani, Matteo Gigli, Cinzia Mannozzi, Juan Pablo Cecchini, Urszula Tylewicz, and Nadia Lotti, Materials 2018, 11, 1980.

[28] Sonam Chouhan, Kanika Sharma, and Sanjay Guleria, Medicines, 2017, 4, 58.

[29] S. Siddiqua, B. A. Anusha, L. S. Ashwini & P. S. Negi, J Food Sci Technol, 2014, 52(9), 5834-5841.

[30] M.A. Del Nobile, A. Conte, A.L. Incoronato, O. Panza, Journal of Food Engineering, 2008, 89, 57–63.

[31] Derya Alkan, Levent Y. Aydemir, Iskender Arcan, Hatice Yavuzdurmaz, Halil I. Atabay, Cagatay Ceylan, and Ahmet Yemenicioglu, J. Agric. Food Chem., 2011, 59, 11003–11010.

[32] Babar Ali, Naser Ali Al-Wabel, Saiba Sham, Aftab Ahamad, Shah Alam Khan, Firoz Anwar, Asian Pac J Trop Biomed, 2015, 5(8): 601–611.

[33] A. Gunia-Krzyzak, K. Sloczynska, J.Popiol, P. Koczurkiewicz, H. Marona, E. Pekala, International Journal of Comestic Science, 2018, 40, 356-366.

[34] Babak Ghanbarzadeh, Abdulrasoul Oromiehie, Mohamad Musavi, Keramat Rezayi, Elhame Razmi, and Jafar Milani, Iranian Polymer Journal, 2006, 15(9), 691-700.

[35] Carolina Pena Serna and José Francisco Lopes Filho, Food Technol. Biotechnol. 2015, 53 (3) 348–353.

[36] Idoya Fernández-Pan, Maite Royo, Juan Ignacio Maté, Journal of Food Science, 2012, Vol. 77(7), 383-390.

[37] Yingling Miao, Ruirui Yang, David Y. B. Deng and Li-Ming Zhang, RSC Adv., 2017, 7, 17711–17719.

[38] E. Kenawy, A.M. Omer, T.M. Tamer, M.A. Elmeligy, M.S Mohy Eldin, International Journal of Biological Macromolecules, 2019, 139, 440-448.

[39] Meenakshi Gautam, Deenan Santhiya, Journal of Drug Delivery Science and Technology, 2019, 53, 101137.

[40] M. Oliviero, E. Di Maio, S.Iannace, Journal of Applied Polymer Science, 2010, 115, 277-287.

[41] Nooshin Vahedikia, Farhad Garavand, Behjat Tajeddin, Ilaria, Seid Mahdi Jafari, Tayebeh Omidi, Zahra Zahedi, Colloids and Surfaces B: Biointerfaces, 2019, 177, 25-32.

[42] Crislene Barbosa de Almeida, Elisângela Corradini, Lucimara Aparecida Forato, Raul Fujihara, and José Francisco Lopes Filho, Polímeros, 2018, 28(1), 30-37.

[43] A. Gómez-Siurana, A. Marcilla, M. Beltrán, D. Berenguer, I. Martínez-Castellanos, S. Menargues, Thermochimica Acta 2013, 573, 146–157.

[44] Huan Yang, Peng Wen, Kun feng, Min H. Zong, Wen Y. Lou, Hong Wu, RCS Adv., 2017, 7, 14939-14946.

[45] E. Parodi, L.E. Govaert, G.W.M. Peters, Thermochimica Acta 2017, 657, 110–122.

[46] Derya Boyaci, Gianmarco Iorio, Gozde Seval Sozbiler, Derya Alkan, Silvia Trabattoni, Flavia Pucillo, Stefano Farris, Ahmet Yemenicioglu, Food Packaging and Shelf Life, 2019, 20, 100316.

[47] Laura Moroni, Cristina Gellini, Pier Remigio Salvi, World Journal of Chemical Education, 2015, 3(3), 59-63.

[48] Barbara Trost, Jochen Stutz, and Ulrich Platt, Atmospheric Environment 1997, 31(23), 3999-4008.

[49] Carla Vilela, Ricardo J.B. Pinto, Joel Coelho, M.R.M. Domingues, Sara Daina, Patrizia Sadocco, Sónia A. O. Santos, Carmen S.R. Freire, Food Hydrocolloids, 2017, 73, 120-128.

[50] Martins, J. T., Cerqueira, M. A., & Vicente, A. A., Food Hydrocolloids, 2012 27(1), 220–227.

[51] Ashraf A. Khalil, Sahar F. Deraz, Somia Abd Elrahman & Gomaa El-Fawal Preparative Biochemistry & Biotechnology, 2015, 45, 551–567.

[52] Ming Zeng, Yiwan Huang, Liyuan Lu, Liren Fan, Cécile Mangavel & Denis Lourdin, Food Biophysics, 2011, 6, 49–57.

[53] Dariusz Kowalczyk, Monika Kordowska-Wiater, Bartosz Sołowiej & Barbara Baraniak, Food and Bioprocess Technology, 2015, 8, 567–579.

[54] Gye Hwa Shin, Yeon Hee Lee, Jin Sil Lee, Young Soo Kim, Won Seok Choi And Hyun Jin Park, J. Agric. Food Chem., 2002, 50, 4608−4614.

[55] Tihminlioglu Funda, Atik İsaDoğan, Ozen Banu, Journal of Food Engineering 2010, 96,

342–347.

# Future Scope

❖ The radiolabeling of bioactive glass and its binding stability in different gastrointestinal pH conducted in the present study can further be explored in an animal model where the whole ADME process (Absorption, Distribution, Metabolism, and Excretion) can be studied when these particles are ingested orally. The pharmacokinetics and pharmacodynamic studies will help in deducing the efficacy of orally delivered bioactive glass in bone regeneration.

❖ Oral delivery of bioactive glass loaded with therapeutic proteins in the polymer-based edible coating can be explored for the targeted drug delivery system

❖ In soft tissue repair, bioactive glass may have a potential application to treat stomach ulcers.

❖ In addition, the practicality of designing dosage forms that are acceptable for human consumption for bioactive glass-based drugs is to be further analyzed and examined in *in-vivo* systems.

# List of Publications

- ❖ <u>Manjot Kaur</u> and Deenan Santhiya. "UV-shielding antimicrobial zein films blended with essential oils for active food packaging." *Journal of Applied Polymer Science* 138.7 (2021): 49832, SCIE Indexed, (Impact factor: 3.057)

- ❖ <u>Manjot Kaur</u> and Deenan Santhiya. "Fabrication of soy film with in-situ mineralized bioactive glass as a functional food for bone health." *Food Bioscience* 47 (2022): 101767, SCIE indexed (Impact factor: 5.318)

- ❖ <u>Manjot Kaur</u>, Deenan Santhiya, Teena Goel and Pooja Srivastava. " In vivo GIT Distribution Study on 99m Tc-Functionalized Bioactive Glass through an Oral Route for Biomedical Applications" (accepeted – Chemistryselect)

- ❖ <u>Manjot Kaur</u> and Deenan Santhiya. "Characterizing Dextran-Sandwiched Collagen Bioactive Glass Film for Enhanced Oral Targeted Delivery: A Physicochemical And Structural Investigation" (Manuscript under review)

# Conference Proceedings

- ❖ Participated in International Conference on Biomaterial-based Therapeutic Engineering and Regenerative Medicine held on 28th November- 1st December 2019 at IIT Kanpur, Kanpur, India

- ❖ Participated in the First International Online conference on Blends, Composites, Bio-Composites, and Nanocomposites (ICNC–2020), held on 9th – 11th October 2020 at Kottayam, Kerala, India, and won fourth prize in an oral presentation (short invited lecture).

- ❖ Took part in the First International Conference on Innovations in Biotechnology and Life Sciences (ICIBLS 2020) organized by the Department of Biotechnology, DTU from 18$^{th}$ -20$^{th}$ December 2020.

- ❖ Delivered Oral Lecture during International e-Conference on Nanomaterials and Nanoengineering (APA Nanoforum) held on 24$^{th}$ -26$^{th}$ February 2022 organized by IIT, Delhi in collaboration with Asian Polymer Association (APA), NPL, India.

- ❖ Presented a paper at the International Conference on Nanotechnology Opportunities and Challenges (ICNOC-2022) held on 28$^{th}$-30$^{th}$ November 2022 organized by the Department of Applied Sciences & Humanities, Faculty of Engineering and Technology, Jamia Milia Islamia, New Delhi, India.